

NASA CR

141735

SKYLAB PROGRAM

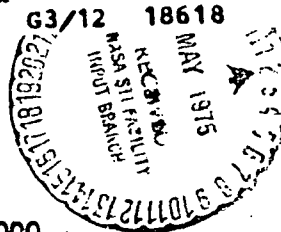
EARTH RESOURCES EXPERIMENT PACKAGE

SENSOR PERFORMANCE EVALUATION FINAL REPORT VOLUME II (S191)

(NASA-CR-141735) EARTH RESOURCES EXPERIMENT
PACKAGE SENSOR PERFORMANCE EVALUATION.
VOLUME 2: S191 Final Report (Martin
Harrington Corp.) 102 p HC \$5.25 CSCI 22A

#75-21304

Unclas
18618

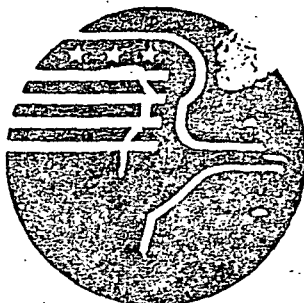


JANUARY 2, 1975

CONTRACT NAS8-24000

AMENDMENT JSC-14S

National Aeronautics and Space Administration
LYNDON B. JOHNSON SPACE CENTER
Houston, Texas



--	--	--	--	--	--	--	--	--

MSC-05546

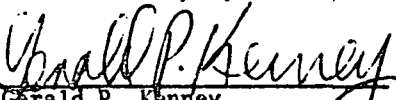
EARTH RESOURCES EXPERIMENT PACKAGE

SENSOR PERFORMANCE EVALUATION
FINAL REPORT

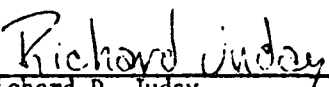
VOLUME II (S191)

January 2, 1975

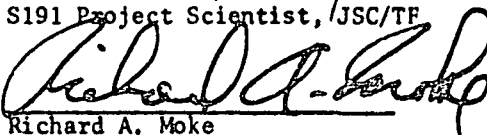
Submitted by:


Gerald P. Kenney
Skylab/ERP Sensor Performance
Evaluation Manager, JSC/HC

Technical
Review by:


Richard D. Juday
S191 Project Scientist, JSC/TF

Approved:


Richard A. Moke
Manager, Systems Analysis and
Integration Office, JSC/HC

Contract NAS8-24000
Amendment JSC-14S

Skylab Program
Lyndon B. Johnson Space Center

--	--	--	--	--	--	--	--

MSC-05546 Volume II

FOREWORD

This volume is Section II of six sections of document MSC-05546, submitted by Martin Marietta Corporation, in accordance with the requirements of Annex I to Exhibit A, Statement of Work, Part I, Data Requirements List, of Contract NAS8-24000, Amendment JSC-14S, Line Item 295, and was prepared under WBS 02216.

CONTENTS

	<u>Page</u>
Foreword	II-11
Contents	II-iii
1. INTRODUCTION	II-1
1.1 Purpose	II-1
1.2 Scope	II-1
1.3 Usage Guide	II-1
1.4 Abstract	II-2
2. APPLICABLE DOCUMENTS	II-3
3. SUMMARY OF SENSOR PERFORMANCE EVALUATION INTERIM REPORT	II-4
3.1 Functional Limit Verification	II-4
3.1.1 Housekeeping	II-4
3.1.2 Zero Radiance Level and Noise Equivalent Spectral Radiance (NESR)	II-6
3.2 Interference Check	II-7
3.3 Wavelength Calibration Check	II-7
3.4 Photographic Image Adequacy for Site Location	II-10
3.4.1 Exposure Setting	II-10
3.4.2 Data Acquisition Camera/Viewfinder Tracking System Resolution	II-11
3.4.3 Crosshair Visibility	II-11
3.4.4 Light-Emitting Diode Visibility	II-11
3.4.5 Data Acquisition Camera Mechanical Performance	II-11
3.5 Determination of Boresight Error and Spectrometer Field of View	II-12
3.5.1 Determination of Boresight Error during Zoom	II-12
3.5.2 Determination of Boresight Error at Maximum Zoom	II-13
3.5.3 In-Flight Alignment Verification	II-14
3.5.4 Field of View and Off-Axis Rejection	II-14
3.6 System Spectroradiometric Response Determination	II-16
3.6.1 Short-Wavelength Radiometric Calibration and Dynamic Range	II-16
3.6.2 Long-Wavelength Radiometric Calibration and Dynamic Range	II-18
3.6.3 Contamination	II-18
3.6.4 Off-Band Radiation	II-20
3.6.5 Drift and Indeterminacy in S191 Outputs	II-20

	<u>Page</u>
4.	SUPPLEMENTARY ANALYSES II-22
4.1	Short-Wavelength Radiometric Calibration . . II-22
4.2	Data Acquisition Camera (DAC) and Viewfinder Tracking System (VTS) Interface Design Considerations II-26
4.2.1	Complete Greenwich Mean Time (GMT) Display II-30
4.2.2	Metered Camera II-30
4.2.3	DAC Mounting Technique II-30
4.2.4	Use of Illuminated Reticles II-31
4.2.5	Variable Control or Multiple Discrete Steps for Light-Emitting Diode (LED) Brightness II-31
4.2.6	Use of High-Resolution Color Film II-31
4.3	S190A, S191, and S192 Radiometric Comparison II-31
4.3.1	Comparison of S190A to S191 II-32
4.3.2	Radiometric Comparison of S190A to S192 . . II-35
4.3.3	Radiometric Comparison of S191 to S192 . . II-36
4.3.4	Radiometric Comparison Summary II-38
4.4	Wavelength Calibration II-39
4.4.1	Calibration Filter Spectra II-39
4.4.2	Equations for Wavelength Calibration . . . II-45
4.5	S191 Viewfinder Tracking System Spectrometer Component Reflectances and Temperatures . . II-48
4.6	Additional Pertinent Studies II-49
5.	FINAL RESULTS II-50
5.1	Significant Performance Degradation II-50
5.2	S191 and EREP System Anomalies II-50
5.3	Summary of Achieved Performance II-51
6.	CONCLUSIONS II-53
7.	RECOMMENDATIONS II-56
7.1	Viewfinder Tracking System Recommendations . II-56
7.2	Infrared Spectrometer Recommendations . . . II-56
7.3	General System Recommendations II-57
8.	NOTES II-59
8.1	Acknowledgements II-59
8.2	Abbreviations II-59

	<u>Page</u>
Appendix A TECHNIQUES ADDENDUM	II-61
I. CALCULATION OF APPARENT SPECTRAL RADIANCE AT THE SPACECRAFT BASED ON GROUND TRUTH MEASUREMENTS	II-62
II. USE OF LAKES AS THERMAL CALIBRATION TARGETS	II-65
III. RADIANCE CALIBRATION OF SEVERAL LUNAR MARIA USING AN S191-IDENTICAL GROUND-BASED SPECTROMETER	II-67
A. Background	II-67
B. Method	II-68
IV. USE OF ABSORPTION FILTERS FOR SPECTROMETER WAVELENGTH CALIBRATION	II-70
V. S191 FIELD OF VIEW, ALIGNMENT, AND OFF-AXIS REJECTION DETERMINATION USING THE LUNAR LIMB	II-71
A. Field of View	II-71
B. Alignment	II-74
C. Off-Axis Rejection	II-74
VI. DETERMINATION OF NOISE IN A LIMITED SET OF REPETITIVE DATA	II-75
VII. INFRARED ATMOSPHERIC CORRECTIONS	II-77
Appendix/B ABSOLUTE RADIANCE OF THREE LUNAR MARIA	II-79

Figures

3.5.4-1	SWL Off-Axis Rejection	II-15
4.1-1	S191 Responsivities Derived from Lunar Calibration Data	II-23
4.1-2	Comparison of S191 Responsivities Derived from Ground Truth and Lunar Calibration Data.	II-27
4.3.1-1	S191 Spectral-Radiance Plot for S190A and S191 Comparison Sites	II-34

	<u>Page</u>
4.3.3-1	S191 Spectral Radiance of Rio Grande Reservoir, SL3 II-37
4.4.1-1	Transmission Spectra of BG-36 Schott Glass as a Function of Ramp Voltage and Wavelength II-40
4.4.1-2	Transmission Spectra of BG-36 Schott Glass as a Function of Ramp Voltage and Wavelength II-41
4.4.1-3	Transmission Spectra of BG-36 Schott Glass as a Function of Ramp Voltage and Wavelength II-42
4.4.1-4	Transmission Spectra of Polystyrene as a Function of Ramp Voltage and Wavelength II-43
4.4.1-5	Transmission Spectra of Polystyrene as a Function of Ramp Voltage and Wavelength II-44
4.4.2-1	S191 Circular Variable Filter Wheel II-45
A.II-1	Reflection from Water Surface at 0, 60, and 80° Incidence Angles II-66
A.II-2	Reflectivity and Emissivity of Water versus Incidence Angle II-66
A.II-3	Thermal Structure of the Sea Boundary Layer II-66
A.III-1	S191 Lunar Calibration Data Flow II-68
A.V-1	Theoretical Field-of-View Determination II-72
A.V-2	Data Acquisition Camera Shutter Time Sequence II-73
A.VII-1	Upwelling Radiance Calculation II-78
B-1	Absolute Radiance of Mare Serentatis II-80
B-2	Absolute Radiance of Mare Tranquillitatis II-85
B-3	Absolute Radiance of Mare Imbrium II-90

Tables

3.1-1	Housekeeping-Parameter Performance Summary II-5
3.1.2-1	Zero Radiance-Level Summary II-6
3.1.2-2	Noise-Equivalent Spectral Radiance Summary (SWL) II-8
3.3-1	Wavelength Calibration II-9
3.5.2-1	Crosshair Position Relative to S191 Field of View (FOV) II-13
3.5.4-1	Field-of-View Determination Summary II-15
3.6.1-1	SWL Responsivity and Dynamic Range Summary II-17
3.6.2-1	LWL Responsivity and Dynamic Range Summary II-19
4.1-1	Short-Wavelength Responsivities Derived from Lunar Calibration Data II-26

MSC-05546

		<u>Page</u>
4.3-1	S190A, S191, and S192 Spectral Bands for Radiometric Comparison	II-32
4.3.1-1	S191 Spectral Radiance for S190A and S191 Comparison Sites	II-33
4.3.1-2	S190A, S191, and Ground-Truth Radiometric Comparison	II-34
4.3.2-1	S190A, S192, and Ground-Truth Radiometric Comparison	II-36
4.3.3-1	S191 Spectral Radiance of Rio Grande Reservoir for Comparison of S191 to S192 . .	II-36
4.3.3-2	S191, S192, and Ground-Truth Radiometric Comparison	II-38
4.4.2-1	S191 Wavelength Coverage	II-46
5.1-1	Significant Performance Degradation	II-50
5.2-1	S191 and EREP System Anomalies	II-51
5.3-1	Evaluation of Achieved Performance	II-52

MSC-05546

1. INTRODUCTION

1.1 Purpose

This document reports the final results of the sensor performance evaluation of the Skylab Earth Resources Experiment Package (EREP) and is based on data and evaluations reported in Volume II of the interim performance evaluation reports (MSC-05528, Volume II, dated September 6, 1974).

1.2 Scope

This document summarizes the results of S191 sensor performance evaluation based on data presented by all contributors (Martin Marietta Corporation, the Science and Applications Directorate, and Lockheed Electronics Company of the Lyndon B. Johnson Space Center) to the sensor performance evaluation interim reports, provides the results of additional analyses of S191 performance, and describes techniques used in sensor performance evaluation (Appendix A). The summarization includes significant performance degradation identified during the Skylab missions, S191, and EREP system anomalies that affected S191 performance, and the performance achieved, in terms of pertinent S191 parameters. The additional analyses include final performance analyses completed after submittal of the SL4 interim sensor performance evaluation reports, including completion of detailed analyses of basic performance parameters initiated during the interim report periods and consolidation analyses to reduce independent mission data (SL2, SL3, and SL4) to determine overall performance during all three Skylab missions.

1.3 Usage Guide

The basic task outline for the EREP sensor performance evaluation was specified EREP Mission Data Evaluation Requirements, JSC-05529, August 31, 1973. The results of these evaluations were subsequently reported in MSC-05528, Earth Resources Experiment Package, Sensor Performance Report, Volumes I through VII, as follows:

Volume I (S190A)	Multispectral Photographic Camera
Volume II (S191)	Infrared Spectrometer
Volume III (S192)	Multispectral Scanner
Volume IV (S193 R/S)	Radiometer/Scatterometer
Volume V (S193 Alt.)	Altimeter
Volume VI (S194)	L-Band Radiometer
Volume VII (S190B)	Earth Terrain Camera

MSC-05546

These volumes were issued after prelaunch testing at KSC and updated after each mission. The single exception is Volume VII (S190B), which was originally issued after SL3, with a single update after SL4.

This document is based on the data and analyses in the first six volumes of the sensor performance report, MSC-05528, (Volume VII, S190B, is not included). The same volume designation used for MSC-05528 has been retained for the individual sensor volumes, with the individual volumes bound in a single cover and identified as MSC-05546. The individual volumes are designed to they can be used independently of the full six-volume report, if desired.

1.4 Abstract

An S191 performance summary based on ground testing and orbital operations in terms of pertinent parameters is provided. Additional tasks covering S191 short-wavelength radiometric calibration, data-acquisition camera, and viewfinder tracking system design criteria, radiometric comparison of S190A, S191, and S192, and wavelength calibration data are included as supplemental analyses. Descriptions of techniques employed in the performance analyses are also discussed. Final results of the evaluations in terms of significant performance degradation, sensor and system anomalies, and achieved performance are presented. Conclusions were based on S191 performance and interaction of S191 with the EREP system. Recommendations for additional analyses and improvements in design and operation are presented.

MSC-05546

2. APPLICABLE DOCUMENTS

- MSC-05528 Earth Resources Experiment Package, Sensor Performance Report, Volume II (S191), Engineering Baseline, SL2, SL3, and SL4 Evaluation; Lyndon B. Johnson Space Center, Houston, Texas, September 6, 1974.
- PHO-TR524,
Revision A Earth Resources Production Data Processing Requirements for EREP Electronic Sensors; Lyndon B. Johnson Space Center, Houston, Texas, May 10, 1973.
- MSC-05531 Ground Truth Data for Test Sites (SL2); Lyndon B. Johnson Space Center, Houston, Texas, August 15, 1974.
- MSC-05537 Ground Truth Data for Test Sites (SL3); Lyndon B. Johnson Space Center, Houston, Texas, March 29, 1974.
- MSC-05543 Ground Truth Data for Test Sites (SL4); Lyndon B. Johnson Space Center, Houston, Texas, April 30, 1974.
- MSC-05548 S191 Lunar Calibration Data Reduction Report; Martin Marietta Corporation, Denver, Colorado, September 30, 1974.
- MSC-05545 S191 VTS Spectrometer Component Reflectances and Temperatures; Martin Marietta Corporation, Denver, Colorado, June 7, 1974.
- JSC-05529 EREP Mission Data Evaluation Requirements; Lyndon B. Johnson Space Center, Houston, Texas, August 31, 1973.
- Intricate Alignment and Timing Facts for S191; Juday, R. D.; Lyndon B. Johnson Space Center, Houston, Texas, November 7, 1974.

MSC-05546

3. SUMMARY OF SENSOR PERFORMANCE EVALUATION INTERIM REPORT

After the preflight testing of EREP experiments at Kennedy Space Center and after each Skylab mission, raw data from preflight tests and each mission were reduced to provide performance data for each EREP sensor. These data were presented by mission in interim sensor performance evaluation reports entitled EREP Sensor Performance Report (Engineering Baseline, SL2, SL3, and SL4 Evaluation), MSC-05528, Volumes I through VII. Preflight test data and selected qualification test data composed the engineering baseline, and flight data were added to this baseline after each Skylab mission. This section summarizes Volume II (S191), Change 3, September 6, 1974 of the sensor performance report paragraph by paragraph. However, sections of the interim report that were similar or contained redundant evaluation data have been combined. To provide traceability, applicable interim report sections in the summary are referenced.

3.1 Functional Limit Verification

The sensor performance evaluation of housekeeping parameters, zero radiance levels, and noise equivalent spectral radiances are summarized in this section. Also presented are summaries of data acquisition camera performance, viewfinder/tracking system (VTS) alignment, and calibration corrections. Detailed evaluations of these parameters are discussed in Section 3 of MSC-05528, Volume II, September 6, 1974.

3.1.1 Housekeeping

S191 housekeeping parameters were monitored throughout prelaunch and orbital operations. A list of these parameters and the maximum and minimum values observed during these operations are summarized in Table 3.1-1. The long-wavelength (LWL) detector temperature measurement exceeded the upper specified limits during SL2 due to the cold Skylab wall near the S191. This condition existed only on the SL2 mission. The upper limit was exceeded during the final EREP pass in SL4 when the Malaker cooler failed to properly cool the thermal detector.

VTS door blackbody sensors indicated off-scale lower limit values consistent with exposure to the space environment when the S191 door failed to close during SL3. Once the door was closed at the end of SL4, on-scale readings were again achieved.

Table 3.1-1 Housekeeping-Parameter Performance Summary

No.	PARAMETER Title	LIMITS			NSC		SL2		SL3		SL4	
		Units	Max	Min	Hi	Lo	Hi	Lo	Hi	Lo	Hi	Lo
A012	Devar Pressure #1	µA	60	0	0	0	0	0	0	0	0	0
A013	Heated Calibration Source Temperature (#9)	°C	50	48	--	49	48	49	49	49	49	49
A013	Heated Calibration Source Temperature (#10)	°C	55	52	53	53	--	--	--	--	--	--
A013	Heated Calibration Source Temperature (#7)	°C	42	40	42	41	--	--	--	--	--	--
A014	Ambient Calibration Source Temperature	°C	42.3	0	31	22	10	23	14	21	15	15
A015	Cooler Case Temperature	°C	43.3	15	38	33	20	32	30	30	26	26
A016	Power Supply Diagnostic	V	2.75	2.25	2.5	2.5	2.5	2.5	2.5	2.5	2.5	2.5
A017	Thermal Reference Source Temperature (#9)	°C	42	40	41	41	--	--	--	41	41	41
A017	Thermal Reference Source Temperature (#5)	°C	10	8	10	10	9	9	9	9	--	--
A017	Thermal Reference Source Temperature (#3)	°C	-6	-8	--	--	--	--	--	-7	-8	-8
A017	Thermal Reference Source Temperature (#2)	°C	-14	-16	--	--	--	-15	-15	-15	-15	-15
A018	Package Temperature	°C	42.3	0	36	30	19	31	25	30	25	25
A019	Dichroic Temperature	°C	42.3	0	33	24	13	26	20	25	20	20
A020	EWL Detector Temperature (*)	°K	110	80	85	85	85	85	85	85	85	86
A021	Devar Pressure #2	µA	60	0	3	3	10	0	2	2	0	0
A023	Calibration Lamp Current (†)	A	4.3	3.9	4.2	4.2	4.2	4.2	4.2	4.2	4.2	4.2
D003	Camera Shutter Pulse	V	5.1	4.5	**	**	5	5	5	5	5	5
D004	Target Data Pulse	V	5.1	4.6	4.9	4.9	4.9	4.9	4.9	4.9	4.9	4.9
D005	Radiance Calibration Wheel Position (OPEN)	V	5.1	4.1	4.1	4.1	4.1	4.1	4.1	4.1	4.1	4.1
D005	Radiance Calibration Wheel Position (SML)	V	1	0	0.4	0.4	0.4	0.4	0.4	0.4	0.4	0.4
D005	Radiance Calibration Wheel Position (HOT)	V	3.6	2.6	3.0	3.0	3.0	3.0	3.0	3.0	3.0	3.0
D005	Radiance Calibration Wheel Position (AMB)	V	2	1	1.5	1.5	1.5	1.5	1.5	1.5	1.5	1.5
D006	Wavelength Calibration Wheel Position (OPEN)	V	5.1	4.4	4.8	4.8	4.8	4.8	4.8	4.8	4.8	4.8
D006	Wavelength Calibration Wheel Position (SML)	V	2.7	1.6	**	**	1.8	1.8	1.8	1.8	1.8	1.8
D006	Wavelength Calibration Wheel Position (LML)	V	3.9	2.9	**	**	3.2	3.2	3.2	3.2	3.2	3.2
D007	Zero Volt Reference	mV	15	0	2	2	0	0	0	0	0	0

(*) Values quoted are those during EREP passes
 (**) KSC values were not available
 (†) Lamp "ON" values only
 §§ Out of limits

MSC-05546

Noise was observed in varying magnitudes on all five blackbody sensors. This noise-level variation correlated to data acquisition camera (DAC) and VTS door operation, with the former being the most significant. However, the noise fluctuations did not affect the derivation of true blackbody temperatures. This was verified in prelaunch testing; averaging the fluctuations yielded the proper temperature.

3.1.2 Zero Radiance Level and Noise Equivalent Spectral Radiance (NESR)

S191 zero-radiance values were determined for all detector channels by observing the S191 output voltage when the input radiances were effectively zero for both prelaunch and orbital operations. Results were found to be consistent and are tabulated in Table 3.1.2-1.

Table 3.1.2-1 Zero Radiance-Level Summary

Channel/ Detector	Zero Radiance Levels (V)			
	KSC	SL2	SL3	SL4
A2 PbS/S1 #3	0.026	0.027	0.027	0.027
A3 S1 #1	0.055	0.055	0.056	0.055
A5 S1 #2	0.025	0.025	0.025	0.025
A1 HgCdTe (-)	0.206	0.206	0.206	0.206
A6 HgCdTe (+)	0.200	0.200	0.200	0.200

MSC-05546

Noise equivalent spectral radiance (NESR) is the radiant flux per unit solid angle per unit area (radiance) per unit wavelength interval at a particular wavelength necessary to yield an output signal equal to the detector noise, i.e. produce a signal-to-noise ratio of one. NESR values were derived by determination of the root-mean-square noise, V_n , present on each of the short-wavelength detector channels and dividing this value by the responsivity at a particular wavelength. The values of V_n were derived for the dark condition only, i.e. with the calibration lamp off. Results of the NESR analyses for short wavelengths are in Table 3.1.2-2. Long-wavelength NESRs were not summarized due to considerable inconsistencies in the results. These inconsistencies were due in part to:

- 1) Off-band radiation effects;
- 2) Different responsivity values derived from internal ambient and heated blackbodies as well as deep space data;
- 3) Inaccurate determination of internal component temperatures, such as the dichroic temperature.

3.2 Interference Check

Stripchart data from KSC and SL2 data were examined to determine whether any interference from external sources affected the S191 system. Sync losses were observed on stripcharts from both KSC and SL2, but were attributable to ground data processing. No noise amplitudes in excess of established criteria of greater than twice the pen width (>4% of full scale) were found.

Some false resets on the filter position ramps were observed on the SL2 data. These were assumed to be related to the low temperature of the Skylab wall near the S191. This cold-wall situation existed up through day of the year (DOY) 156. A few false resets were experienced after DOY 156, but correlation with other sources of potential interference was not indicated. These evaluations were discussed in MSC-05528, Volume II, September 6, 1974, Section 4.

3.3 Wavelength Calibration Check

Evaluation of S191 wavelength calibration indicated that the instrument's calibration did not change during the Skylab

Table 3.1.2-2 Noise-Equivalent Spectral Radiance Summary (SML)

Channel/ Detector	Wavelength (μm)	KSC			SL2			SL3			SL4		
		V_n (mV)	R_A (*)	NEQR (**)	V_n (mV)	R_A (*)	NEQR (**)	V_n (mV)	R_A (*)	NEQR (**)	V_n (mV)	R_A (*)	NEQR (**)
A2 (PbS/Sl #3)	0.4	13.15	No Data	---	7.70	0.432	17,824	7.50	0.403	16,610	7.90	0.920	8,587
	0.5	11.40	---	2591(†)	---	6.205	1,241	---	3.371	2,225	---	4.310	1,833
	0.6	---	---	---	11.32	11.32	680	---	6.271	1,208	---	7.034	1,123
	0.7	10.55	---	910(†)	16.5	16.5	467	---	9.032	879	---	11.6	683
	0.7	6.75	---	614(†)	17.0	17.0	453	---	9.477	862	---	11.0	719
	0.8	---	---	---	19.6	19.6	393	---	10.3	735	---	12.0	658
	1.0	---	No Data	---	71.6	71.6	108	---	30.8	244	---	36.6	216
A3 (Sl #1)	1.3	8.80	111.8	79	7.70	453	17	7.50	183	41.0	7.90	361	21.9
	0.4	7.50	176	43	5.45	35.6	153	5.15	30.2	171	6.00	31.4	191
	0.5	5.70	446	13	---	Saturated	Saturated	---	341	15.1	---	Saturated	18.3
	0.6	---	678	---	---	---	---	---	Saturated	Saturated	---	Saturated	Saturated
	0.7	5.10	Saturated	4(†)	---	---	---	---	---	---	---	---	---
	0.7	5.05	---	5(†)	---	---	---	---	---	---	---	---	---
	0.8	---	Saturated	---	---	---	---	---	---	---	---	---	---
A5 (Sl #2)	1.0	---	208	---	---	454	12	---	207	25.2	---	244	24.6
	1.3	NA	NA	NA	NA	NA	NA	NA	NA	NA	NA	NA	NA
	0.4	0.90	No Data	51(†)	0	3.892	0	0	3.091	0	0	3.374	0
	0.5	0	44.0	0	---	57.2	---	---	34.3	---	---	33.0	---
	0.6	---	67.7	---	100	100	---	---	55.3	---	---	63.3	---
	0.7	0	116	0	153	153	---	---	83.6	---	---	105	---
	0.7	0	110	0	147	147	---	---	83.2	---	---	99.4	---
0.8	---	108	---	180	180	---	---	91.2	---	---	103	---	
1.0	---	20.2	---	45.0	45.0	---	---	20.6	---	---	24.1	---	
1.3	NA	NA	NA	NA	NA	0	0	NA	0	0	NA	0	

(*) $V/W/\text{cm}^2\text{-}\mu\text{m-ster}$

(**) $\mu\text{W}/\text{cm}^2\text{-}\mu\text{m-ster}$

(†) values derived indirectly from gain relationships

MSC-05528

missions. This evaluation was based on data from a minimum of three auto cal periods from each mission. The results of these evaluations are summarized in Table 3.3-1, together with vendor data for comparison.

Table 3.3-1 Wavelength Calibration

FILTER SEGMENT	WAVELENGTH (μm)	BLOCK'S CAL TEST REPORT	FINAL KSC PRELAUNCH TEST	SL2	SL3	SL4
		V_{fc}	V_{fc}	V_{fc}	V_{fc}	V_{fc}
NUMBER 1 (0.39 - 0.73 μm)	0.497	---	---	---	2.848	2.843
	0.525	---	2.943	2.942	2.942	2.939
	0.580	---	3.137	3.137	3.136	3.135
NUMBER 2 (0.68 - 1.4 μm)	0.744	3.82	3.810	3.810	3.808	3.809
	0.805	3.90	3.893	3.894	3.893	3.892
	0.876	4.00	4.005	4.002	4.005	4.004
	1.215	4.50	4.528	4.529	4.531	4.531
NUMBER 3 (1.34 - 2.51 μm)	1.503	0.40	0.411	0.409	0.403	0.401
	1.69	0.73	---	---	---	---
	1.74	---	0.847	0.847	0.847	0.849
	1.910	1.16	1.168	1.170	1.164	1.163
NUMBER 4 (5.82 - 11.4 μm)	6.238	2.91	2.938	2.942	2.945	2.943
	8.467	3.78	3.811	3.806	3.803	3.806
	9.345	---	4.160	4.161	4.165	4.169
	9.724	4.29	4.324	4.317	4.327	4.332
NUMBER 5 (8.3 - 15.99 μm)	8.467	0.36	0.366	0.353	0.359	0.353
	9.724	0.76	0.775	0.775	0.766	0.770
	11.035	1.13	1.154	1.143	1.141	1.143
	11.876	1.37	1.378	1.388	1.388	1.390
	13.83	---	1.946	1.949	1.950	1.946

ORIGINAL PAGE IS
OF POOR QUALITY

MSC-05546

Graphs of values tabulated in Table 3.3-1 originally presented in MSC-05528, Volume II, September 6, 1974, Section 5, were approximated by a straight-line fit. Subsequent analyses have indicated that most of the filter-wheel segments did not provide a straight-line variation of ramp voltage with wavelength, but were better approximated by second-order polynomial equations. A discussion of these new wavelength calibration equations and other supplemental calibration information is given in paragraph 4.4.

3.4 Photographic Image Adequacy for Site Location

The purpose of the data acquisition camera was to indicate the location of the S191 spectrometer's field of view. Light-emitting diode displays along the edge of the scene gave the time and pointing angles with reference to the spacecraft axes. The resolution and exposure of the imagery, and the camera's mechanical performance, were described by mission in MSC-05528, Volume II, September 6, 1974, Sections 3 and 6. Ground target lists were produced that provide times and locations for S191 spectra and data acquisition camera imagery.

3.4.1 Exposure Setting

For SL2 and most of the prelaunch tests, Eastman Kodak 3401 black-and-white film was used. The optimum exposure setting was selected from prelaunch testing. Unfortunately, the combination of improper shutter speed and forced development resulted in overexposure of the SL2 flight imagery. Although most of the ground targets were still identifiable, the required high-contrast reproduction greatly increased duplicate film granularity and resulted in poor imagery. Due to an extremely short shutter setting (1/500 or 1/1000 sec) inadvertently left on the camera after another use, the pass 11 imagery was badly underexposed.

For SL3 and SL4, Eastman Kodak SO-168 and SO-368 color film were used and a new shutter speed was selected. After viewing the SL2 imagery, it was decided that the added dimension in color film would help identify targets and that the proper exposure setting was now known so that the lower dynamic range of color film would not be a problem. The results of using color film and proper exposure were excellent, and the imagery was of good quality. However, some difficulty was encountered in recognizing targets that were shaded by clouds.

One magazine (C1-90) exhibited noticeably poorer image quality during SL4. The magazine was filled with SO-368 film; the optimum emulsion was SO-168, but all four magazines of the latter were exhausted toward the end of the mission. The SO-368 was used as a

MSC-05546

3.4.2 Data Acquisition Camera/Viewfinder Tracking System Resolution

Prelaunch testing indicated that system ground resolution with 3401 black-and-white film would be about 350 feet for high-contrast targets and 500 feet for low-contrast. The resolved ground distance for SL2 was about 300 feet for very high-contrast targets (land-sea interface), and moderate-contrast targets gave resolutions of about 1000 feet with the poorly exposed 3401 film. For SL3 and SL4, using SO-168 color film, the very high-contrast land-sea interfaces gave ground resolutions of approximately 200 feet, while other high-contrast targets gave resolutions of approximately 300 feet. Areas of medium to low contrast varied from 450- to 750-foot resolution, with most agricultural scenes near the 750-foot value.

3.4.3 Crosshair Visibility

The SL3 and SL4 crosshair visibility was generally good, except for deep space where the crosshairs were not visible. In a few cases on the poorly exposed SL2 imagery, the crosshairs were difficult to see. This also occurred in lunar imagery and for very bright objects such as clouds and deserts. For frames in which the crosshairs could not be seen, lines were drawn on the projection screen (from adjacent scenes when the crosshairs were visible) to establish the location of the field of view. This method of determining field of view when the crosshairs were not visible assumed that the crosshair position did not change during sequential projection. The accuracy of the assumption was verified on frames in which the crosshairs were visible.

3.4.4 Light-Emitting Diode Visibility

The light-emitting diode display images were also included on data acquisition camera imagery. These displays indicated time and pointing direction relative to spacecraft coordinates. For SL2, the displays were visible (in some cases very faint) for all passes except for day of year 165. On this day, the displays were not visible at all during either the lunar or terrestrial passes. For SL3 and SL4, the displays were clearly visible on all imagery.

3.4.5 Data Acquisition Camera Mechanical Performance

This evaluation was performed by microscopic examination of random frames from a second generation positive. The SL2, SL3, and SL4 films indicated excellent mechanical operation of

MSC-05546

the data acquisition camera, with only a few incidences of streaking, scratches, light leaks, and emulsion digs. Most of these features were along the edge of the film outside the primary image and did not hamper the camera's primary purpose of target identification and S191 pointing. However, some light leaks during SL4 caused the imagery to be seriously washed out.

In certain instances, the data acquisition camera was improperly installed on the VTS mount. The resulting imagery was rotated by $\pm 90^\circ$, depending on each particular occurrence. While these occurrences proved an annoyance during evaluation, they did not affect image quality. During several SL4 film advance periods, two of the light-emitting diode displays failed to light for a brief period. These anomalies were apparently associated with particular VTS functions because they were only observed during several film advance periods. The cause could not be determined from the available data.

One additional anomaly occurred during SL2 that was not included in the interim report. This was an interface problem between the data acquisition camera and viewfinder tracking system that had occurred during ground testing. The crew reported that the data acquisition camera continued to run after the camera control switch on the viewfinder tracking system control panel was placed in the OFF position. The crewman reseated the data acquisition camera magazine, and the problem was eliminated.

3.5 Determination of Boresight Error and Spectrometer Field of View

The boresight errors at maximum zoom and during zoom, and the spectrometer field of view are summarized in this section. These analyses are described in detail in Sections 3, 6, and 7 of MSC-05528, Volume II, September 6, 1974.

3.5.1 Determination of Boresight Error during Zoom

The position of the spectrometer field of view relative to crosshair position on the data acquisition camera film during zoom was investigated on SL2. This evaluation was not made for the other missions. Evaluation results were normalized to give zero difference at maximum zoom. (The boresight error at maximum zoom is given in paragraph 3.5.2 in this report.) At minimum versus maximum zoom, the spectrometer field of view changed

MSC-05546

positions relative to the imagery crosshairs by about 150 milliradians (which corresponds to ~60 kilometers on the ground) in both forward-aft and left-right axes. Therefore, corrections were necessary for data taken at less than maximum zoom. Data for making these corrections are given in Section 6.2.5.1.1 of MSC-05528, Volume II, September 6, 1974.

3.5.2 Determination of Boresight Error at Maximum Zoom

The maximum-zoom alignment error between the crosshair position and the spectrometer's actual field of view was determined from lunar data takes on each mission. This determination was made by comparing the distance between the time when the crosshairs reached the moon's limb and when the spectrometer field of view was half on and half off the limb. Knowledge of this time difference, the rate of drift of the crosshairs across the limb, and the fact that the moon's disk subtends 9 milliradians when viewed from earth (or Skylab), led to determination of alignment error. The results of this determination in both axes are summarized in Table 3.5.2-1.

Table 3.5.2-1 Crosshair Position Relative to S191 Field of View (FOV)

MISSION	CROSSHAIR ALIGNMENT ERROR RELATIVE TO DETECTOR FOV (mrad)	
	Forward-Aft Axis	Left-Right Axis
SL2	0.1 Forward*	No Data
SL3	0.1 Forward*	0.55 Left*
	0.34 Forward†	0.62 Left†
SL4	0.09 Forward†	0.39 Left†

* Values measured by JSC/S&AD

† Values measured by Martin Marietta Corporation

MSC-05546

As indicated by this table, different values of crosshair alignment were obtained independently by two S191 sensor performance evaluation teams. The SL3 forward-aft results were rechecked by both teams, but the difference still remained. Different data periods and slightly different evaluation methods were used. It was concluded that these measurements had an error of ± 0.1 milliradian and that the two measurements were at either end of the value range.

The SL4 results were determined from 45° and 135° scans (measured clockwise from the forward axis) instead of forward-aft and left-right scans off the lunar limb. A resultant vector plot was made and the forward-aft and left-right components of this resultant were taken from the plot. The results are given in Table 3.5.2-1. These errors must be added to any zoom errors described in Section 3.5.1. These measurements were made at small values of the displayed forward angle. The boresighting between the spectrometer and the crosshairs as a function of forward angle is described in the report referenced on page II-49.

3.5.3 In-Flight Alignment Verification

For SL2, no changes in alignment were made by the astronauts after the original checkout. In SL3, a realignment of the crosshairs was made by the astronauts, but the change was less than 0.1 milliradian. No alignment changes were made for SL4, but the alignment was checked with the door closed so that the alignment procedure check could be made. The astronauts estimated that the crosshairs were 0.2 milliradian forward and 0.4 milliradian to the left of the spectrometer field of view. This was in excellent agreement with the SL4 results given in Table 3.5.2-1.

3.5.4 Field of View and Off-Axis Rejection

Measurements of the S191 field of view were made both before launch and in orbit, using two different methods. At the time of initial mating of the viewfinder tracking system with the spectrometer, a special task was performed using a 0.09-milliradian mask. The mask was placed in the collimator focal plane and moved in a raster scan in 0.1-milliradian increments in two axes while the short-wavelength output of the highest-gain silicon channel was monitored. Results of this test are summarized in Figure 3.5.4-1. No measurements were made in the long-wavelength channels. The field-of-view values given in Table 3.5.4-1 are for the 50% points on Figure 3.5.4-1.

ORIGINAL PAGE IS
OF POOR QUALITY

MSC-05546

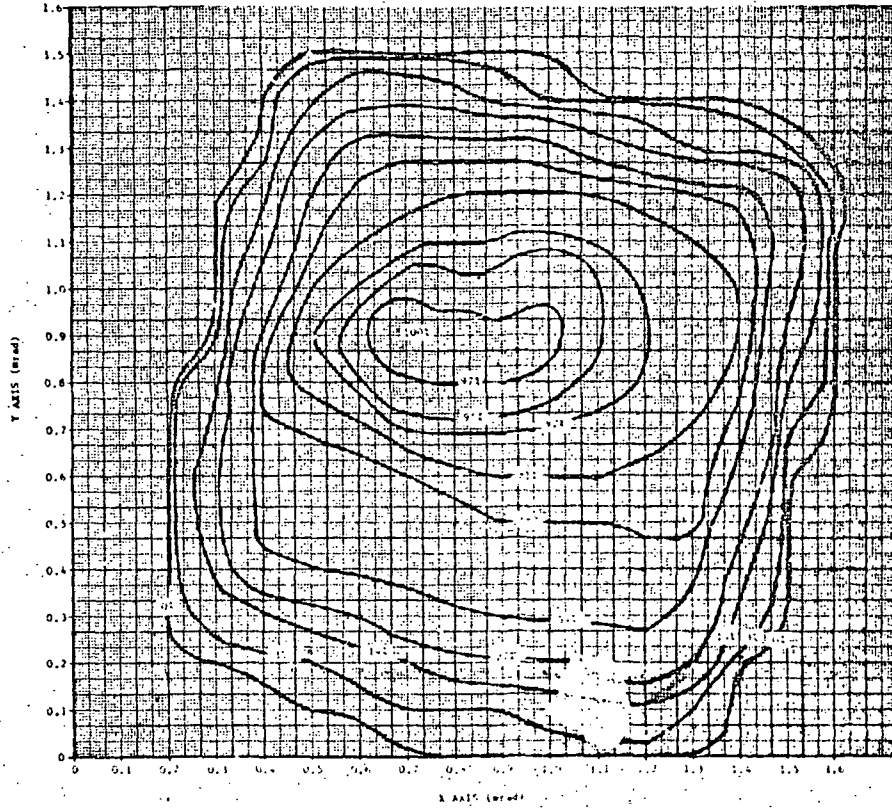


Figure 3.5.4-1 SWL Off-Axis Rejection

Table 3.5.4-1 Field-of-View Determination Summary

WAVELENGTH (μm)	PRELAUNCH		SL3		SL4 (mrad)
	Forward-Aft Axis (mrad)	Left-Right Axis (mrad)	Forward-Aft Axis (mrad)	Left-Right Axis (mrad)	
0.5	---	---	1.39	1.01	1.38
0.63	1.01	1.05	---	---	---
0.8	---	---	1.48	1.36	1.44
2.0	---	---	1.45	1.25	1.22
8.0	---	---	1.95	1.56	1.08
13.0	---	---	1.72	1.15	1.38

MSC-05546

Scans were made across the edge of the moon during lunar calibration passes to determine the field of view. No analysis was made during SL2 due to the lack of the light-emitting diode displays. The SL3 analysis provided data from both right-left and forward-aft axes. Because the scan off the moon was made at $45^{\circ}/135^{\circ}$ during SL4, there was a 35° long-wavelength and 36° short-wavelength angle between the field-of-view edge and the lunar edge. Nevertheless, this evaluation was performed in the same manner as for SL3 to see if any large change had occurred. The determination was made in only one direction because the other scan would have given the same results. (See Section 7.4.8, MSC-05528, Volume II, for detailed explanation.) The field-of-view values obtained in these analyses are summarized in Table 3.5.4-1. The on-orbit values are about 30% greater than the prelaunch values. This difference may be attributable to the few data points available for on-orbit values. The long wavelengths at 8 and 13 micrometers seem to exhibit a field of view that is larger than expected.

Off-axis rejection was not measured on orbit because very few data points were available to define this parameter. Nevertheless, from the data available, it appears that the good off-axis rejection exhibited in Figure 3.5.4-1 was present on orbit.

3.6 System Spectroradiometric Response Determination

Results of the various analyses leading to determination of the spectroradiometric response of the S191 system are summarized in this section. These analyses were described in detail in Section 7 of MSC-05528, Volume II, September 6, 1974.

3.6.1 Short-Wavelength Radiometric Calibration and Dynamic Range

Short-wavelength responsivities and dynamic ranges were determined for prelaunch and orbital operations and are summarized in Table 3.6.1-1. Responsivity values were derived by dividing the detector output voltage (less bias offset) by the target radiance. Dynamic range values were derived by dividing the maximum detector output voltage (~ 5.117 V) by the responsivity.

The significant differences between the KSC, SL2, SL3, and SL4 responsivities are due to difficulties in calculating the responsivities for the KSC results and the presence of clouds near the Willcox Playa ground truth site during SL2. SL3 and

MSC-05546

SL4 results agree well and should be taken as the valid responsivities, except for the lowest-gain (S1 #3) silicon channel, which is adversely affected by a very low signal level.

Table 3.6.1-1 SWL Responsivity and Dynamic Range Summary

Channel/ Detector	Wavelength (μm)	KSC		SL2		SL3		SL4		
		Responsivity (*)	Dynamic Range (**)	Responsivity (*)	Dynamic Range (**)	Responsivity (*)	Dynamic Range (**)	Responsivity (*)	Dynamic Range (**)	
A2 (PbS/S1 #3)	0.4	No Data	No Data	0.432	11.8	0.403	12.697	0.920	5.562	
	0.5	↑	↑	6.205	0.825	3.371	1.518	4.310	1.187	
	0.6			11.32	0.453	6.271	0.816	7.034	0.727	
	0.7	↓	↓	16.5	0.310	9.082	0.563	11.6	0.441	
	0.7			17.0	0.301	9.477	0.540	11.0	0.463	
	0.8	No Data	No Data	19.6	0.261	10.3	0.497	12.0	0.426	
	1.0			71.6	0.071	30.8	0.164	36.6	0.140	
	1.3			112	0.046	453	0.011	183	0.028	361
A3 (S1 #1)	0.4	176	0.079	35.6	0.144	30.2	0.169	31.4	0.163	
	0.5	446	0.011	Saturated	Saturated	361	0.015	328	0.016	
	0.6	678	0.008	↑	↑	Saturated	Saturated	Saturated	Saturated	
	0.7	Saturated	Saturated			Saturated	Saturated	Saturated	Saturated	Saturated
	0.7	Saturated	Saturated	Saturated	Saturated	Saturated	Saturated	Saturated	Saturated	
	0.8			Saturated	Saturated	Saturated	Saturated	Saturated	Saturated	Saturated
	1.0			208	0.025	454	0.011	207	0.025	244
	1.3	NA	NA	NA	NA	NA	NA	NA	NA	
A5 (S1 #2)	0.4	No Data	No Data	3.892	1.315	3.091	1.655	3.374	1.517	
	0.5	44.0	0.116	57.2	0.089	34.3	0.149	33.0	0.155	
	0.6	67.7	0.076	100	0.051	55.3	0.093	63.3	0.081	
	0.7	116	0.044	153	0.033	83.6	0.061	105	0.049	
	0.7	110	0.046	147	0.035	83.2	0.062	99.4	0.051	
	0.8	108	0.047	180	0.028	91.2	0.056	103	0.050	
	1.0	20.2	0.253	45.0	0.114	20.6	0.249	24.1	0.212	
	1.3	NA	NA	NA	NA	NA	NA	NA	NA	

(*) $\text{V}/\text{V}/\text{cm}^2\text{-}\mu\text{m-ster}$
 (**) $\text{W}/\text{cm}^2\text{-}\mu\text{m-ster}$

ORIGINAL PAGE IS
 OF POOR QUALITY

MSC-05546

Another method of calibration using the moon and the S191 backup unit in conjunction with on-module calibrator data was used to check the accuracy of the preflight KSC calibration. The technique used in the lunar calibration is described in Appendix A, Section III of this volume. The results of the investigation were put into the form of a correction table -- factors by which to multiply the production processed S191 short wavelength data, given as a function of wavelength. The table has been published SKYLAB INSTRUMENTATION CALIBRATION DATA, VOLUME IV, as Table 3.7.13.1 in change 3. It is also included here as Table 3.6.1-2. The results of the instrument calibration are further described in paragraph 4.1.

TABLE 3.6.1-2

$\lambda(\mu)$	CF(A3&A5)	$\lambda(\mu)$	CF(A3&A5)	CF(A2)	$\lambda(\mu)$	CF(A2)
0.400	3.98	0.72	0.920		1.38	1
0.405	3.25	0.73	0.929		1.40	1
0.410	2.21	0.74	0.938		1.44	1
0.415	1.63	0.75	0.946		1.48	1
0.420	1.37	0.76	0.955		1.50	1.021
0.425	1.34	0.77	0.973		1.52	1
0.430	1.45	0.78	0.982		1.54	1.008
0.435	1.39	0.79	0.991		1.56	1.025
0.440	1.24	0.80	0.991		1.58	1.042
0.445	1.107	0.81	0.982		1.60	1.042
0.45	1.067	0.82	0.973		1.62	1.047
0.46	1.047	0.83	0.964		1.64	1.042
0.47	1.057	0.84	0.973		1.66	1.021
0.48	1	0.85	0.982		1.68	1
0.49	1.057	0.86	0.991		1.70	0.979
0.50	1.067	0.88	1		1.72	0.967
0.51	1.028	0.90	1		1.74	0.971
0.52	1	0.92	1		1.76	0.996
0.53	0.964	0.94	1		1.78	1
0.54	0.938	0.96	1		1.80	1
0.55	0.895	0.98	1		1.84	0.996
0.56	0.895	1.00	1	4.00x10 ⁸	1.88	0.928
0.57	0.912	1.02	1	2.60x10 ⁸	1.92	0.971
0.58	0.895	1.04	1	2.00x10 ⁸	1.96	1.008
0.59	0.887	1.06	1	1.67x10 ⁸	2.00	1
0.60	0.879	1.08	1	1.49x10 ⁸	2.04	1
0.61	0.863	1.10	1	1.32x10 ⁸	2.08	1
0.62	0.871	1.12		1.018	2.12	1
0.63	0.871	1.14		1	2.16	1
0.64	0.887	1.16		0.982	2.20	0.898
0.65	0.887	1.18		0.965	2.24	0.883
0.66	0.895	1.20		1.012	2.28	0.932
0.67	0.912	1.22		1.018	2.32	0.890
0.68	0.912	1.24		1.018	2.36	0.872
0.69	0.887	1.26		1.012	2.40	0.812
0.70	0.871	1.28		0.965	2.44	0.857
0.71	0.904	1.30		0.965	2.48	1.056
		1.32		0.965		
		1.34		0.970		
		1.36		0.959		

NOTE: CF = Correction Factor
A2, A3, A5 = Scientific data channels

MSC-05546

3.6.2 Long-Wavelength Radiometric Calibration and Dynamic Range

Long-wavelength responsivities and dynamic ranges determined for prelaunch and orbital operations are summarized in Table 3.6.2-1. Responsivity values were derived by dividing the detector output voltage (less bias offset) by the radiance difference calculated using the equations used in the production data processing system.* However, there were some sizeable responsivity differences between deep space, external blackbody, and ambient/heated auto cal responsivities. These differences were assumed to be due to the combined effects of:

- 1) Not knowing the actual surface temperature of the dichroic;
- 2) Not knowing the temperatures of the viewfinder tracking system mirrors;
- 3) Off-band radiation discussed in Section 3.6.4.

The ambient and heated blackbody responsivities were also somewhat different, but the two values were averaged for the summary Table 3.6.2-1.

3.6.3 Contamination

Mare Serenitatis was used as the lunar target for the contamination analyses during all orbital missions. SL2 and SL3 data comparisons were made looking for evidence of water vapor at 1.9 micrometers and 6.3 micrometers and carbon dioxide at 2.0 micrometers and 15.0 micrometers. Because similar spectral shapes were obtained from SL2 and SL3, no evidence of these contaminants was found. Similar comparisons of SL4 data against the SL2 and SL3 analyses indicated some variations in spectral shapes in the short-wavelength region, but no conclusive evidence identifying water vapor and carbon dioxide contaminants was found. In the long-wavelength region between 8 and 10 micrometers, some large variations in spectral shape were observed from mission to mission. Some correlation between these spectra and those of Coolanol-15 and S13G paint was seen. Both constituents were known to be in the atmosphere surrounding the spacecraft.

* Earth Resources Production Data Processing Requirements for EREP Electronic Sensors, PHO-TR524 Rev. A, NASA/JSC, 10 May 1973.

MSC-05546

Table 3.6.2-1 LWL Responsivity and Dynamic Range Summary

WAVELENGTH (nm)	KSC		SL2		Deep Space		SL3		SL4	
	Ambient/Heated Responsivity (s)	Dynamic Range (db)	External Blackbody (Mean) Responsivity (s)	Dynamic Range (db)	Ambient/Heated Responsivity (s)	Dynamic Range (db)	External Blackbody (Mean) Responsivity (s)	Dynamic Range (db)	Ambient/Heated Responsivity (s)	Dynamic Range (db)
6.0	1034	4.95	1265	4.05	1103	1280	4.00	925	5.53	No Data
6.26	No Data	No Data	No Data	No Data	No Data	1285	3.98	870	5.68	No Data
8.00	2062	2.46	2223	2.30	2026	1955	2.62	2045	2.50	No Data
8.41	No Data	No Data	No Data	No Data	No Data	2135	2.40	2345	2.18	No Data
10.00	2654	1.93	2862	1.79	2724	2605	1.96	2990	1.71	No Data
10.50	No Data	No Data	No Data	No Data	No Data	2810	1.82	3090	1.66	No Data
10.00	2968	1.71	3241	1.58	3069	2915	1.76	3450	1.48	No Data
10.50	No Data	No Data	No Data	No Data	No Data	3085	1.66	3495	1.46	No Data
11.00	No Data	No Data	No Data	No Data	No Data	No Data	No Data	No Data	No Data	No Data
11.20	No Data	No Data	No Data	No Data	No Data	4175	1.23	5030	1.02	No Data
11.5	No Data	No Data	No Data	No Data	No Data	No Data	No Data	No Data	No Data	No Data
12.05	No Data	No Data	No Data	No Data	No Data	3850	1.33	4710	1.09	No Data
12.5	No Data	No Data	No Data	No Data	No Data	No Data	No Data	No Data	No Data	No Data
13.0	3077	1.66	3620	1.41	3294	3520	1.45	3975	1.29	No Data
13.5	No Data	No Data	No Data	No Data	No Data	No Data	No Data	No Data	No Data	No Data
14.05	No Data	No Data	No Data	No Data	No Data	4040	1.27	5350	0.96	No Data
14.5	No Data	No Data	No Data	No Data	No Data	No Data	No Data	No Data	No Data	No Data
15.0	3848	1.33	5043	1.01	4883	4925	1.04	5375	0.93	No Data

(s) V/W/cm²-micrometer
(db) cal/cm²-micrometer

ORIGINAL PAGE IS
OF POOR QUALITY

3.6.4 Off-Band Radiation

The presence of off-band radiation (energy at wavelengths other than in the designed spectral bandpass that passes through the instrument to the detector) was the greatest anomaly found in the S191. This unwanted radiation was high at wavelengths at which the instrument's responsivity or target radiance was low. The wavelength regions affected were 0.4 to 0.5, 1.0 to 1.1, 2.0 to 2.5, 6.0 to 8.0 micrometers, and above 14 micrometers.

The circular variable interference filter in the S191 spectrometer was primarily responsible for the off-band leakage. The off-band component leakage of the filter was determined by the manufacturer to be only 0.01%, but when this leakage was integrated over a large spectral interval, the resultant energy falling on the detector was significant. Corrections for this effect are discussed in MSC-05528, Volume II, September 6, 1974, Section 7.4.2.1.3. Because the target's spectral shape must be known to make the correction, an iterative technique must be used. Inaccuracies in the knowledge of some parameters (notably the circular variable filter transmission) has precluded some studies. The problem is roughly that of obtaining the transmission of off-band wavelengths (about 0.0001) to an accuracy of 5% by measuring a non-flight-unit filter and then assuming that the flight filter has the same characteristics. Doing this in an absolute sense is not reasonable, but individual principal investigators may well be able to juggle the parameters within the framework of the algorithms mentioned above to obtain off-band corrected radiances.

3.6.5 Drift and Indeterminacy in S191 Outputs

Two additional anomalies were uncovered during the sensor performance evaluation:

- 1) Output drift was found between data-take periods. Initial attempts to use one set of responsivities for all passes in one mission, therefore, led to appreciable errors. In addition, short-term drifts during each data take were found, so that both the prepass and postpass auto cal should be used for the most accurate calibrations. The relative short-term drift was attributed to electronic gain changes. The short-term drift in both the long wavelengths and short wavelengths was 3% over a 20-minute period of a data take. The error of using a single set of responsivities for all passes in one mission and not generating a new responsivity from each prepass auto cal was about 12% peak-to-peak for all wavelengths.

MSC-05546

2) The second anomaly was indeterminacy in certain housekeeping parameters used in radiometric calibration of the spectrometer. These parameters were auto cal lamp radiance repeatability, external mirror temperatures, and actual temperature and reflectivity of the dichroic surface. The auto cal lamp seemed to have a large radiance decrease between initial testing and on-orbit operation. The external viewfinder tracking system mirrors did not have temperature sensors. Thermal modeling was performed, which resulted in reasonable temperatures, but some indeterminacy still remained. The dichroic temperature sensor was 3.8 centimeters (1.5 inches) from the surface and the dichroic material was not a good thermal conductor.

The dichroic reflectivity is such a key quantity for absolute radiometric calculations that this reflectivity should have been measured much more carefully. Because of all these unknowns, indeterminacy still exists. Absolute radiometric calibrations have been performed in the short wavelengths via the lunar calibrations discussed in Section 4.1 and Appendix A, Section III. For long wavelengths, radiometric calibrations were highly dependent on off-band radiation, and the best calibration target was deep space.

MSC-05546

4. SUPPLEMENTARY ANALYSES

This section presents the results of analyses completed after the submittal of the interim report, MSC-05528, Volume II, September 6, 1974. These analyses address performance trends over the operational life of the Skylab EREP system and specific problems and inconsistencies observed in the S191 performance data.

4.1 Short-Wavelength Radiometric Calibration

Short-wavelength responsivities derived from prelaunch and orbital operations were found to be inconsistent, due principally to uncertainties in truth-site atmospheric corrections. An alternative method, using designated lunar maria (Serenitatis, Tranquillitatis, and Imbrium) as radiance sources for the S191 flight instrument and an identical ground based instrument, is described in Appendix A, Section III, of this volume. Flight instrument responsivities were derived from lunar maria radiances, and plots of responsivity versus wavelength for the three short-wavelength channels are shown in Figure 4.1-1. Each data point in the figure represents a mean value of six measurements taken from available data extending over all three missions. Tranquillitatis was examined during SL2, SL3, and SL4; Serenitatis during SL2 and SL4; and Imbrium only during SL4. Error bars on the figures indicate the 70% confidence intervals, using small-sample statistics.* Mean values of responsivity versus wavelength for all three short-wavelength detector channels are in Table 4.1-1.

* P. G. Hoel: Introduction to Mathematical Statistics, 2nd ed., New York: Wiley, 1954, paragraph 11.5.1.

MSC-05546

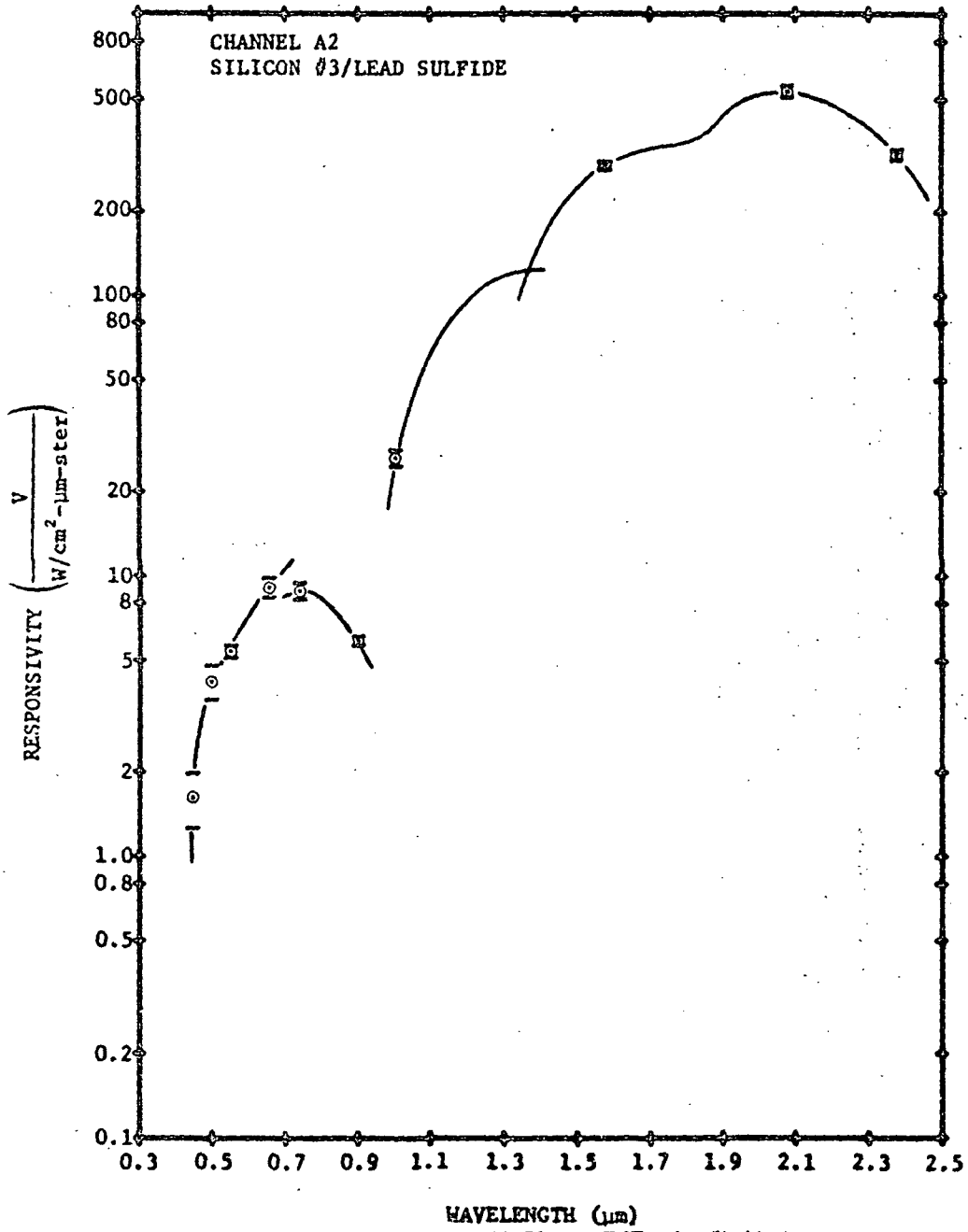


Figure 4.1-1 S191 Responsivities Derived from Lunar Calibration Data

MSC-05546

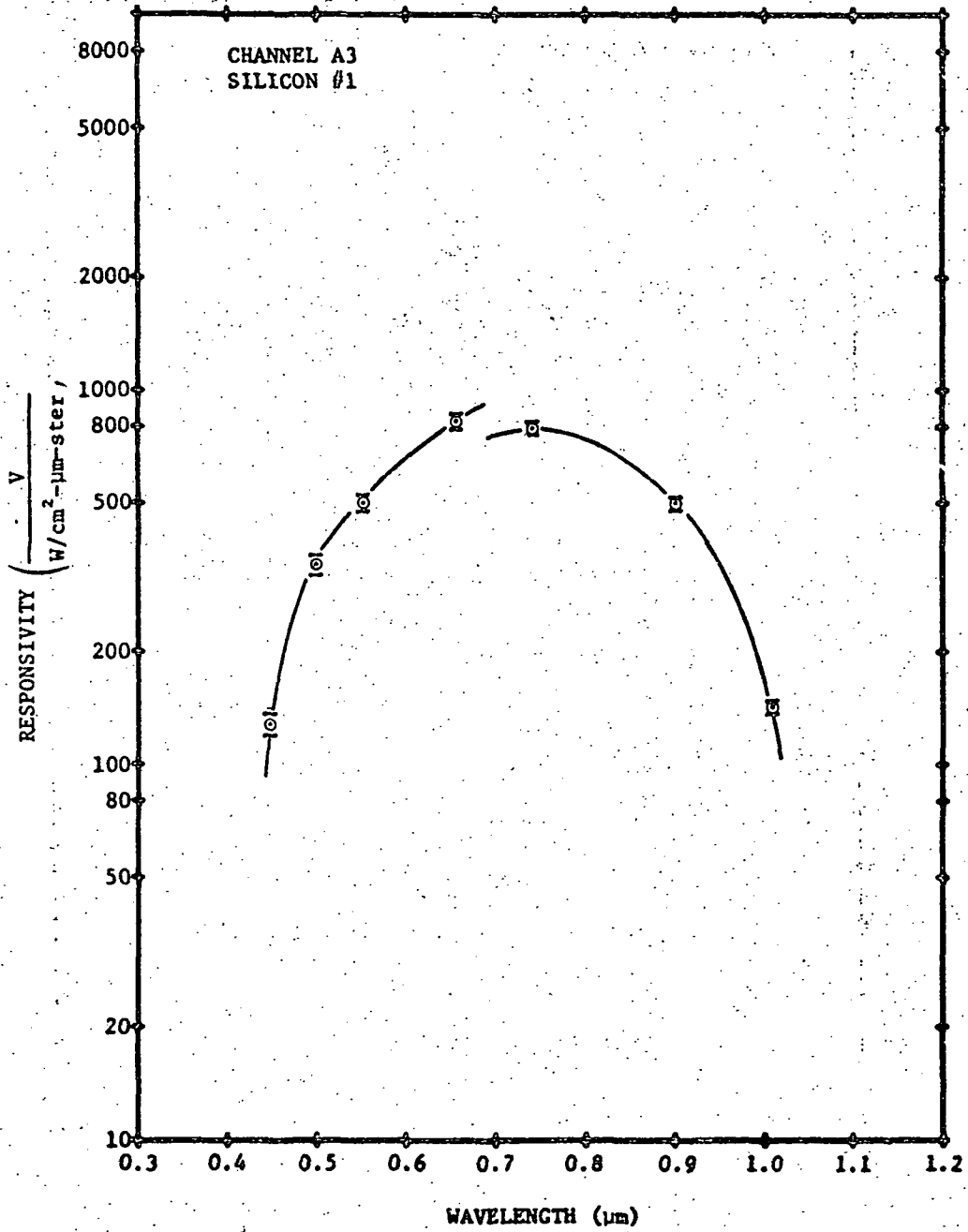


Figure 4.1-1 (continued)

MSC-05546

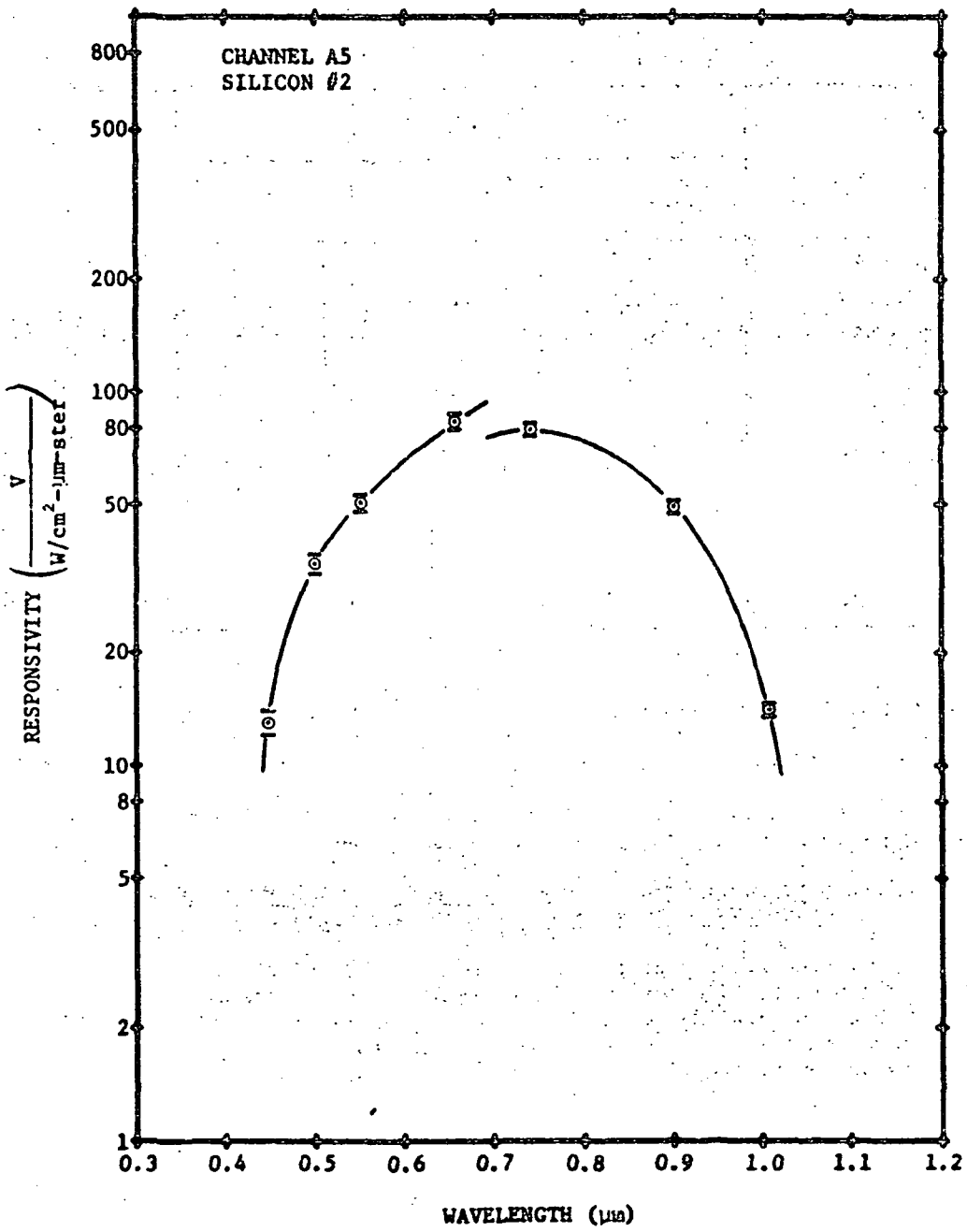


Figure 4.1-1 (concluded)

Table 4.1-1 Short-Wavelength Responsivities
Derived from Lunar Calibration Data

WAVELENGTH (μm)	RESPONSIVITY $\left(\frac{V}{W/\text{cm}^2-\mu\text{m-ster}}\right)$		
	CHANNEL A2 Si #3/Pbs	CHANNEL A3 Si #1	CHANNEL A5 Si #2
0.448	1.61	128	13.0
0.500	4.18	343	34.7
0.552	5.35	501	50.4
0.657	9.06	830	83.3
0.741	8.80	794	79.3
0.901	5.86	500	49.3
1.008	26.3	143	14.1
1.578	291.	N/A	N/A
2.078	533.	N/A	N/A
2.379	318.	N/A	N/A

Responsivity values calculated from ground truth data for SL2, SL3, and SL4 were compared to values derived from lunar calibration. The results are shown for channels A2 and A3 in Figure 4.1-2. The silicon #1 detector (channel A3) was saturated for all ground truth data in the wavelength region of interest. SL3 responsivity values appeared to agree more closely with the lunar calibration values. SL3 and SL4 values were found to be more accurate because of improved ground site conditions.

4.2 Data Acquisition Camera (DAC) and Viewfinder Tracking System (VTS) Interface Design Considerations

S191 evaluation reported in Section 3 of MSC-05528, Volume II, September 6, 1974 resulted in a number of recommendations that should be considered in the design of future instruments. These recommendations are presented to facilitate the analysis and reduction of experiment data, most of which depends on DAC film as the basis for data interpretation.

MSC-05546

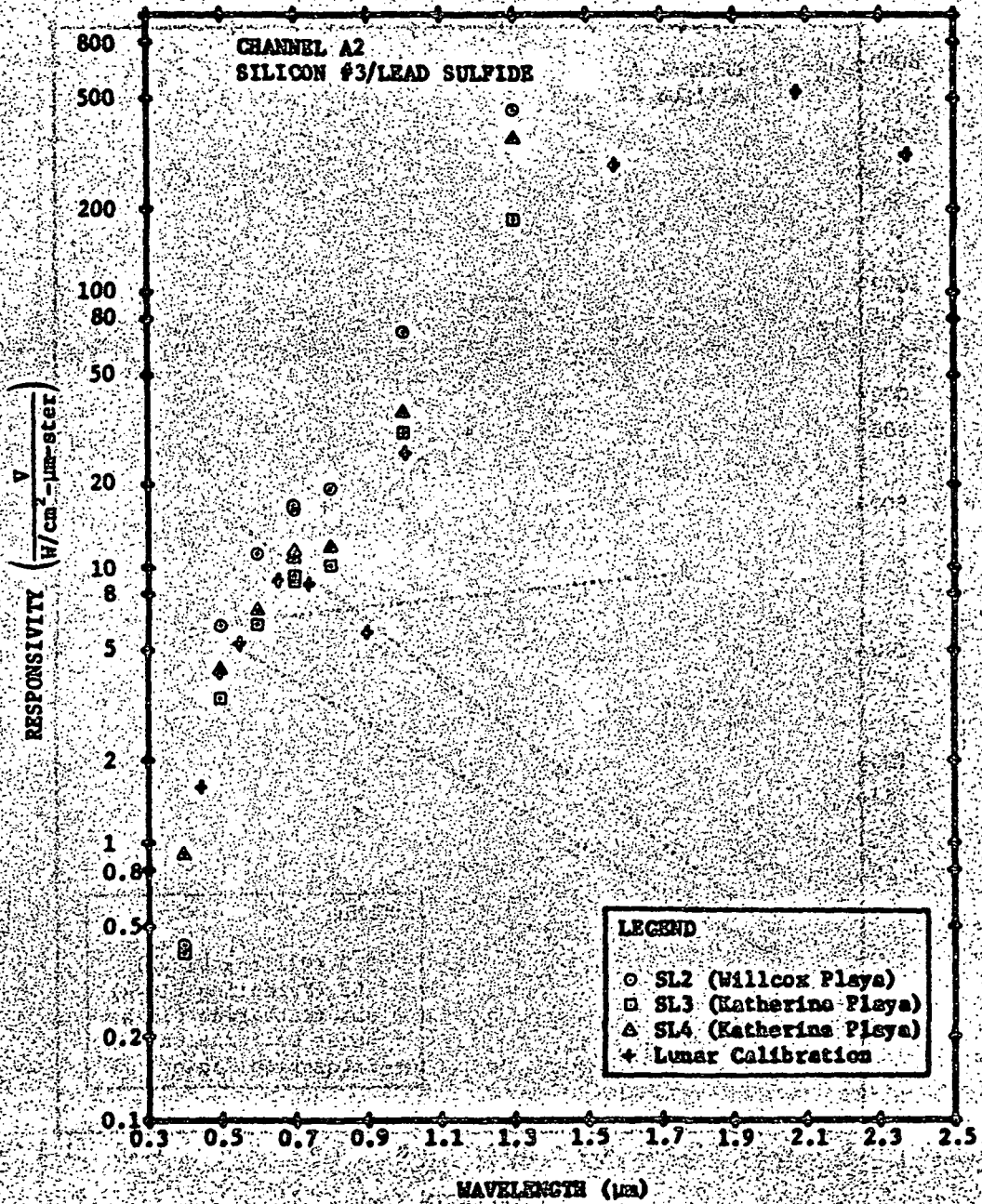


Figure 4.1-2 Comparison of S191 Responsivities Derived from Ground Truth and Lunar Calibration Data

NSC-05546

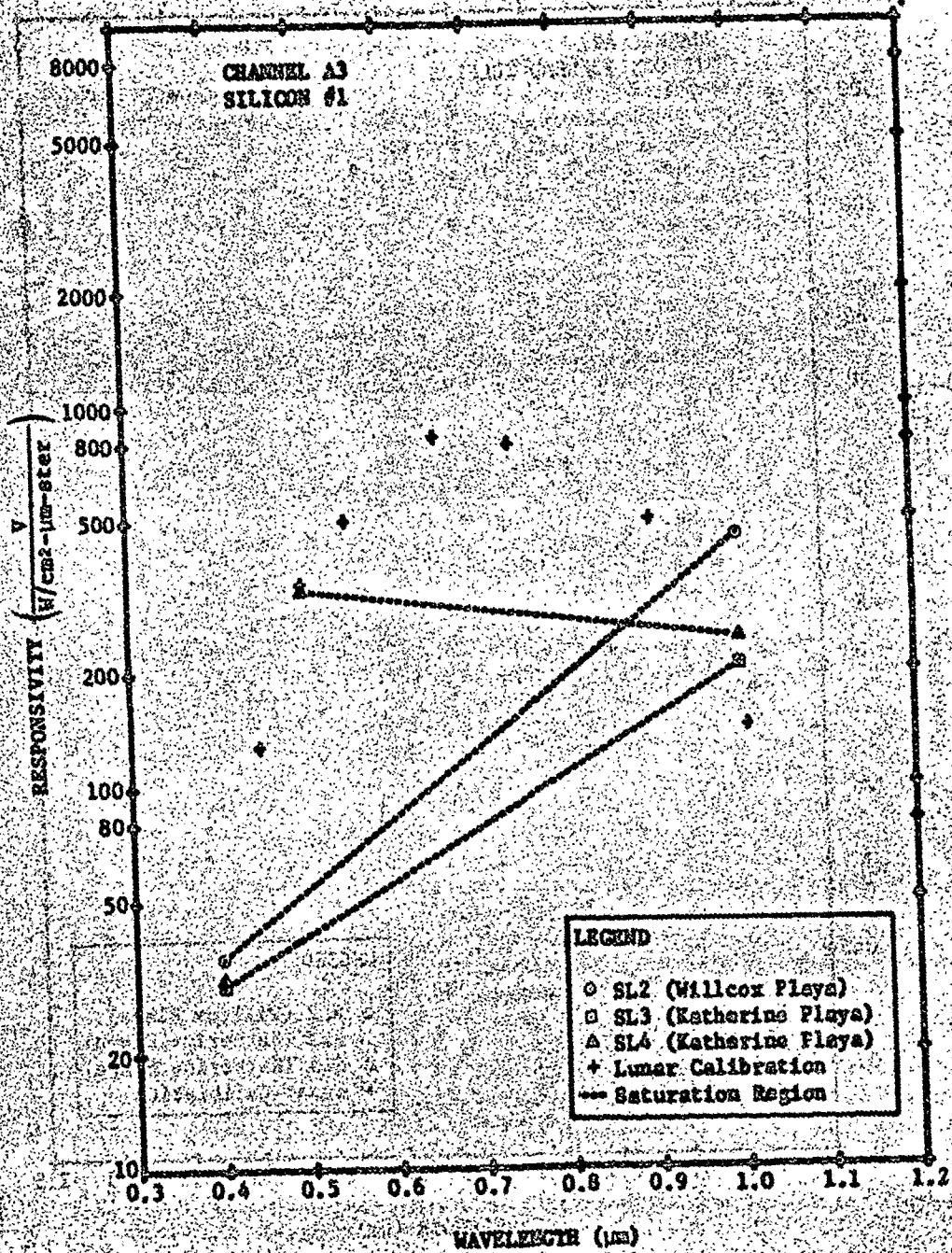
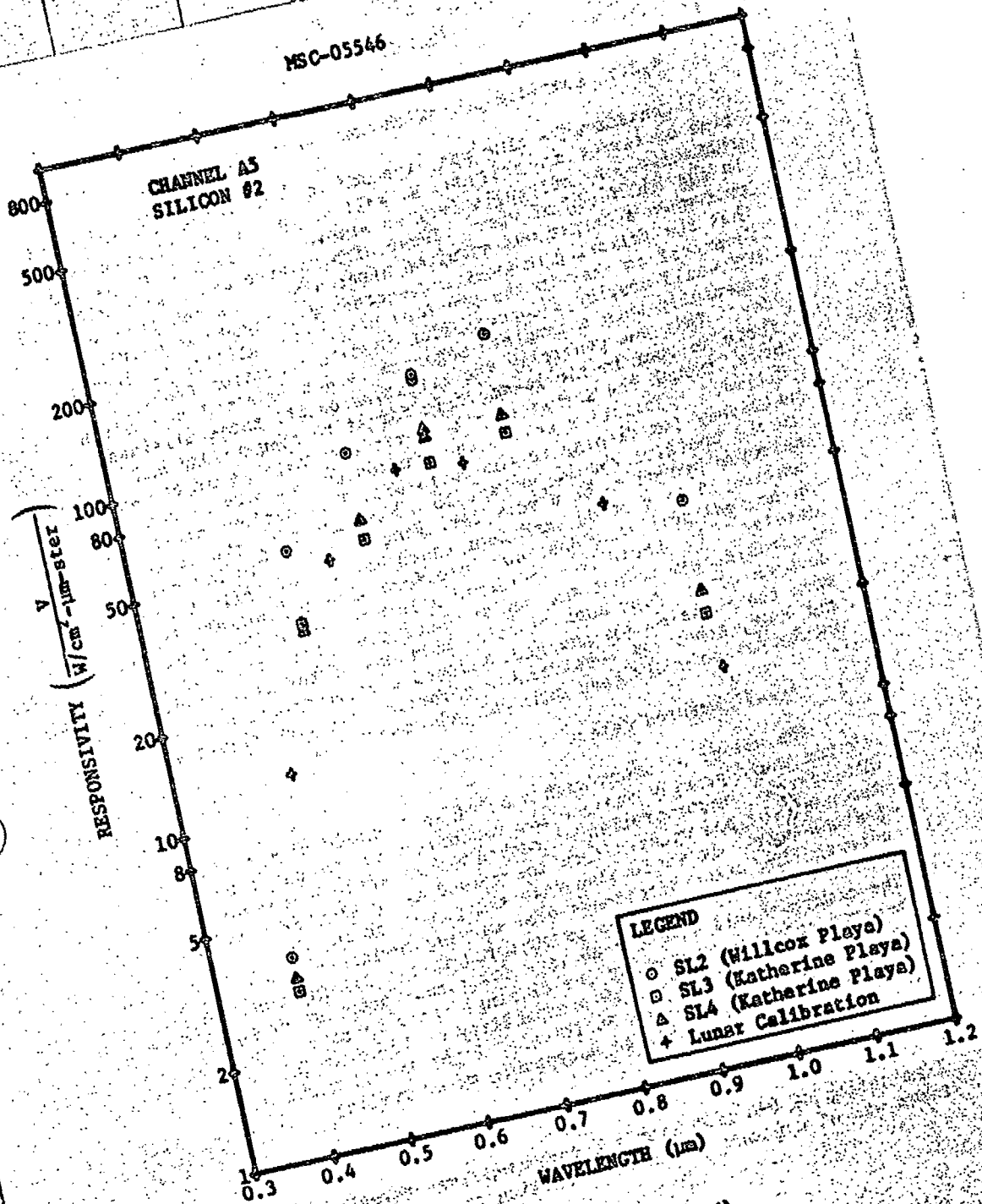


Figure 4.1-2 (continued)

MSC-05546

CHANNEL A5
SILICON 82



LEGEND
○ SL2 (Wilcox Playa)
□ SL3 (Katherine Playa)
△ SL4 (Katherine Playa)
+ Lunar Calibration

Figure 4.1-2 (concluded)

MSC-05546

4.2.1 Complete Greenwich Mean Time (GMT) Display

Considerable time was expended in determining the date and time of target acquisition, as well as identities of targets themselves, by relying solely on minutes and seconds displayed in the DAC field of view. These efforts were especially difficult when a target was acquired after a break in the pass so that the following minutes and seconds displayed was nearly identical to that in the previous pass. The ability to display DOY would provide a conservation in data reduction time, especially when a complete magazine is not depleted on a given day. This was generally the situation on all three missions. There is room in the 16-mm. film format to display day and hour, though the format of the operator's image is pretty well filled. Information beyond the minutes and seconds is not necessary for display to the operator. The displays presented to the operator should be kept to a bare minimum; the items selected proved to be a very satisfactory set. The logical conclusion is that day and hour could be put into film through an optical path that does not interfere with the operator's display. It should be considered a luxury rather than a highly desirable item to put the day and hour onto film; the mission documentation, plus such clues as portions of the film exposed when the magazine was changed, allowed a reconstruction of day and hour, albeit at considerable effort. Less than rigorous documentation would have made the job impossible.

4.2.2 Metered Camera

The use of a camera with a built-in light-level metering system would greatly enhance the capability of the complete DAC system. Incorporation of such a device would eliminate the need for pad updates from the ground as to shutter speeds, f-stops, etc. It would also take the guesswork out of anticipating scene brightness over varying terrain and the inherent brightness changes encountered in the zooming process. The camera should have the ability for manual override of the metered settings by opening (or closing) the diaphragm by one or possibly two f-stops. This capability would be useful during situations in which anticipated light levels might be too low (or too high) for an acceptable meter reading.

4.2.3 DAC Mounting Technique

Examination of DAC film from the three missions revealed that there was an apparent problem in mounting the DAC on the VTS

MSC-05546

mount in the proper orientation to the telescope body. With the adapter ring used on Skylab, the DAC could theoretically be mounted in any one of four positions (one for each of four mounting tabs, each 90 degrees apart). In practical operation, only three of the four positions were actually possible because the camera body would come in contact with the telescope in the fourth position. To alleviate the problem of mounting confusion, an orange alignment dot was placed on the DAC mounting port so that the DAC could be properly aligned and locked in its normal operating position. However, a review of DAC film revealed that the mounting problem had not completely disappeared. While the incorrect mounting incidents were few, they nevertheless did occur, and future designs should incorporate foolproof mounting features. All bayonet-mounted single-lens reflex cameras have an alignment dot, but only a single slot for tab insertion, so that locking the lens into its proper place is assured.

4.2.4 Use of Illuminated Reticles

Special lunar calibration data taken where deep space backgrounds were involved revealed the problem that the pointing reticle could not be seen. Consideration should be given to the illumination of reticles with variable intensity control. Such a system is generally required only when the darkened reticles can not be distinguished from the background. The majority of the targets viewed from Skylab did not require reticle illumination.

4.2.5 Variable Control or Multiple Discrete Steps for Light-Emitting Diode (LED) Brightness

Problems with LED brightness encountered during SL2 and some overexposed images encountered in subsequent missions indicated a need for a wider selectivity in brightness steps for the LED displays rather than a three-position switch. Future designs should consider a variable control or multiple step of LED brightness to obtain the desired contrast for data takes.

4.2.6 Use of High-Resolution Color Film

Future programs should consider recent developments in high resolution color film for applications similar to DAC photography. The color film used during SL3 and SL4 proved to be far superior to the black-and-white film used during SL2. A thorough survey of the film market should be made and preflight testing implemented to determine the optimum material to provide the highest resolution possible within the capabilities of the camera. The film choice (or at least a recommendation) should be a part of the contract for

MSC-05546

the development of any similar equipment. The contractor should be required to demonstrate the film as part of system functional verification.

4.3 S190A, S191, and S192 Radiometric Comparison

Each EREP optical sensor (S190A, S191, and S192) was designed and calibrated to provide absolute spectroradiometric data. These sensors also covered common wavelength regions, which facilitated a radiometric comparison. However, the spectral bands and bandwidths were different and required band averaging to accomplish the comparison. The spectral bands for each sensor are given in Table 4.3-1. The radiometric values output from these sensors were converted to common units. The S190A output data were converted to units of spectral radiance ($\text{mW}/\text{cm}^2\text{-}\mu\text{m-ster}$) by dividing the S190A total radiance output ($\text{mW}/\text{cm}^2\text{-ster}$) by the bandwidth of each station. The bandwidth equalled the difference between the limits of integration used to calculate the S190A radiance output from equation A.II.12, Appendix A, Section II of Volume I of this report.

MSC-05546

Table 4.3-1 S190A, S191, and S192 Spectral Bands for Radiometric Comparison

S190A		S192		S191*		
Station	Wavelength Band (μm)	Band	Wavelength Band (μm)	Segment	Wavelength Range (μm)	Wavelength Resolution (μm)
6	0.48 to 0.63	1	0.41 to 0.45	1	0.39 to 0.73	0.0115
		2	0.45 to 0.51			
		3	0.50 to 0.56			
5	0.58 to 0.72	4	0.54 to 0.60			
		5	0.60 to 0.66			
1	0.68 to 0.78	6	0.65 to 0.74	2	0.68 to 1.43	0.0185
2	0.75 to 0.90	7	0.77 to 0.89			
		8	0.93 to 1.05			
		9	1.03 to 1.19			
		10	1.15 to 1.28			
		11	1.55 to 1.73	3	1.34 to 2.50	0.015 $\times \lambda$
		12	2.10 to 2.34			
				4	5.82 to 11.40	0.019 $\times \lambda$
		13	10.07 to 12.68	5	8.30 to 15.99	0.019 $\times \lambda$

* S191 had a continuously variable filter; definable narrow bands are given by the wavelength resolution.

The radiometric comparison as planned was to have compared radiance values when all three sensors were observing the same target. However, due to mission scheduling difficulties only one ground truth site suitable for radiometric evaluation was observed simultaneously by all three sensors. This site was the Willcox Playa observed during SL2 when there were small cumulus clouds near the site, and which probably influenced the results. However, common sites were available for comparing S190A to S191, S190A to S192, and a limited comparison of S191 to S192. Based on data from these sites the overall comparison of all three sensors could be made.

4.3.1 Comparison of S190A to S191

Comparison of S190A to S191 was based on the three sites:

<u>Mission</u>	<u>Date</u>	<u>Site</u>
SL2	6/3/73	Willcox Playa, Arizona
SL3	8/11/73	Katherine Playa, New Mexico
SL4	2/1/74	Katherine Playa, New Mexico

MSC-05546

The spectral radiance of each site was first calculated from the S191 data for 13 narrow wavelength bands over the spectral range of the S190A (0.44 to 0.9 μm). These data were calculated using S191 responsivity derived from ground-based lunar mare measurements made with the S191 backup spectrometer. This responsivity is presented in Figure 4.1-1 for channel A5. The resulting spectral radiance values for the three sites are listed in Table 4.3.1-1 and plotted in Figure 4.3.1-1. These data were then averaged over each of the S190A spectral bands to obtain the average spectral radiance comparable to each S190A station. The resulting average spectral radiance for both sensors and that derived from the ground truth measurement are listed in Table 4.3.1-2. Radiance ratios were also calculated and listed to provide a basis for intersensor comparison.

Table 4.3.1-1 S191 Spectral Radiance for S190A and S191 Comparison Sites

Wavelength (μm)	SPECTRAL RADIANCE VALUE ($\text{mW}/\text{cm}^2\text{-}\mu\text{m}\text{-ster}$)		
	Willcox Playa, SL2	Katherine Playa, SL3	Katherine Playa, SL4
0.448	17.63	12.05	8.542
0.475	18.64	12.50	8.975
0.500	17.09	11.45	8.853
0.552	15.40	10.1	8.828
0.600	15.04	10.0	9.267
0.657	15.78	10.9	10.286
0.675	15.65	10.5	10.199
0.700	14.61	9.21	9.866
0.725	15.58	10.04	10.468
0.741	15.29	10.65	10.474
0.800	14.46	9.86	9.920
0.850	12.42	8.75	8.454
0.901	9.28	5.97	6.418

MSC-05546

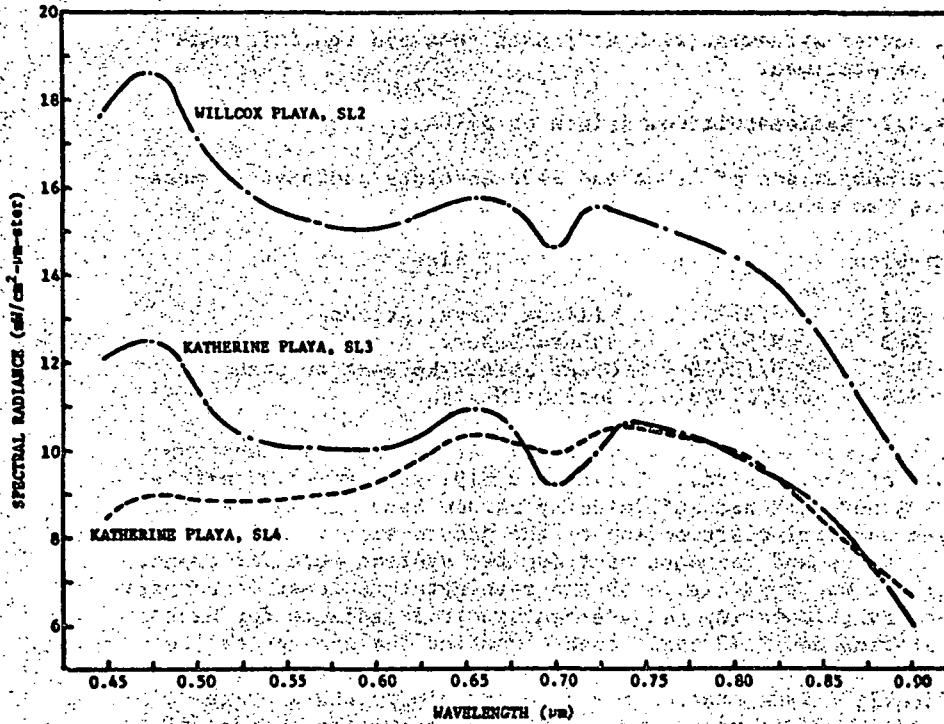


Figure 4.3.1-1 S191 Spectral-Radiance Plot for S190A and S191 Comparison Sites

Table 4.3.1-2 S190A, S191, and Ground-Truth Radiometric Comparison

MISSION	SITE	DATE	SPECTRAL RADIANCE (mW/cm ² -µm-ster)			RADIANCE RATIO			WAVELENGTH BAND (µm)
			S190A	S191	Ground Truth	S190A/S191	S190A/ Ground Truth	S191/ Ground Truth	
SL2	Willcox Playa	6/3/73	11.93	16.93	10.27	0.70	1.16	1.65	0.48 - 0.63
			14.79	16.28	10.00	0.91	1.68	1.63	0.58 - 0.71
			11.21	14.95	7.16	0.75	1.57	2.09	0.68 - 0.87
			10.93	13.93	6.07	0.78	1.60	2.29	0.75 - 0.90
SL3	Katherine Playa	8/11/73	9.47	11.27	12.00	0.84	0.79	0.94	0.48 - 0.63
			10.79	10.86	11.57	0.99	0.93	0.94	0.58 - 0.72
			6.89	10.16	8.95	0.68	0.77	1.14	0.68 - 0.87
			6.60	9.60	8.20	0.67	0.78	1.17	0.75 - 0.90
SLA	Katherine Playa	2/1/76	9.27	9.67	9.93	0.96	0.93	0.97	0.48 - 0.63
			9.07	10.37	10.14	0.88	0.89	1.04	0.58 - 0.72
			No Data	10.21	8.05	--	--	1.27	0.68 - 0.87
			8.00	9.33	7.33	0.84	1.09	1.30	0.75 - 0.90

This comparison shows that the spectral radiance values derived from S191 were consistently higher than those from S190A, with an average about 18% higher. The large ratios for both S190A and S191 with ground truth data for Willcox Playa indicate that local atmospheric conditions caused the ground truth calculations to give erroneously low spectral radiance values, particularly in the near-infrared bands. This result supports the suspicions of that data.

MSC-05546

The camera stations operating in the visible spectral region showed better agreement with S191 data than did the infrared-sensitive stations.

4.3.2 Radiometric Comparison of S190A to S192

The comparison of S190A and S192 absolute radiometric measurements was based on four ground sites:

<u>Mission</u>	<u>Date</u>	<u>Site</u>
SL2	6/3/73	Willcox Playa, Arizona
SL3	9/2/73	Sahara Desert, Africa
SL3	9/13/73	Great Salt Lake Desert, Utah
SL3	9/17/73	Gulf of Mexico

No ground truth measurements were made at the Sahara Desert and the Gulf of Mexico sites. Unlike the S191 spectrometer, neither the S190A nor S192 had sufficiently narrow bands to define the detailed spectral distribution of the ground sites. Also, the spectral bands and response of these two systems were different. However, it was possible to obtain meaningful radiometric comparison data by calculating the average spectral radiance for each S190A station and S192 band; then computing the average of the S192 bands covering the spectral range of each S190A station. Specifically, S190A station 6 was comparable to the average of S192 bands 3 and 4; station 5 was comparable to the average of bands 5 and 6; station 1 was comparable to the average of bands 6 and 7; and station 2 was comparable to S192 band 7. The spectral ranges of these stations and bands are given in Table 4.3-1.

The average spectral radiance values and radiance ratios for the S190A, S192 and the ground truth measurements are given in Table 4.3.2-1. The S192 Willcox Playa data were recorded on pass 3 of SL2 before installation of the attenuators. The "off scale" listed in the table means the output signal was above the upper limit for bands 4 and 5. This condition was later corrected by installation of the attenuators. Review of this table shows similar error magnitude in the Willcox Playa ground truth data as in the comparison of S190A to S191. The data also indicate good agreement between S190A and S192 radiance values, with no apparent systematic error, or bias, in the comparison.

MSC-05546

Table 4.3.2-1 S190A, S192, and Ground-Truth Radiometric Comparison

MISSION	SITE	DATE	AVERAGE SPECTRAL RADIANCE (mW/cm ² -μm-ster)			RADIANCE RATIO			COMPARATIVE OUTPUT		
			S190A	S192	Ground Truth	S190A/S192	S190A/ Ground Truth	S192/ Ground Truth	S190A (Station)	S192 (Beads)	
SL2	Willcox Playa	6/3/73	11.93	off scale	10.27	--	1.16	--	6	3,4 average	
			14.79	off scale	10.00	--	1.48	--	5	5,6 average	
			11.21	11.56	7.16	0.97	1.57	1.57	1	6,7 average	
			10.93	11.32	6.07	0.97	1.80	1.86	2	7	
SL3	Sahara Desert	9/2/73	7.75	8.10	--	0.96	--	--	6	3,4 average	
			12.25	10.68	--	1.15	--	--	5	5,6 average	
			-----No Data Available-----			-----No Data Available-----			--	1	6,7 average
			7.92	9.36	--	0.85	--	--	2	7	
SL3	Great Salt Lake Desert	9/13/73	13.27	11.39	11.00	1.17	1.21	1.04	6	3,4 average	
			13.21	11.12	10.43	1.19	1.27	1.07	5	5,6 average	
			9.00	9.78	7.79	0.92	1.16	1.26	1	6,7 average	
			8.73	9.17	6.93	0.95	1.26	1.32	2	7	
SL3	Gulf of Mexico	9/17/73	4.15	3.43	--	1.21	--	--	6	3,4 average	
			2.06	1.62	--	1.27	--	--	5	5,6 average	

4.3.3 Radiometric Comparison of S191 to S192

Only two ground sites suitable for radiometric comparison of S191 to S192 were available. They were the SL2 Willcox Playa site discussed in paragraphs 4.3.1 and 4.3.2 and the Rio Grande Reservoir, Colorado, site observed on 8/8/73 during the SL3 mission. The absolute spectral radiance values based on S191 data for Willcox Playa are listed in Table 4.3.1-1 and plotted in Figure 4.3.1-1. The S191 spectral radiance for the Rio Grande Reservoir is given in Table 4.3.3-1 and plotted in Figure 4.3.3-1.

Table 4.3.3-1 S191 Spectral Radiance of Rio Grande Reservoir for Comparison of S191 to S192

Wavelength (μm)	Spectral Radiance (mW/cm ² -μm-ster)
0.448	4.94
0.475	4.48
0.50	3.69
0.552	2.74
0.60	1.72
0.657	1.42
0.675	1.37
0.70	1.41
0.725	1.42
0.741	1.46
0.80	1.37
0.85	1.12
0.901	0.80

MSC-05546

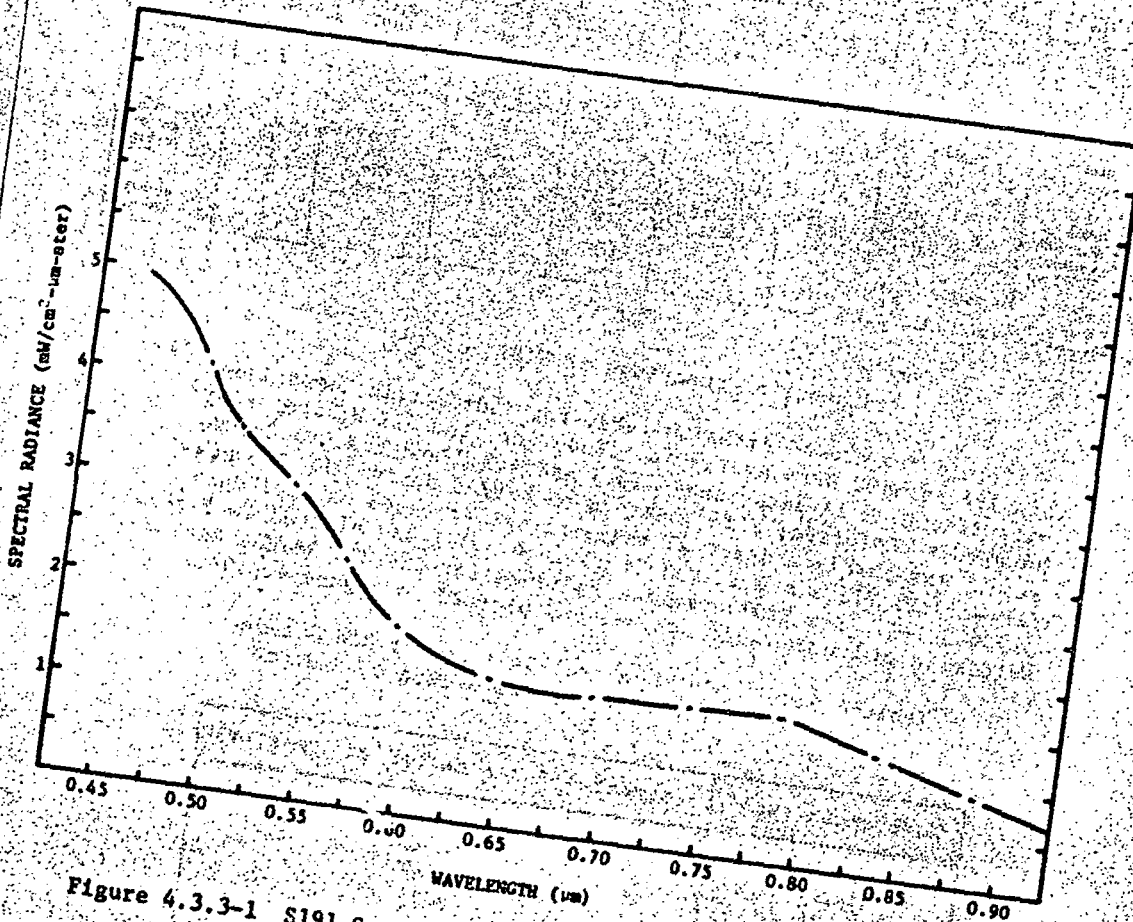


Figure 4.3.3-1 S191 Spectral Radiance of Rio Grande Reservoir, SL3

The comparison of S191 to S192 was achieved by taking the average of the S191 spectral radiance over each corresponding S192 band. Infrared wavelengths greater than 0.901 μm were not considered due to a lack of analysis time. The resulting comparative data are listed in Table 4.3.3-2.

MSC-05546

Table 4.3.3-2 S191, S192, and Ground-Truth Radiometric Comparison

MISSION	SITE	DATE	AVERAGE SPECTRAL RADIANCE (mW/cm ² -μm-ster)			RADIANCE RATIO			S192 SPECTRAL BAND
			S191	S192	Ground Truth	S192/S191	S191/ Ground Truth	S192/ Ground Truth	
SL2	Willcox Playa	6/3/73	17.8	9.51	10.8	0.534	1.648	0.881	2
			16.1	10.13	9.4	0.629	1.713	1.078	3
			15.3	off scale	9.4	---	1.628	---	4
			15.4	off scale	9.7	---	1.588	---	5
			15.3	11.54	8.6	0.754	1.779	1.342	6
			13.0	11.32	5.6	0.870	2.321	2.021	7
			SL3	Rio Grande Reservoir	8/8/73	4.43	3.49	Not available	0.788
3.20	2.70	↑ ↓				0.844	---	---	3
2.92	2.38					0.815	---	---	4
1.51	1.60					1.060	---	---	5
1.36	1.05					0.772	---	---	6
1.17	1.03					Not Available	0.880	---	---

A review of this table for Rio Grande Reservoir shows the S191-derived spectral radiance is higher than that for S192 by approximately 16%. The S192 results for Willcox Playa differ significantly from those of S191. No attenuators had been installed in S192 and other problems were associated with these data. The differences with Willcox Playa ground truth are again apparent.

4.3.4 Radiometric Comparison Summary

The derived spectral radiances from various targets agree closely for S190A and S192. The S191 values were about 16 to 18% higher than those for S190A and S192. The values are given in Tables 4.3.1-2, 4.3.2-1, and 4.3.3-2. The agreement among the three sensors was judged to be excellent considering that a recent study* showed the variation in radiometric calibrations made at various standards laboratories to be approximately ±10% (total variation 20%) from the consensus. Considering the space environment, the variations in spectral bands, and the less-than-optimum calibration procedures available before launch, the relative radiometric absolute accuracy of these three instruments was considered excellent.

* Franc Grum and Joseph Cameron: "Detector Intercomparison Results," Electro-Optical Systems Design, Vol 6, November 1974, p 82.

MSC-05546

These data also showed that, based on the S190A and S192 data, the lunar radiance values calculated using the Lane and Irvine data* were approximately 25% high.

4.4 Wavelength Calibration

To more adequately describe the nature of the wavelength calibration of the S191 instrument, two additional analyses were performed after the publication of the interim report. These analyses were:

- 1) Generation of spectra of BG-36 Schott glass and polystyrene as resolved by the S191 instrument for comparison to laboratory-produced spectra;
- 2) Derivation of equations applicable to specific wavelength regions covered by the S191 instrument.

4.4.1 Calibration Filter Spectra

To demonstrate the quality of the wavelength calibration, the transmission of both filter materials (Schott glass and polystyrene) was plotted against ramp voltage. Representative auto calcs from all three missions were used in the evaluation. All five physical segments of the circular variable filter were examined. Three of these segments (0.4 to 2.5 μm) use the Schott glass filter for wavelength calibration; two segments (6 to 16 μm) use polystyrene.

The ratio of detector output voltage with the calibration filter in place to the same detector output voltage with the calibration filter removed was calculated. This ratioing technique effectively compensated for background slope effects that would shift the position of the absorption minimum. The results were corrected for drifts in ramp voltage by multiplying the ramp voltage by the factor 4.86 divided by the average maximum ramp voltage. Four sets of data were taken with the calibration filter in the field of view, and five sets were taken with the calibration filter removed. (Each set corresponded to one revolution of the filter wheel with an approximate rotation rate of one revolution per second.) Therefore, the average maximum ramp used was the mean of nine data sets. The spectra obtained in these analyses are shown in Figures 4.4.1-1 through 4.4.1-5. The appropriate wavelength scale is included on each plot and representative resolution values are noted at specified wavelengths.

* A. P. Lane and W. M. Irvine, "Monochromatic Phase Curves and Albedos for the Lunar Disk," The Astronomical Journal, Vol 78, No. 3, 1972.

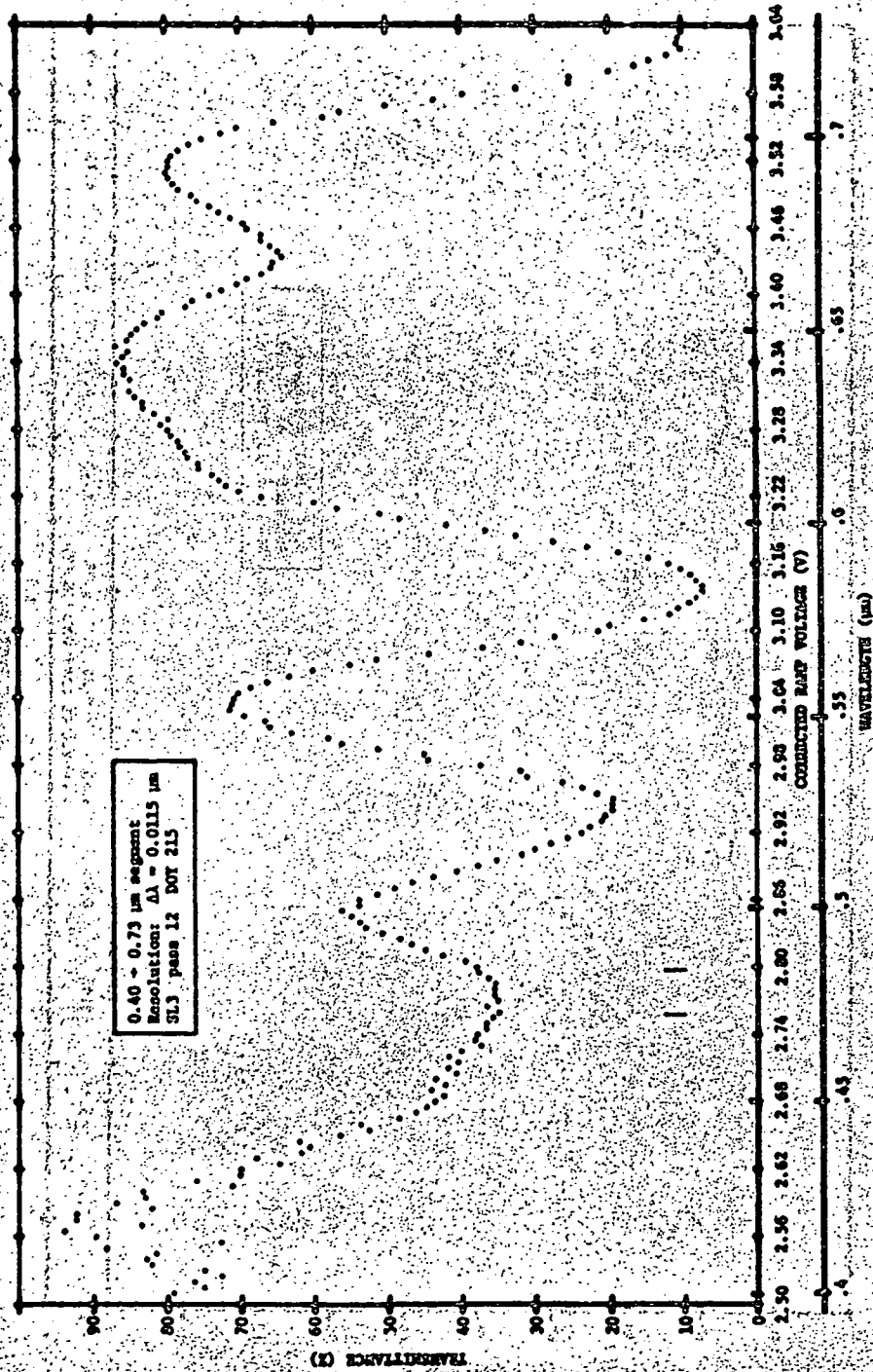


Figure 4.4.1-1 Transmission Spectra of BG-36 Schott Glass as a Function of Ramp Voltage and Wavelength

MSC-05546

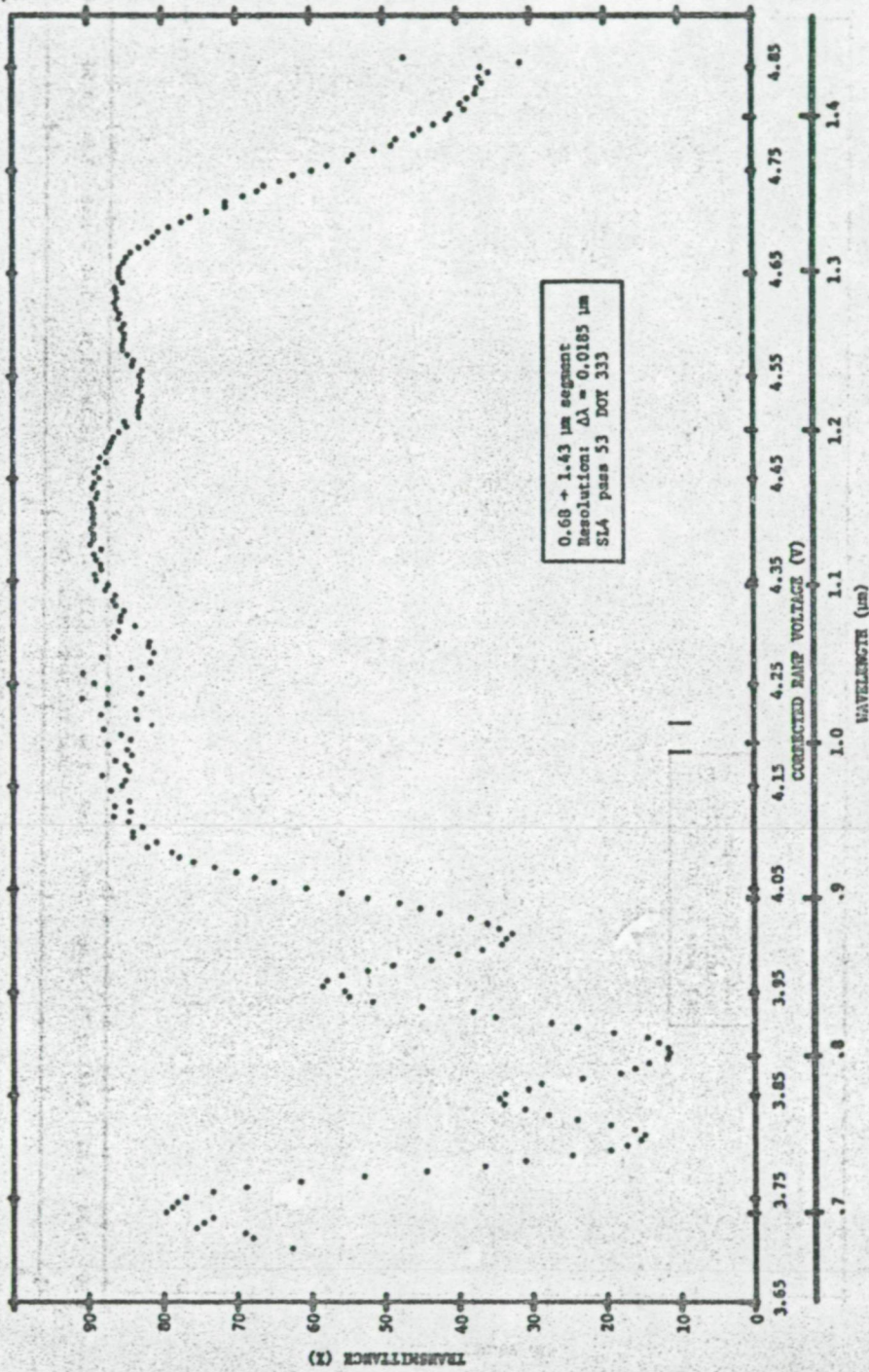


Figure 4.4.1-2 Transmission Spectra of EG-36 Schott Glass as a Function of Ramp Voltage and Wavelength

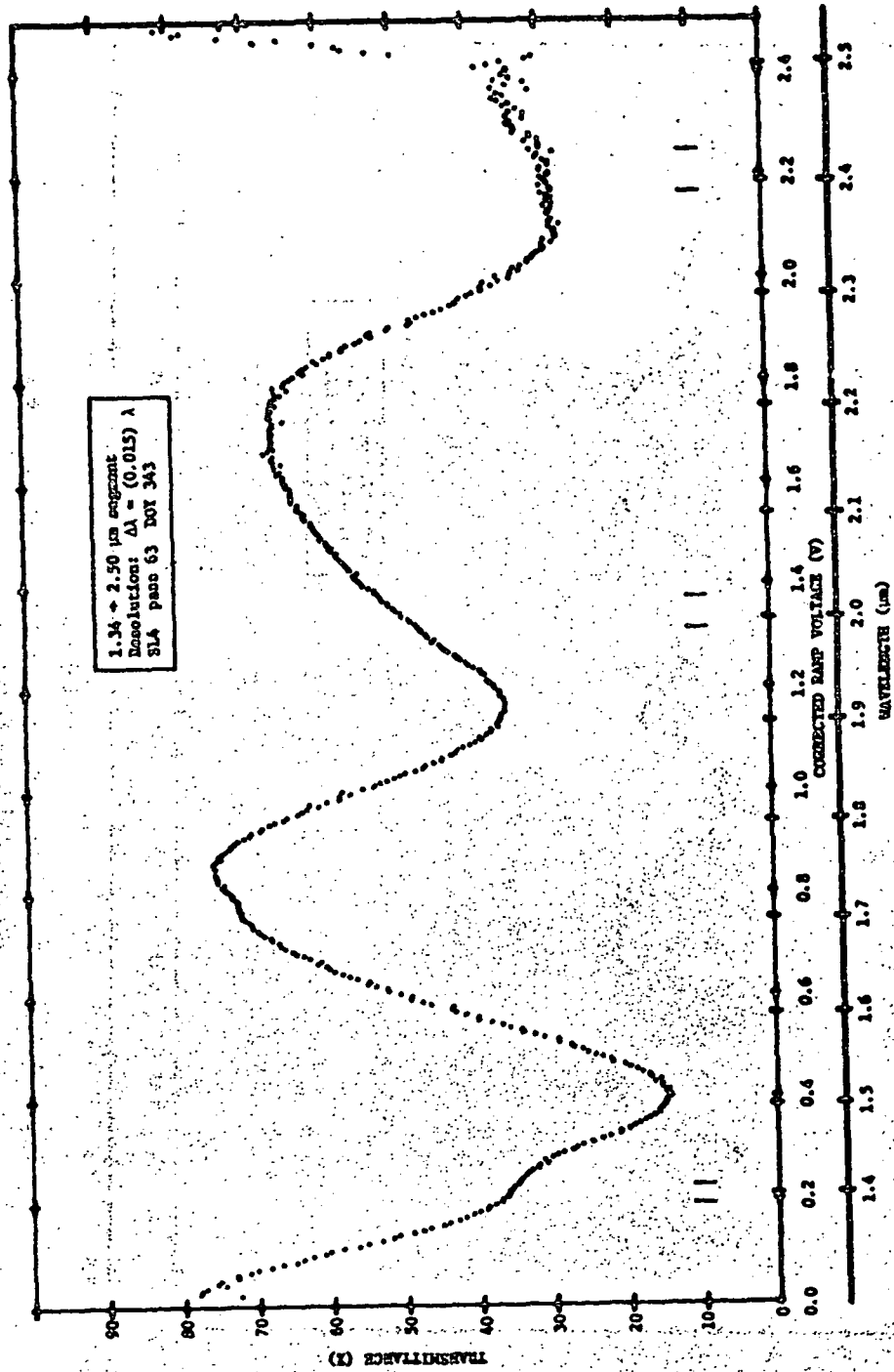


Figure 4.4.1-3 Transmission Spectra of EC-36 Schott Glass as a Function of Ramp Voltage and Wavelength

MSC-05546

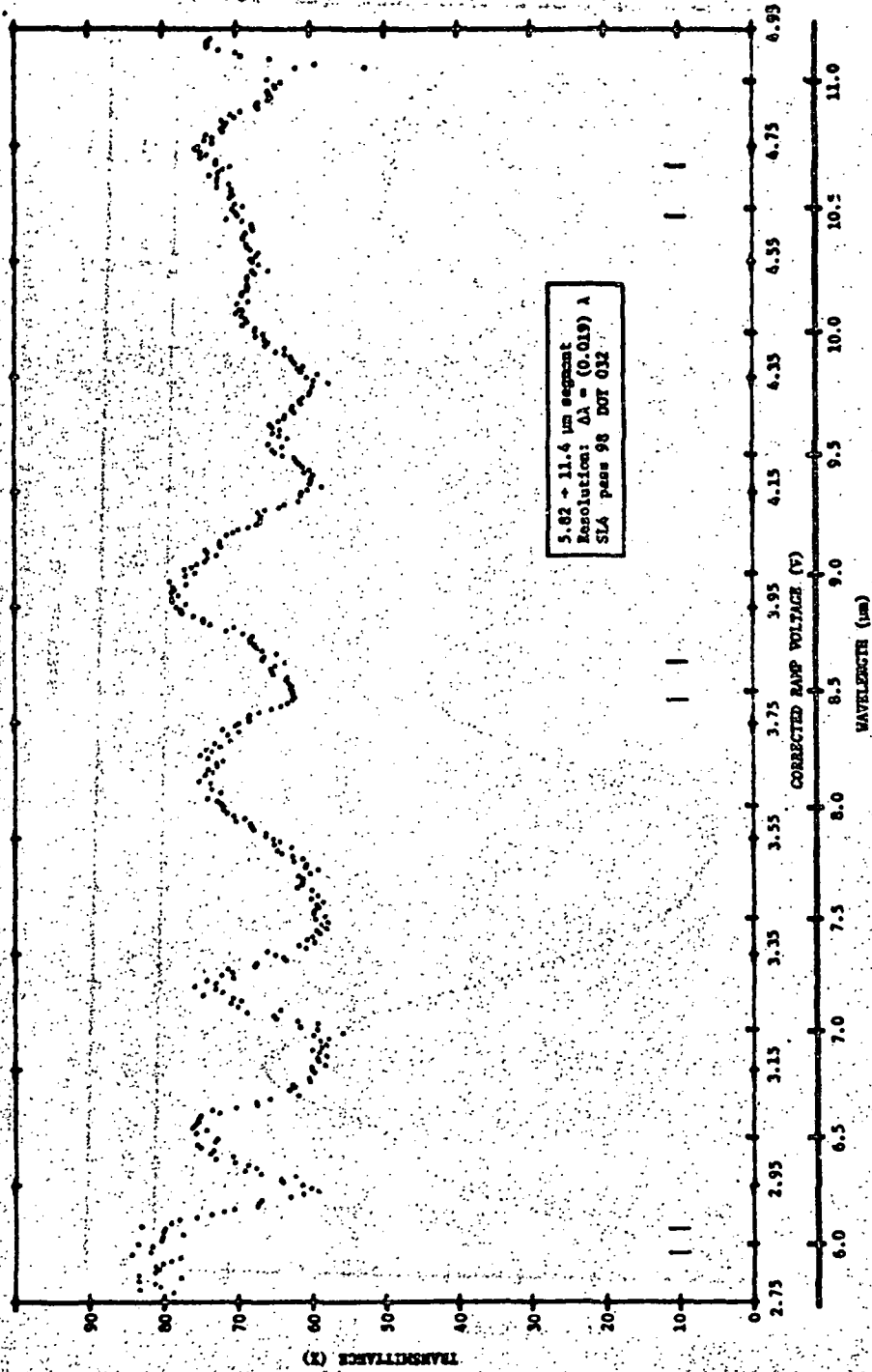


Figure 4.4.1-4. Transmission Spectra of Polystyrene as a Function of Ramp Voltage and Wavelength

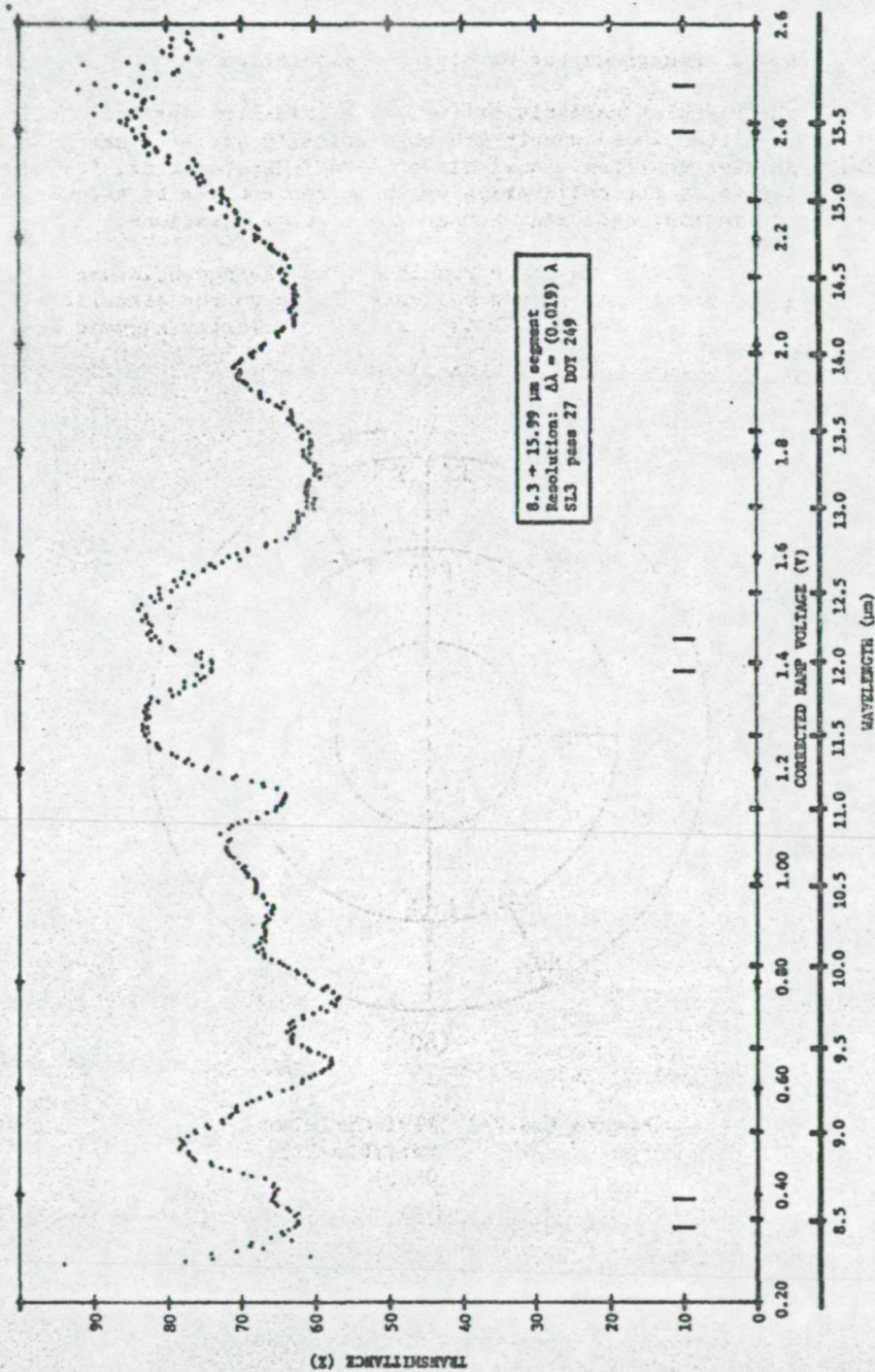


Figure 4.4.1-5 Transmission Spectra of Polystyrene as a Function of Ramp Voltage and Wavelength

MSC-05546

4.4.2 Equations for Wavelength Calibration

The circular variable filter was a thin-film optical interference filter whose wavelength theoretically varied linearly with angular position. Analysis of data indicated that, for certain segments, the calibration was best represented by second-order polynomial equations rather than linear equations.

Some confusion may have resulted from the nomenclature defining the particular filter segments making up the circular variable filter. Figure 4.4.2-1 is provided to clarify segment designations.

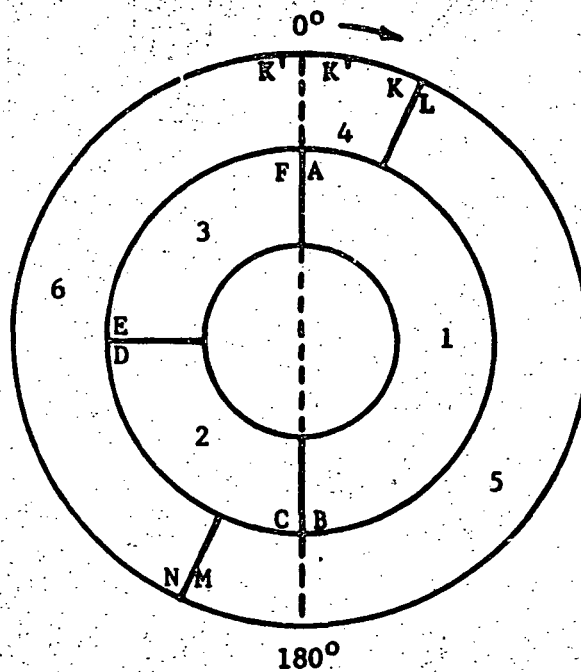


Figure 4.4.2-1 S191 Circular Variable Filter Wheel

MSC-05546

The filter wheel was designed so that the short-wavelength (0.4- to 2.5- μm) segments, 1, 2, and 3 comprised an inner annulus and the long-wavelength (6- to 16- μm) segments 4, 5 and 6, the outer annulus. The 0-degree position on the filter wheel corresponded to the ramp reset, and, as the wheel rotated, a sawtooth waveform would be generated so that the peak was nominally 4.86 volts. One of the segment changes on the 0.4- to 2.5- μm annulus was coincident with the ramp reset. However, on the 6- to 16- μm annulus, the ramp reset preceded the segment change by approximately 10 degrees. There were only five physical segments, but a sixth "segment" was formed by the small portion of the 6- to 11.4- μm segment that followed the ramp reset. The wavelength range of these six segments is identified in Table 4.4.2-1. Segment numbers and approximate range limits are shown in Figure 4.4.2-1.

Table 4.4.2-1 S191 Wavelength Coverage

Segment	Range Limits		Wavelength Range (μm)	
1	A	B	1.34	2.50
2	C	D	0.40	0.73
3	E	F	0.68	1.43
4	K'	K	11.0	11.4
5	L	M	8.3	15.99
6	N	K'	5.82	11.0

Determination of absorption minimums and in some instances, maximums, from plots similar to those of Figures 4.4.1-1 through 4.4.1-5 were presented in Table 3.3.1-1. Both these values and those derived by the vendor were used to formulate a series of equations applicable to specific wavelength increments. Within the five physical segments, there is some wavelength overlap, and a particular wavelength may have two ramp voltages. Reference should be made to the wavelength region specified in a particular equation rather than in the region covered by one of the five segments. The corrected ramp voltage value is denoted by V_{fc} . These equations are:

- 1) For $0.40 \leq \lambda \leq 0.71 \mu\text{m}$,

$$V_{fc} = A_0 + A_1 \lambda + A_2 \lambda^2 \quad [4.4.2.1]$$

where

$$\begin{aligned} A_0 &= 1.14527 \\ A_1 &= 3.41492 \\ A_2 &= 0.0237844 \end{aligned}$$

MSC-05546

- 2) For $0.72 \leq \lambda \leq 1.36 \mu\text{m}$,

$$V_{fc} = A_0 + A_1 \lambda + A_2 \lambda^2 \quad [4.4.2.2]$$

where

$$\begin{aligned} A_0 &= 2.67633 \\ A_1 &= 1.52349 \\ A_2 &= 0 \end{aligned}$$

- 3) For $1.38 \leq \lambda \leq 2.48 \mu\text{m}$,

$$V_{fc} = A_0 + A_1 \lambda + A_2 \lambda^2 \quad [4.4.2.3]$$

where

$$\begin{aligned} A_0 &= -1.64778 \\ A_1 &= 0.966462 \\ A_2 &= 0.265708 \end{aligned}$$

- 4) For $6.0 \leq \lambda \leq 9.2 \mu\text{m}$,

$$V_{fc} = A_0 + A_1 \lambda + A_2 \lambda^2 \quad [4.4.2.4]$$

where

$$\begin{aligned} A_0 &= 0.975941 \\ A_1 &= 0.266592 \\ A_2 &= 0.00798181 \end{aligned}$$

- 5) For $9.2 \leq \lambda \leq 12.7 \mu\text{m}$,*

$$V_{fc} = A_0 + A_1 \lambda + A_2 \lambda^2 \quad [4.4.2.5]$$

where

$$\begin{aligned} A_0 &= -3.12383 \\ A_1 &= 0.490235 \\ A_2 &= -0.00932054 \end{aligned}$$

* Two sets of coefficients were required to accurately describe the physical segment covering the 8.3- to 15.99- μm range.

6) For $12.7 \leq \lambda \leq 16 \mu\text{m}$,*

$$V_{fc} = A_0 + A_1 \lambda + A_2 \lambda^2 \quad [4.4.2.6]$$

where

$$A_0 = -2.04175$$

$$A_1 = 0.288636$$

$$A_2 = 0$$

4.5 S191 Viewfinder Tracking System Spectrometer Component Reflectances and Temperatures

A separate study† was done to determine the following three parameters calculated from actual Skylab data:

- 1) Dichroic reflectivity versus wavelength;
- 2) Combined Viewfinder Tracking System (VTS) mirror reflectivity versus wavelength;
- 3) Time and temperature profiles for the VTS gimbal and Cassegrainian mirror surfaces.

Each of these parameters is required for an accurate 6- to 16-micrometer radiometric calibration and were either in question or not available from ground calibration or housekeeping data. The equations involved in determining these three parameters were developed and discussed.

In the process of calculating the dichroic reflectivity, it was discovered that the assumption of linear detector response did not accurately describe the results in the 6- to 8-micrometer region. However, at the longer wavelengths the calculations gave stable responsivities consistent with a linear detector response. The dichroic and VTS mirror reflectivities above 8 micrometers were calculated and tabulated in the report. Valid parametric values for calculation of radiometric response were obtained. Subsequent studies indicate that off-band radiation was severe in the 6- to 8-micrometer region; this radiation caused the difficulties in this wavelength region mentioned above. Off-band radiation is discussed in Section 7.4.2.1 of MSC-05528, Volume II.

* Two sets of coefficients were required to accurately describe the physical segment covering the 8.3- to 15.99- μm range.

† S191 VTS Spectrometer Component Reflectances and Temperatures, MSC-05545, Martin Marietta Corporation, Denver, Colorado, June 7, 1974.

MSC-05546

VTS mirror temperature profiles were developed using available flight temperature data as inputs to a simplified thermal model. The model equations were developed and the assumptions given. Each EREP pass was individually evaluated. A representative temperature for the VTS gimbal and Cassegrainian mirror was tabulated for each EREP pass. The resulting temperature values represented an orbital average, about which a $\pm 3^{\circ}\text{C}$ variation was expected throughout one orbit. The detailed results are given in S191 VTS Spectrometer Component Reflectances and Temperatures.*

4.6 Additional Pertinent Studies

Additional information on data acquisition camera film format, spectrum timing, and registration and alignment is in a report by R. D. Juday.†

The data acquisition camera film format section contains format information on the data acquisition camera scenes and indicated that 5.6 millimeters on the film corresponds to 2.1-degree field of view. A pass-by-pass conversion between the airlock module time displayed on the film and Greenwich Mean Time is also given.

The spectrum timing section gives the fractional distance into each scan when the spectrometer was examining particular wavelengths. This information was particularly useful for nadir scans and on some occasions when there was motion across a non-uniform target.

The method by which the location of the S191 data acquisition camera crosshairs can be calculated from spacecraft coordinates and gimbal angle readout is discussed in the experiment/Skylab alignment section. The alignment between the crosshairs and the spectrometer field of view and the changes with zoom are included. The registration of the 0.4- to 2.5-micrometer with the 6- to 16-micrometer wavelength region changed as a function of forward gimbal angle. The method of applying this correction is also given.

* S191 VTS Spectrometer Component Reflectances and Temperatures, MSC-05545, Martin Marietta Corporation, Denver, Colorado, June 7, 1974.

† R. D. Juday: Intricate Alignment and Timing Facts for S191, Lyndon B. Johnson Space Center, Houston, Texas, November 7, 1974.

MSC-05546

5. FINAL RESULTS

Based on evaluations for all three missions, the overall performance of the S191 system was good. Notable exceptions to satisfactory performance in terms of degradation and specific sensor anomalies are described in paragraphs 5.1 and 5.2, respectively. Paragraph 5.3 summarizes achieved performance in terms of pertinent sensor parameters.

5.1 Significant Performance Degradation

Items resulting in significant degradation to sensor performance are in Table 5.1-1.

Table 5.1-1 Significant Performance Degradation

ITEM	CAUSE	REMARKS	REF PARA
Off-band radiation	Radiant energy leakage through circular variable filter wheel	Affected wavelength regions were 0.4 - 0.43, 6 - 8, & 14 - 16 μ m	3.6.1
Loss of all long-wavelength data before DOY 160 during SL2	Unusually cold Skylab wall in vicinity of S191	Malaker cooler could not generate cold enough temperatures for proper detector operation	3.1.1
Degraded long-wavelength data on final EREP pass of SL4	Failure of Malaker cooler	Lifetime operating constraints exceeded	3.1.1
Loss of S191 door blackbody data & alignment verification capability during SL3 & most of SL4	Inability to close S191 door	S191 door blackbody data & alignment verification achieved during final SL4 pass	3.1.1
Poor DAC imagery on SL2	Improper exposure & forced development of EK3401 black-and-white film	Color film used on SL3 and SL4; proper exposure & good results achieved	3.4.1
Poor image quality on DAC magazine CI-90	Increased film storage degradation due to ionizing radiation dosage	Film data useable but degraded	3.4.1

5.2 S191 and EREP System Anomalies

Sensor anomalies and those specific EREP system anomalies directly affecting S191 are in Table 5.2-1.

MSC-05546

Table 5.2-1 S191 and EREP System Anomalies

S191 EREP	ANOMALY DESCRIPTION	CAUSE	REMARKS
X	Malaker cooler failure during final EREP pass of SL4	Assumed due to loss of working gas	Cooler operating life-time was exceeded during SL4. Long-wavelength data are recoverable.
X	S191 door would not close after a pass completion in SL3	Unknown; contamination from thruster pod, which later outgassed, was suspected	Door was left open during remainder of SL3, between SL3 & SL4, and all of SL4 to avoid potential inability of reopening after closure. Door was successfully closed after last pass of SL4.
X	Data-acquisition camera would not shut off when switch was thrown (SL2)	Film magazine improperly seated on camera	Magazine was reseated & operation continued normally.
X	In several cases during SL4, 2 of 4 light-emitting diode units of GNT display in telescope field of view failed to light	Unknown; attempts to correlate these incidents with external phenomena such as circuit breaker or switching action were unsuccessful.	No significant number of film frames were lost. Events were apparently associated with film advance periods.

5.3 Summary of Achieved Performance

Table 5.3-1 summarizes the performance of the S191 sensor in terms of pertinent parameters, which were selected as the most significant for evaluation of any spectrometer system.

MSC-05546

Table 5.3-1 Evaluation of Achieved Performance

SIGNIFICANT PARAMETER	RESULTS & REMARKS
Temperature Sensors (Housekeeping)	All housekeeping parameter values were observed to fall within specified limits except for the S191 door blackbody sensors & long-wavelength detector temperature early in SL2 & on the final SL4 pass. In both cases, the sensors correctly responded to anomalous situations.
Wavelength Calibration	The instrument's calibration did not change appreciably during the three missions. A series of equations were derived that adequately define all wavelength regions covered by the experiment.
Radiometric Calibration (Short wavelength)	Instrument responsivities were determined based on ground truth & backup-unit lunar-calibration data. Lunar calibration data were taken as the standard. SL3 & SL4 ground truth data compared reasonable well. SL2 data from Willcox Playa yielded higher values of responsivity, but clouds observed near the Playa when measurements were taken made these data questionable. A radiometric comparison between S190A, S191 and S192 indicated agreement within 15%.
Radiometric Calibration (Long wavelength)	Instrument responsivities were determined from deep space, S191 door blackbody, & internal blackbodies. Substantial variation in values were observed in 6 - 8 μm & 14 - 16 μm regions. These variations were attributed to off-band radiation effects & inaccurate determination of internal component temperatures. Good calibration was obtained only in the 8 - 14 μm region. Some evidence of contamination was observed but no specific effects on radiometric calibration could be determined.
Zero Radiance Level	Values obtained from the three mission analyses were found to be very consistent & agreed well with ground test values.
Noise-Equivalent Spectral Radiance (NESR)	<p>Because the short-wavelength NESR values depended on instrument responsivities derived from each ground truth target, similar variations as discussed in "Radiometric Calibration" were found. Detector noise values varied from mission to mission, but not by significant amounts. For most wavelengths, prelaunch test data did not agree with orbital data. This was attributed to refinements in the ground processing of data.</p> <p>Long-wavelength NESRs were not tabulated due to inconsistencies encountered in responsivity determination discussed in "Radiometric Calibration (Long-Wavelength)." Because lunar calibration data did not include the longer wavelengths, no comparisons could be made.</p>
Instrument Pointing Accuracy	The spectrometer field-of-view was observed to change position relative to the viewfinder tracking system crosshairs by approximately 150 mrad when moving from minimum to maximum zoom. The boresight error at maximum zoom was determined. The best evaluation of the error was that the crosshairs were approximately 0.1 mrad forward & approximately 0.5 mrad to the left of the actual instrument field of view.
Field of View	<p>Prelaunch measurements with a special mask determined that the spectrometer field of view was approximately 1 mrad square. On-orbit values were determined at specific wavelengths & were found to be somewhat larger, but consistent with measurements made on each mission. No data were available for SL2. The larger values were attributed to the relatively small number of data points compared to prelaunch measurements.</p> <p>Long-wavelength & short-wavelength field-of-view positions were a function of forward gimbal angle & differed from each other. Actual positions relative to telescope crosshairs were determined.</p>
Support Equipment	The data-acquisition camera used to provide supporting film coverage for target acquisition & determination of instrument pointing performed as expected throughout the missions. Exposure-setting difficulties, combined with forced development of black-and-white film from SL2, resulted in subsequent use of color film for SL3 & SL4. Imagery from the color film was excellent.

MSC-05546

6. CONCLUSIONS

The objectives of the S191 system were to obtain earth resources data from orbital altitudes in the 0.4- to 2.5-micrometer and 6- to 16-micrometer regions, and to provide a means of evaluating the usefulness of such remotely sensed data from space. Despite certain shortcomings in instrument design that became apparent during sensor performance evaluations, the instrument performed as intended. The unique features of an astronaut selecting quality targets, evaluating their quality, and acquiring and tracking the targets while data were being taken, were very successful. The ability of a crewman to respond to secondary targets when the primary targets were inaccessible proved extremely valuable.

All design specifications were met except for the failure of the Malaker cooler in the final SL4 EREP pass and the unexplained failure of the S191 door closure during SL3. Technically, the Malaker cooler operating life of 225 hours had been exceeded at the time of failure. Because the S191 Malaker unit was not updated with a special end-cap modification before launch, and because the cooler was exposed to "cold-start" problems early in SL4, it was assumed that the failure was due to loss of the working gas. Previous Malaker cooler failures during ground testing had similar problems, which resulted in the end-cap modifications. However, these modifications were not incorporated in the S191 cooler because it had no tendency to be a problem during testing, and the removal and replacement of the cooler would have delayed the launch.

The failure of the S191 door during SL3 resulted in a decision to leave the door open for the remaining portion of SL3, the entire period between SL3 and SL4, and practically all of SL4. This decision was warranted on the basis that, without some indication of the cause, closure of the door and subsequent failure to reopen would result in a total loss of experiment data. No significant conclusion could be made regarding the failure. There was some evidence that indicated contamination from the thruster quad on the command and service module might have temporarily induced a binding in the door-motor gear train. While this is speculation, the fact that the door closed nominally at the end of SL4 provides some credence because the contaminant(s) could have outgassed by then. The decision to leave the door open for most of SL3 and all of SL4 resulted in a loss of door blackbody data and alignment verification, the latter being somewhat more critical.

MSC-05546

The performance evaluation identified certain instrument design "shortcomings." One of these was that the data reduction algorithms were not implemented on computation machine for bootstraps aid in the calibrations. In the "bootstraps" technique, rough or dummy calibration data was used to process the spectrometer's output when activated with calibration sources; deductions made from the processed data refined or generated final calibration constants. That technique has proven powerful in the calibrations of the other spectrometers in the S191 program (the backup unit used for lunar observations and the helicopter unit). The data reduction algorithms to be used with spectrometer data are fundamentally a part of the system and should be included in a system calibration. Another shortcoming was limited wavelength calibration. While the vendor used external emission-line sources in his factory calibration, two faults remain: the measurement of the voltage representative of wavelength was not made to the accuracy of which the spectrometer is capable (particularly in light of using the computer algorithms as a bootstrap as discussed above), and also the wavelength versus ramp voltage was not as nearly linear as was expected. The latter consideration leads one to the conclusion that a finer mesh of line sources should have been used in the calibration, and that careful attention to the on-orbit verification of the wavelength calibration was required. (Note that in the case of S191, there is no indication of a change in the wavelength calibration during the flight.) Another "shortcoming" resulted from analysis of the data acquisition camera film. It was concluded that a camera with an automatic metering system that would compensate for changing light levels would have been preferred. In addition, the time display in the telescope field of view (visible on the film image) included only minutes and seconds. This resulted in additional data reduction time being required because any given magazine included many passes, which made it difficult to determine the hour and the day of year. The cross-hair visibility was adequate in most cases, except on lunar calibration passes where the crosshairs were allowed to drift off the moon's limb into deep space (or vice versa) so they were not visible against the blackness of space.

An examination of crew comments regarding the operation of the S191 revealed a lack of adequate restraints while operating the control panel and tracking targets. This did not preclude proper operation of the S191. The SL2 crew mentioned that operation of the viewfinder tracking system was much better on orbit than in the ground simulator, but that they would have preferred to have a wider field of view for target acquisition.

One of the objectives of the S191 experiment was to obtain data and correlate these data with ground truth measurements. Therefore,

MSC-05546

it was advantageous to provide adequate ground truth coverage. Obviously, this was a difficult task because weather conditions were often unsuitable and personnel staffing of such expeditions was limited. Only three ground truth data collections yielded data usable for S191 evaluation. This was inadequate for the three Skylab missions.

The test phase of the EREP sensors provided the baseline for S191 performance evaluation. The complexity of the hardware interfaces, the inadequacy of some ground support equipment, lack of complete end-to-end checkout of the system, and rigid schedule of design, delivery, and checkout, all contributed to an unpredictable test program. The spectrometer entered the test program without having been factory tested and calibrated with its counterpart, the viewfinder tracking system, and attempts to radiometrically calibrate the S191 system end-to-end using the on-module calibrator were not successful. This became a primary problem in the S191 flight data evaluation. A new program, using the S191 backup unit, had to be instituted in order to obtain the flight unit calibration. The behavior of the Malaker coolers under certain test conditions was very unpredictable, and resulted in a number of special test constraints. The test program was conducted in an ambient atmospheric environment as opposed to a vacuum. This also created testing problems. Effective dissipation of heat generated by long-term experiment operation was extremely difficult because many components, including the circular variable filter and lead sulfide detector, were heat sensitive. These testing problems made it difficult to determine specific parameter values for the performance baseline.

A radiometric comparison in the 0.44- to 0.90-micrometer region between S190A, S191, and S192 was made. Common targets were identified and the radiance of the target calculated from the best available calibration constants for each instrument. The derived spectral radiances from these common targets agreed closely for S190A and S192, but the S191 values were 16 to 18% higher. This agreement was within expectations, considering that various standards laboratories only agree to within $\pm 15\%$. Agreement was good with the ground truth data obtained on days when ideal atmospheric conditions prevailed. The path radiance model used for the ground truth radiance calculations above the atmosphere did not adequately consider local atmospheric conditions for less than an ideal atmosphere. Additional effort in this area is indicated. The Lane and Irvine lunar data* were about 25% higher than the values obtained by S190A and S192.

* A. P. Lane and W. M. Irvine: "Monochromatic Phase Curves and Albedos for the Lunar Disk," The Astronomical Journal, Vol 78, No. 3, 1972.

7. RECOMMENDATIONS

Based upon the extensive performance evaluation of S191 during prelaunch testing and orbital operation, a number of recommendations concerning potential improvements in instrument design, operation, and performance analysis are provided. No priority has been assigned to these recommendations but where possible, these recommendations are presented separately for the viewfinder tracking system and spectrometer portions of the S191 instrument. Recommendations which were considered applicable to both major components or to the system in general are presented in a separate category.

7.1 Viewfinder Tracking System Recommendations

Recommendations for the viewfinder tracking system are:

- 1) Use a wider angle lens system for easier target acquisition;
- 2) Modify the telescope to incorporate illuminated crosshairs for deep space scans;
- 3) The time display data block in the margin of the telescope (and camera) field of view should include complete time information (day of year, hour, minutes, and seconds) to facilitate postmission target identifications;
- 4) Reduce the alignment errors associated with the telescope zoom process and those induced as a function of forward look angle;
- 5) Incorporate a magnification indicator in the camera field of view or record these data on magnetic tape to facilitate data reduction;
- 6) Employ a data acquisition camera with an automatic exposure metering system to compensate for constantly changing light levels, a technique that allows only one mounting position of the camera, and high-resolution color film to improve target definition.
- 7) Record the gimbal angles in the housekeeping data, to allow automatic calculation of the look-point on the ground. The experiment was used in ways not anticipated in the design, such as in a nadir-swath mode and with the camera either not attached (TV passes) or not being operated; it was either impossible or meaningless to use the film displays to calculate the look point in those cases.

7.2 Infrared Spectrometer Recommendations

Recommendations for the infrared spectrometer are:

- 1) Obtain accurate preflight measurements of spectral band shapes, including off-band radiation effects;
- 2) Minimize the use of temperature-dependent components such as the circular variable filter and lead sulfide detector because application of appropriate temperature correction factors greatly increases data reduction time and decreases reliability in the output parameters;
- 3) Investigate the use of a reliable cryogenic system for long-wavelength detector cooling that minimizes cool-down time;
- 4) Modify the instrument's internal calibration to allow at least 10 seconds for each portion of the wavelength and radiometric calibration sequence. The S191 system employed 8 seconds with calibration filter removed and 4 seconds with filter in the field of view. The amount of time allowed for lamp turn-on and stabilization was excessive and should be reduced;
- 5) Provide emission line sources and/or interference filters, in addition to existing filters, for wavelength calibration;
- 6) A slower scan rate (up to 5 seconds per scan) could be incorporated if this improves the noise-equivalent spectral radiance or makes possible a preferable field of view. When considering altering the scan rate of the instrument, note that the computer processing can be done so as to integrate several scans to reduce noise. That approach would have the benefit of causing fewer cases of incomplete spectral scans of targets.

7.3 General System Recommendations

- 1) Perform developmental testing on the combined spectrometer/viewfinder tracking system;
- 2) Incorporate temperature sensors on all mirrored surfaces, including the dichroic, and on all other temperature-sensitive components, such as detectors;

MSC-05546

- 3) Accurately determine the emissivities and reflectivities of all components lying in the optical path of the instrument;
- 4) Nadir tracks should not be used for targets with less than a 7.1-kilometer-long uniform surface. The average ground velocity was 7.1 kilometers per second and the wavelength scan took 1 second. Therefore, smaller targets only provided data for a portion of the spectrometer wavelength coverage;
- 5) Provide in-depth sensor experience gained in the performance evaluations to the principal investigators (PI) to assist them in their studies. It is important that the PIs have a complete understanding of all physical aspects of the sensor parameters;
- 6) Provide continued analysis of the off-band radiation problem, especially in the LWL region because this would lead to a calculation of the true LWL responsivity of the S191;
- 7) Expand lunar calibration data reduction to improve the accuracy of the analysis. Additional data processing will be required;
- 8) Explore the causes of discrepancies between ground truth and lunar radiometric calibrations.
- 9) Synch the autocalibration cycle to scan periods of the spectrometer rather than allowing the control of the calibration sources to run free.

MSC-05546

8. NOTES

8.1 Acknowledgements

The effort covered by this report was sponsored by the Earth Resources Program Office of the Lyndon B. Johnson Space Center. It is based on the results of a concerted effort by numerous individuals in:

Science and Applications Directorate
Lyndon B. Johnson Space Center,

Lockheed Electronics Company, Incorporated
Lyndon B. Johnson Space Center,

Block Engineering, Incorporated
Cambridge, Massachusetts.

Particular acknowledgement is due the late Mr. Charles K. Williams of the Skylab Program Office at JSC for his conception and implementation of the EREP sensor performance evaluation. His dedication and leadership were essential to the successful completion of these evaluation studies. Acknowledgement is also made to Mr. Richard D. Juday, Science and Applications Directorate, of the Johnson Space Center, for his efforts as Technical Coordinator of the S191 experiment. Through his efforts, a substantial amount of additional work was initiated that ultimately led to a radiometric calibration of the instrument.

This volume was prepared by Lloyd P. Oldham, J. William Helbron, and Roger H. Kleen of the Martin Marietta Corporation, Denver Division.

8.2 Abbreviations

Abbreviations in common usage have been used for English units of measure. International units (SI) have been abbreviated in accordance with E. A. Mechtly's NASA SP-7012, The International System of Units, 2nd Rev, National Aeronautics and Space Administration, Washington, D.C., 1973--except for steradian, which has been abbreviated to ster.

AFCRL

Air Force Cambridge Research
Laboratories

amb

Ambient

MSC-05546

b/u	Backup unit
cal	Calibration
DAC	Data acquisition camera
DOY	Day of the year
EREP	Earth Resources Experiment Package
F/U	Flight unit
FOV	Field of view
GMT	Greenwich Mean Time
IR	Infrared
JSC	Johnson Space Center
KSC	Kennedy Space Center
LED	Light-emitting Diode
LWL	Long wavelength
MSC	Manned Spacecraft Center
NBS	National Bureau of Standards
NESR	Noise-Equivalent Spectral Radiance
NOAA	National Oceanic and Atmospheric Administration
OMC	On-module calibrator
Para	Paragraph
PI	Principal Investigator
REF	Reference
S&AD	Science and Applications Directorate
SKYBET	Skylab Best Estimate of Trajectory Ephemeris Data
SL	Skylab
SWL	Short wavelength
SWLI	Radiance at the sensor aperture
VTS	Viewfinder Tracking System

--	--	--	--	--	--	--	--

MSC-05546

APPENDIX A

TECHNIQUES ADDENDUM

This appendix describes in detail the techniques used to evaluate S191 performance as presented in the Sensor Performance Evaluation Report, MSC-05528, Volume II, dated September 6, 1974. These descriptions of the techniques include both the theoretical approach and the mechanics of application.

I. CALCULATION OF APPARENT SPECTRAL RADIANCE AT THE SPACECRAFT BASED ON GROUND TRUTH MEASUREMENTS

To determine the radiometric calibration of the S191, the apparent spectral radiance at the spacecraft ($N_{S\lambda}$) is required. The value for this parameter is calculated from ground truth measurements made by Martin Marietta ground truth field teams concurrently with EREP overpasses. The detailed results of these ground truth measurements were reported for each Skylab mission*.

The expression relating $N_{S\lambda}$ to the quantities measured on the ground is:

$$N_{S\lambda} = \frac{\rho}{\pi} H e^{-\tau \sec \theta} + N_{a\lambda} \quad \text{[A.I.1]}$$

where

$N_{S\lambda}$ = apparent spectral radiance from the target area at the spacecraft

H = total (direct and diffuse) solar spectral radiance incident on the target

ρ = target reflectivity (as a function of wavelength)

τ = atmosphere optical depth

θ = sensor view angle with respect to the normal

$N_{a\lambda}$ = atmospheric-path spectral radiance

The methods used to measure H , ρ , τ and $N_{a\lambda}$ are as follows:

1) Total solar radiance, H , (direct and diffuse) incident on the target. A spectral scanning spectroradiometer with a wavelength range from 400 to 1300 nanometers was used to measure the total solar radiation incident on the target.

* MSC-05531 Ground Truth Data for Test Sites (SL2), August 15, 1973
 MSC-05537 Ground Truth Data for Test Sites (SL3), March 29, 1974
 MSC-05543 Ground Truth Data for Test Sites (SL4), April 30, 1974

2) Target reflectivity, ρ , (as a function of wavelength). The same spectroradiometer used to measure H was used to measure the radiance reflected from the target area. The ratio of the values of H and ρ gives the target reflectivity.

3) Atmospheric optical depth, τ . This quantity was calculated by using measurements of the direct solar radiance as functions of the solar incidence angle.

A pyr heliometer, a spectral scanning spectroradiometer equipped with a collimator, was used. It was pointed directly at the sun and produced a meter reading, M , proportional to the direct solar radiance at the surface. Using the expression

$$M = M_0 e^{-\tau \sec \theta_0} \quad [\text{A.I.2}]$$

where

M_0 = value of M that would be observed by the pyr heliometer if it were above the atmosphere

θ_0 = solar incidence angle (with respect to the normal),

rewriting the equation by taking logs of both sides and transposing

$$\tau \sec \theta_0 = \log M_0 - \log M \quad [\text{A.I.3}]$$

by measuring values of M at various values of θ_0 , simultaneous equations can be written and solved for τ and M_0 . In practice, the solution technique used is to plot values of M versus $\tau \sec \theta$ (which gives the relative air path length with respect to a vertical path) on a semilog plot. The slope of the line is τ , and the extrapolated line intercept with the vertical axis gives the value of M_0 . This technique allows a convenient least squares fit of the data to determine M_0 .

4) Atmospheric path spectral radiance, $N_{a\lambda}$. This is a calculated quantity derived from an atmospheric radiative transfer computer model*. Required inputs to the computer program are:

* W. A. Malila, et.al.: "Studies of Spectral Discrimination," Report No. NAS CR-WRL 31650-22-T, Contract NAS9-9784, May 1971.

MSC-05546

- a) altitude of the sensor;
- b) target reflectivity;
- c) target background reflectivity;
- d) solar zenith angle;
- e) solar-sensor azimuth angle;
- f) sensor view angle;
- g) atmosphere visual range.

These values were available from field observations, Skylab Best Estimate of Trajectory Ephemeris Data (SKYBET) mission tapes, and ephemeris data.

The apparent radiance calculated using Equations A.I.1 was used to determine S191 flight unit responsivities, as described in Sections 3.8 and 4.4.

II. USE OF LAKES AS THERMAL CALIBRATION TARGETS

The use of lakes as infrared calibration targets in the 6- to 16 micrometer region was especially useful because their emissivity is greater than 0.98 over most of this spectral region for measurements made at normal incidence. Figures A.II-1* and A.II-2* show that the emissivity remains high (reflectivity low) at incident angles up to 60°. For radiometric accuracies corresponding to about $\pm 0.5^\circ\text{C}$, the water temperature can be measured by a conventional thermometer and 0.5°C subtracted from it to account for the lower surface temperature. The radiance is then calculated from the Planck blackbody radiation equation. However, for the 0.1°C accuracy desired on Skylab, a radiation thermometer was used to accurately determine the surface temperature. Figure A.II-3† illustrates effect of evaporation on the surface. The figure was plotted from data taken during low wind and medium humidity. When the humidity is low, there is an even greater temperature gradient at the surface, but no data were available describing the magnitude of this effect at lower or higher humidities. It is reasonable to assume that the surface radiometric temperature may be from 0 to 1°C lower than the water temperature a few centimeters below the surface, depending on wind and humidity conditions.

For lakes viewed by Skylab a correction for atmospheric constituent absorption was made. This correction was made by the method described in Section VII of this appendix. To minimize the amount of absorber between the lake's surface and Skylab, lakes were selected at the highest possible altitude consistent with their required size. Water vapor is the primary absorber in the infrared, and total water content (precipitable centimeters) decreases dramatically for lakes above 3000 meters. Lake Titicaca (3812 meters) is high enough so that no atmospheric correction was needed, except in the strongly absorbing water bands.

Because the reflectivity of the lakes from 6 to 16 micrometers is low, calculations were made that showed that the sun's reflected energy did not cause an appreciable error in the assumption that all the energy emanates from the lake surface.

* H. O. McMahon: "Thermal Radiation from Partially Transparent Reflecting Bodies," *J. Opt. Soc. Am.*, 40, June 1950, p 376-380.

† E. D. McAlister, "Application of Infrared-Optical Techniques for Oceanography," *J. Opt. Soc. Am.*, 52, May 1963, p 607.

MSC-05546

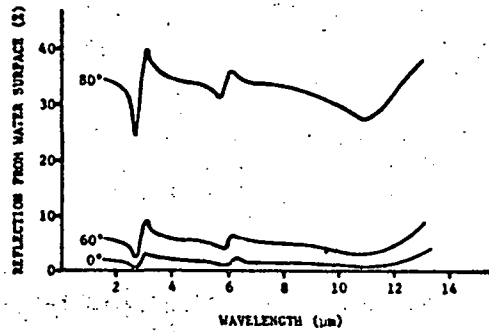


Figure A.II-1 Reflection from Water Surface at 0, 60, and 80° Incidence Angles

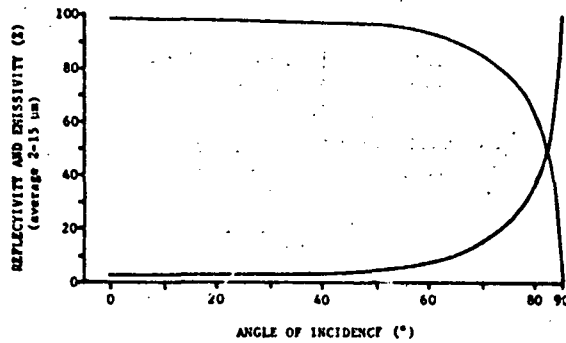


Figure A.II-2 Reflectivity and Emissivity of Water versus Incidence Angle

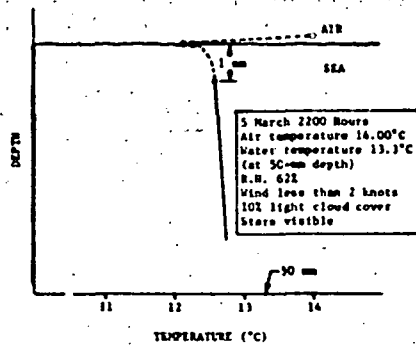


Figure A.II-3 Thermal Structure of the Sea Boundary Layer

III. RADIANCE CALIBRATION OF SEVERAL LUNAR MARIA USING AN S191-IDENTICAL GROUND-BASED SPECTROMETER

Absolute radiance values for three lunar maria (Serenitatis, Tranquillitatis, and Imbrium) were derived and plotted against phase angle. The values were derived from ground observations made with the S191 backup unit in November and December 1973 and January and March 1974. The data were used to calibrate the S191 system. Data were tabulated for ten wavelengths in the 0.4- to 2.5-micrometer range, and for phase angles between -30° and $+30^\circ$.

A. Background

A reliable absolute calibration was not achieved prior to Skylab launch. The light bulb in the ground calibration source failed during measurements of the radiance of that source, which were being made after the activation of the flight system prior to launch. The failure gave cause for concern with respect to the stability of the radiance of the source between time of the flight system activation and the radiance measurements. Determinations of instrument responsivity based on ground truth site measurements were made for each of the three missions. These determinations were not consistent. The cause was ascribed to uncertainties in correcting for atmospheric effects. An alternative approach for calibrating the flight spectrometer, which would eliminate most of these uncertainties, was developed.

This alternative method consisted of using designated lunar maria as reference sources for both the S191 flight spectrometer and an identical ground-based instrument that had been calibrated against the Scale of Spectral Irradiance of the National Bureau of Standards (NBS). This calibration was effected by means of an on-module calibrator (OMC) used to transfer the NBS standard to the S191 unit.

The product of the ground measurements was a set of curves* for the absolute spectral radiance of the lunar maria as a function of phase angle.

The major remaining element of uncertainty in the lunar maria spectral radiance curves was in the correction for atmospheric attenuation effects for the ground based measurements. The correction for atmospheric attenuation was derived from a plot of radiance measurements made over a range of viewing incidence angles with a consequent variation of air-mass values. The zero-air-mass radiance

MSC-05546

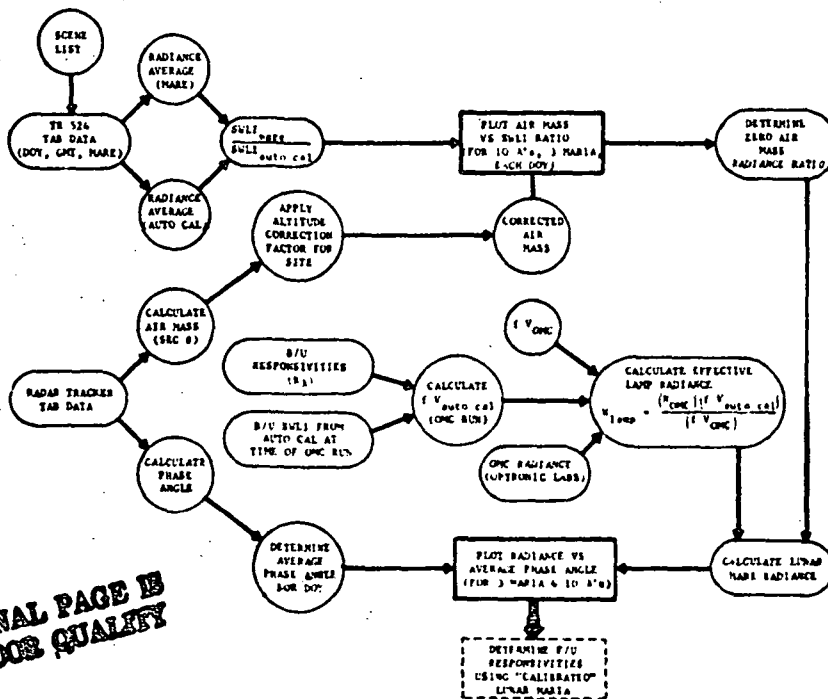
value was derived by an extrapolation of this plot. It was assumed that attenuation effects were relatively constant during the time required to make the measurements. Observations were made at night to avoid the effects of scattered sunlight.

* MSC-05548, S191 Lunar Calibration Data Reduction Report,
September 30, 1974.

II-67a

B. Method

The sequence of calculations required to produce the lunar spectral radiance curves is shown in Figure A.III-1. Acceptable data sets were selected for analysis based on examination of photographs taken concurrently with the ground data by the S191 data acquisition camera. TR524 data products giving radiance at the sensor aperture (SWLI) were averaged over the period of observation and ratioed with the corresponding value of SWLI for the period corresponding to that portion of the auto cal cycle when the lamp was on and the integrating sphere capped. This radiance ratio was plotted as a function of air mass for each wavelength interval, mare, and day of the year (DOY). Lunar viewing angles used to calculate air-mass values were determined from an existing Apollo lunar rover computer program in which designated lunar-mare and the ground-based test-site latitudes and longitudes were considered. These values were then multiplied by an altitude correction factor based on test-site atmospheric pressure at the time of observation.



ORIGINAL PAGE IS
OF POOR QUALITY

Figure A.III-1 S191 Lunar Calibration Data Flow

MSC-05546

Zero-air-mass radiance ratio values were determined by applying a least squares fit of the existing data points. Other data, such as OMC radiance values, instrument responsivities, SWLI from the auto cal at the time of the OMC run, and spectrometer output voltages when observing the OMC, were used to calculate the effective backup unit lamp radiance as a function of wavelength. These values, together with the zero-air-mass radiance ratio values, provided radiance values for the three lunar maria.

Phase-angle calculations were derived from the ARMP, Apollo Reference Mission Profile. Because these angles were continuously varying, they were averaged over each night's observations. Maria radiances were then plotted as functions of average phase angle for each of the ten wavelengths.

The entire data analysis and results of the lunar calibration task were presented in MSC-05548, S191 Lunar Calibration Data Reduction Report, September 30, 1974. Plots of maria radiances as functions of average phase angle that were presented in Appendix D of MSC-05548 were discovered to require a refit of the data points. These modifications were based on

- 1) Derivation of additional data points;
- 2) The "weighting" of specific data points.

The additional data points, which provide values of zero radiance, were derived from purely geometrical relationships based on terminator location and approximate longitude of each mare. Knowledge of these data points, together with radiance values derived from phase angles of $\geq 20^\circ$, realistically defines the slope of the linear portion of the curves. In cases where the radiance ratio/air-mass curves exhibited a positive slope, i.e., did not indicate an increase in the radiance ratio value when extrapolated back to zero air mass, the mean value of radiance ratio had been used to define the data point corresponding to the phase angle for that day's observation. Upon examination of other radiance ratio/air-mass plots at other wavelengths, (which did not exhibit positive slopes) for the same mare and day, certain assumptions were made as to the what the slopes should have been, thereby defining a radiance ratio value at zero air mass. While these points were not plotted, they were used as guides when the resulting curves were drawn. Data points for phase angles of -29.6 and $+21.2^\circ$ were considered inaccurate because of too few data points in the radiance ratio/air-mass curves.

Flight-unit responsivities were then calculated using the radiance values derived from the three lunar maria. The new plots of lunar maria radiance as a function of phase angle are included as Appendix B.

IV. USE OF ABSORPTION FILTERS FOR SPECTROMETER WAVELENGTH CALIBRATION

During developmental testing of the S191, Block Engineering, Inc., Cambridge, Massachusetts used external mercury and argon emission-line sources in the laboratory wavelength calibration of two of the five circular variable filter segments. Only mercury-line sources were used to calibrate the 0.39- to 0.73-micrometer segment; no internal calibration data points were used. While these line sources provided an extremely accurate calibration, there was no method of comparing these results to later test or flight data because the line sources were outside the spectrometer system.

For internal wavelength calibration, two filter materials were incorporated in the S191. A 1.0-millimeter (0.040 in.) thick piece of BG-36 Schott glass was used in calibrating the three short-wavelength segments and a 0.15-millimeter (0.006 in.) thick piece of polystyrene film was used for the two long-wavelength segments. During sensor performance evaluation, at least three points in each of the five segments were used in the wavelength calibration. The number of points was limited to absorption minimums and maximums in the filter material used for wavelength calibration. While absorption minimum locations of Schott glass and polystyrene were readily available from published literature, maximum locations were not, and special laboratory spectra were obtained to determine their specific locations. These locations proved to be useful calibration points, provided the maximums were not too broad spectrally. For example, only one maximum point (11.83 micrometers) was determined to be useful in the long-wavelength calibration.

For the range of wavelengths covered by the five circular variable filter segments, more calibration points were required to adequately cover the entire range of each segment. The circular variable filter theoretically provided a linear variation of wavelength as a function of angle. However, final calibration of the flight instrument indicated that optimum curve fits were obtained in the majority of the segments with a second-order polynomial rather than a straight line. The theoretical straight line for the wavelength versus angle is a manufacturing goal, not a mathematical fallout of the filter design. The fact that the curves did not fit the theoretical straight-line fortified the need for additional data points, especially at extremes of the segment range.

A meaningful curve fit for the 1.34- to 2.5-micrometer segment should have required a calibration point between 2.0 and 2.5 micrometers. However, no acceptable minimum or maximum in this range was available from the BG-36 Schott glass filter.

V. S191 FIELD OF VIEW, ALIGNMENT, AND OFF-AXIS REJECTION
DETERMINATION USING THE LUNAR LIMB

The S191 field of view, alignment, and off-axis rejection evaluation used the bright-dark step intensity function of the moon's edge. Because there was no atmosphere between Skylab and the moon, there were no scattering effects, and the step function was exceptionally sharp. The small amount of lunar curvature in the S191 field of view did not appreciably effect the results.

A. Field of View

When the S191 field of view was slowly scanned from the lunar center into deep space, a silicon or lead-sulfide detector output at a particular wavelength exhibited the curve shown in Figure A.V-1. The width of the field of view can be measured directly on the abscissa as the distance from A to C. The determination was made in both axes and at various wavelengths. For the HgCdTe detector 6- to 16-micrometer region the ordinate was both positive and negative because the reference temperature was between that of the sunlit lunar surface and deep space. The break points at A and C were still a measure of the S191 field of view in these wavelengths.

This method had limitations:

- 1) S191 rectangular field of view was not exactly aligned with the lunar edge.
- 2) There were not enough data points to adequately describe the curve.

The first condition causes the curve in Figure A.V-1 to change slope somewhat and have rounded corners. No attempt was made to develop these curves theoretically and correct the results because the actual scans of the lunar edge were fast and not enough data points were available to adequately fit a curve. The assumption was made that the curve in Figure A.V-1 was correct and the line AC was drawn from the available data.

The milliradian scale on the abscissa of Figure A.V-1 was determined from data acquisition camera film measurements of crosshair distance from the limb. These measurements were made with a variable-rate 16-millimeter projector. Because the crosshairs could not be seen in deep space, they were marked on the screen and measurements were made to these screen marks.

MSC-05546

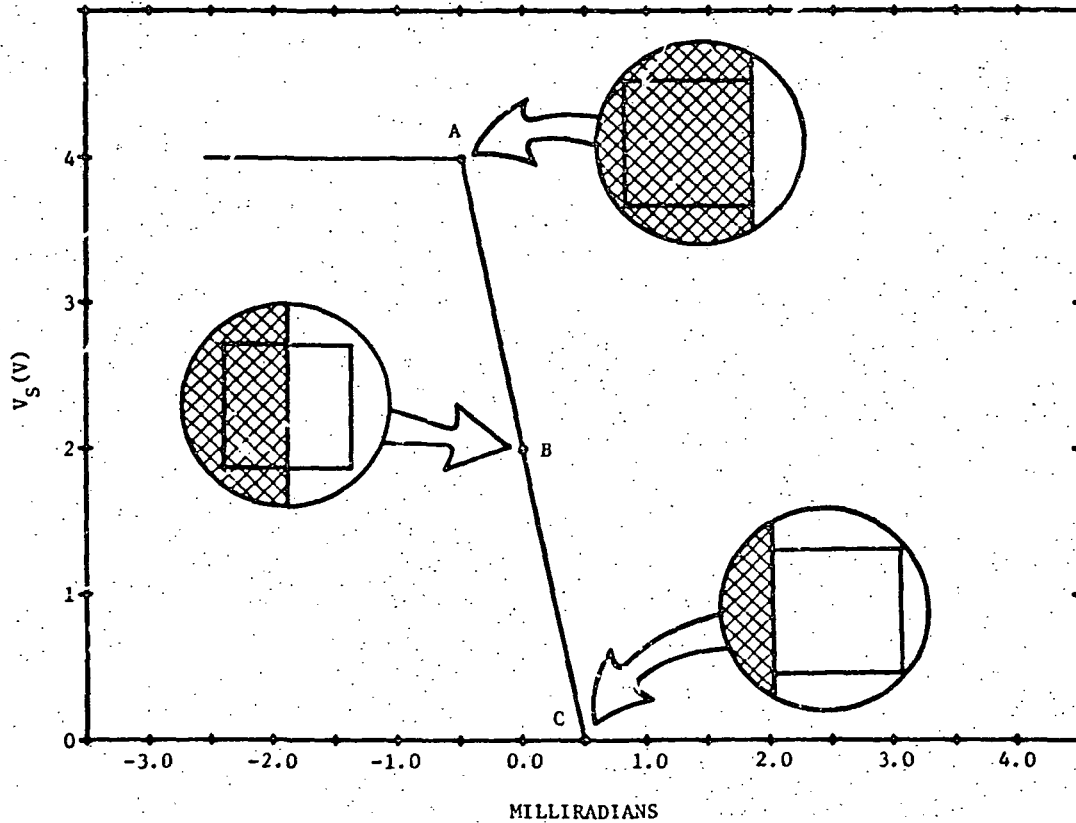


Figure A.V-1 Theoretical Field-of-View Determination

Small changes were observed in screen crosshair position from frame to frame. These were corrected by marking light-emitting diode position on the screen and using these reference indicators to make the required small corrections. The moon's diameter was also measured so that the previous measurements could be converted to milliradians.

Time was used to correlate detector output data to each data acquisition camera frame, but the frames only recorded time to the nearest second. This was much too gross a measure and the times recorded in the housekeeping tabs for each camera actuation were used. However, this camera shutter pulse time was not the same as the data acquisition camera exposure time and a correction had to be made. Figure A.V-2 illustrates the shutter operation and shows that the housekeeping camera shutter pulse initiation time was 7 milliseconds after the data acquisition camera frame exposure time.

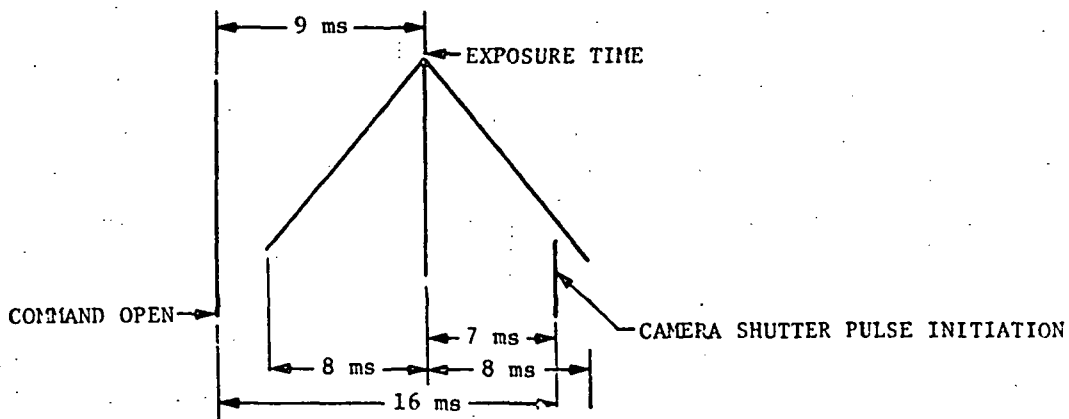


Figure A.V-2 Data Acquisition Camera Shutter Time Sequence

Because housekeeping functions were only sampled every 47 milliseconds, the exact time when the camera shutter pulse was initiated was not available. The housekeeping tabs merely indicated the presence of a pulse when this function was sampled. The width of the pulse was known to be 40 ± 14 milliseconds. The frame rate was 2 frames per second ($\pm 3\%$). Because the frame rate was accurately known and constant, a sequence of camera shutter pulse times was examined. The earliest observed time (subtracting the major multiple of $1/2$ second) was used to establish the first, second, and third decimal points for the camera shutter pulse initiation times. This procedure may still give errors of up to 10 milliseconds.

Now that the crosshair position (in milliradians from the lunar limb) had to be correlated to the detector outputs, a figure like Figure A.V-1 was drawn and the distance from A to C measured directly.

B. Alignment

The alignment at each wavelength and in each direction could be assessed by directly reading the position of point B,

$\left(\frac{V_s(A) - V_s(C)}{2} \right)$, on the abscissa of Figure A.V-1 because the 0-milliradian position corresponded to the data acquisition camera crosshairs alignment on the edge of the moon.

Because Figure A.V-1 contained a small number of data points for each wavelength presented, an alternative procedure was used to obtain better accuracy. This procedure consisted of determining point B directly by examination of the data and finding the time when the detector output was 50% of the same wavelength's output when the field of view was completely on the illuminated lunar surface. For the 6- to 16-micrometer range, the deep-space background had to be subtracted. This time was then compared to the corrected exposure time derived in the manner discussed in Section A.V and the actual alignment values interpolated.

C. Off-Axis Rejection

If the instrument's field of view did not show a sharp drop-off at its edge, the curve in Figure A.V-1 would have rounded response at points A and C. On the other hand, a flat response up to A and after C would have shown that there was a sharp fall-off. There were not enough data on S191 lunar limit tranverses to make an exact analysis, but this technique was applied and indicated that off-axis energy outside the primary field of view was small.

VI. DETERMINATION OF NOISE IN A LIMITED SET OF REPETITIVE DATA

This technique was developed for use on S191 spectra when only a limited number of scans of the same target were available. The uncertainty of a measurement is inversely proportional to the square root of the number of samples taken. Because means and standard deviations were determined by hand, a crossover point between reliability and effort falls at about 30 data samples. Because only 10 data samples were available in most of the data and it was felt that this introduced too much uncertainty, the following technique was developed.

Three data sets were used that corresponded to the detector outputs at a selected wavelength and the two detector outputs adjacent in wavelength on either side of the desired wavelength. It was most important to use the following relations for determining three separate standard deviations because the means can change significantly from one sampled wavelength to another.

Mean values for all sample groups were calculated by

$$\bar{X} = \frac{1}{M} \sum_{k=1}^M \bar{x}_k \quad [\text{A.VI.1}]$$

where

\bar{X} = resultant mean value from the two or three sample groups

M = number of sample groups

\bar{x}_k = mean value of the kth sample group

The standard deviation using a sample mean was defined as

$$\sigma_k^2 = \frac{1}{n_k - 1} \sum_{i=1}^{n_k} (x_i - \bar{x}_k)^2 \quad [\text{A.VI.2}]$$

where

σ_k = standard deviation for the kth sample group

n_k = number of data words forming the sample group

x_i = the value of a particular data word

\bar{x}_k = the sample mean for the kth sample group

For M sample groups,

$$\sigma^2 = \frac{\sum_{i=1}^{n_1} x_i - \bar{x}_1)^2 + \sum_{i=1}^{n_2} x_i - \bar{x}_2)^2 + \dots + \sum_{i=1}^{n_M} (x_i - \bar{x}_M)^2}{n_1 + n_2 + \dots + n_M - M} \quad [\text{A.VI.3}]$$

where σ = standard deviation for all sample groups.

If the sample groups have the same number of data words, i.e. $n_1 = n_2 = \dots = n_M = n$, then

$$\sigma^2 = \frac{\sum_{k=1}^M \left[\sum_{i=1}^n (x_i - \bar{x}_k)^2 \right]}{M(n-1)} \quad [\text{A.VI.4}]$$

$$\text{and } \sigma = \sqrt{\frac{\sum_{k=1}^M \sigma_k^2}{M}} \quad [\text{A.VI.5}]$$

The technique assumed that the standard deviation was the same magnitude or at least had a linear variation over the range of sample sets used, and that the S191 data had the same magnitude of standard deviation over the adjacent wavelength ranges used.

VII. INFRARED ATMOSPHERIC CORRECTIONS

When viewing any target below about 4000 meters above sea level (99% of all targets) corrections for atmospheric absorption and re-emission were required at wavelengths longer than 0.82 micrometers.

Atmospheric transmission was calculated by using a basic program developed by R. F. Calfee, National Oceanic and Atmospheric Administration (NOAA), Boulder, Colorado. This program calculates transmission by dividing the atmosphere into layers. The required inputs are average temperature, pressure, and total water content for each layer. These temperature inputs were derived from humidity profiles. For most Skylab targets, radiosondes were balloon launched or dropped from a helicopter at the time of Skylab overflight. Radiosonde data were supplemented by adjacent NOAA network radiosonde data. The NOAA data, as well as the ground-truth-team radiosonde data, were then plotted on skew T, log P diagrams. The ground-truth radiosonde data were most heavily weighted in the meteorological analysis performed to arrive at a "composite" water-vapor temperature profile for a particular Skylab observation, but weather features like cold fronts were also taken into account in developing the "composite" curves. The atmosphere was then divided into convenient layers based on the "composite" profile and water content and representative temperatures estimated for each layer. The resulting temperature, water content, and thickness for each layer were used as input parameters to the Calfee atmospheric transmission program.

The basic Calfee program uses the "compressed line" data*. However, this program does not take into account the amount of radiation from the target and the upwelling radiance from each layer. The Calfee program was therefore modified according to the following equations (See Figure A.VII-1):

$$R_{\lambda} = (\tau_1 - 1) B_1 + (\tau_2 - \tau_1) B_2 \tau_1 + \dots + (\tau_n - \tau_{n-1}) B_n \tau_{n-1} + B_c \tau_n \quad [\text{A.VII.1}]$$

* R. McClatchy et al.: AFCRL Atmospheric Absorption Line Parameter Compilation, AFCRL Environmental Research Laboratory, Publication Number 434, Bedford, Massachusetts, 1972.

R. F. Calfee and R. Schweisow: Nu Averaged Infrared Absorption Coefficients of Water Vapor, NOAA Technical Report #ERL 274-WPL24, Boulder, Colorado, 1972.

where

R_λ = radiance above atmosphere at a particular wavelength

B_n = blackbody radiance of nth layer (starting at the top atmospheric layer)

B_t = blackbody radiance of target

τ_n = transmission from space through nth layer

The effective upwelling radiance includes the instrument wavelength response function and is given by

$$R_{\text{eff}} = \frac{\sum_{\lambda=1}^m R_\lambda \cdot g_\lambda}{\sum_{\lambda=1}^m g_\lambda} \quad [\text{A.VII.2}]$$

where

R_{eff} = effective radiance seen by instrument with particular instrument function

g_λ = instrument response function normalized to one at the peak

m = number of increments in instrument function characterization.

The radiance, R_{eff} , was then taken as the effective radiance at the spacecraft aperture corrected for the particular sensor's response function.

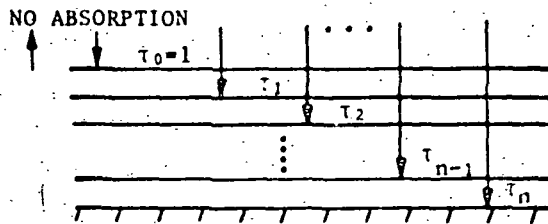


Figure A.VII-1 Upwelling Radiance Calculation

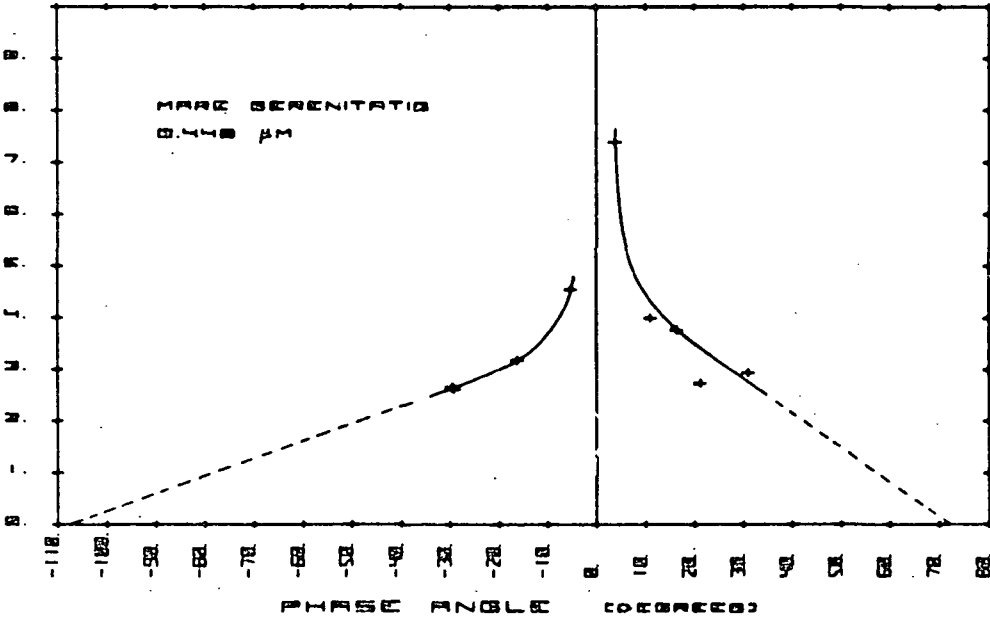
MSC-05546

APPENDIX B

ABSOLUTE RADIANCE OF THREE LUNAR MARIA

This appendix contains the plots of absolute radiance of Mare Serenitatis, Mare Tranquillitatis, and Mare Imbrium as a function of phase angle at ten wavelengths. A description of these plots is in Section III of Appendix A.

IRRADIANCE (10^{-3} WATTS/CM²/MICROMETER/STER)



IRRADIANCE (10^{-3} WATTS/CM²/MICROMETER/STER)

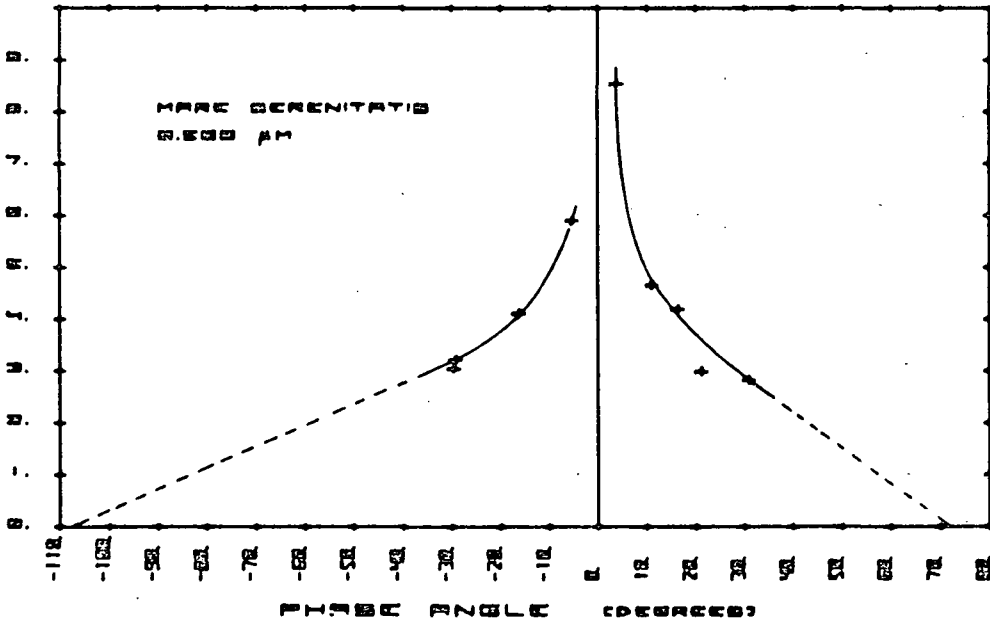
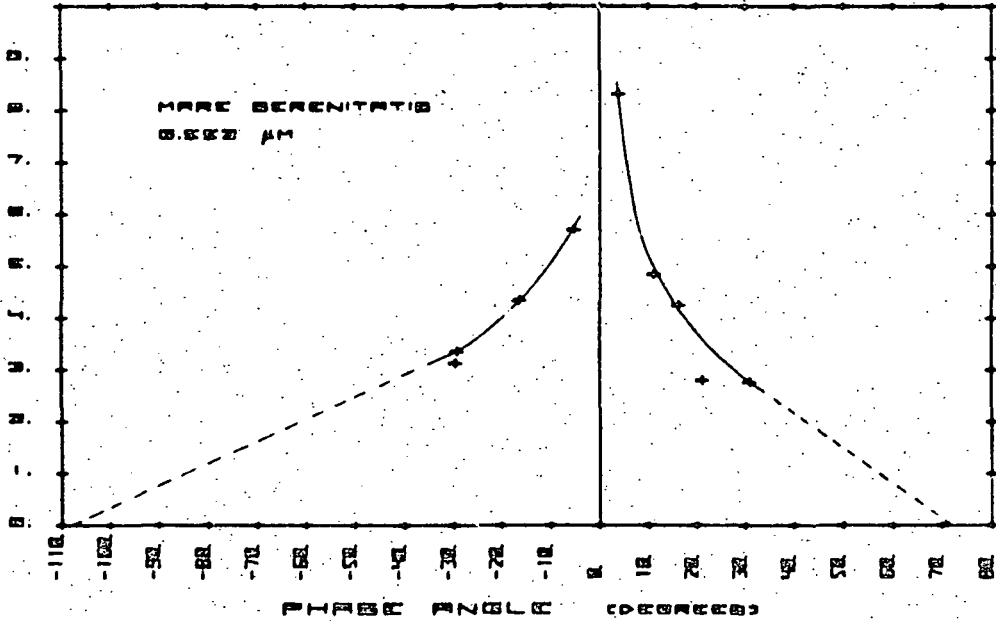


Figure B-1 Absolute Radiance of Mare Serenitatis

IRRADIANCE (10^{-3} WATTS/CM²/MICROMETER/STER)



IRRADIANCE (10^{-3} WATTS/CM²/MICROMETER/STER)

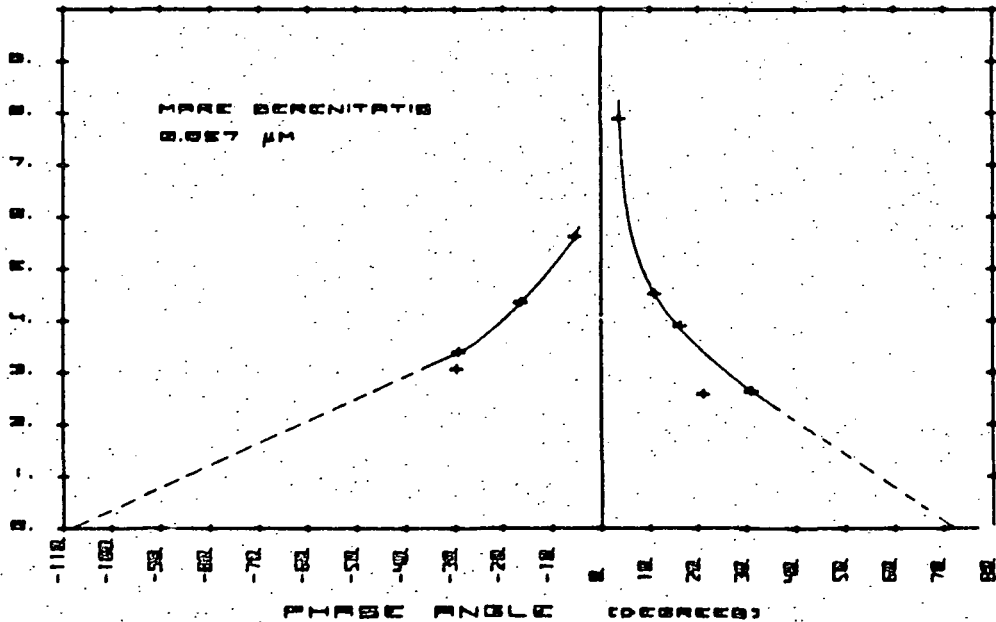
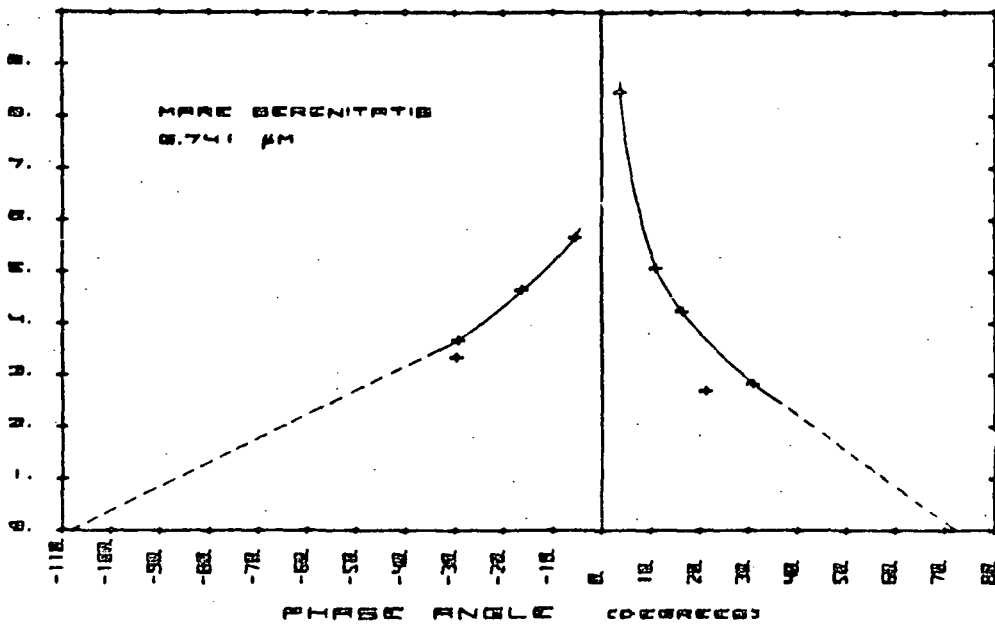


Figure B-1. (continued)

IRRADIANCE (10⁻³ WATTS/CM²/MICROMETER/STER)



IRRADIANCE (10⁻³ WATTS/CM²/MICROMETER/STER)

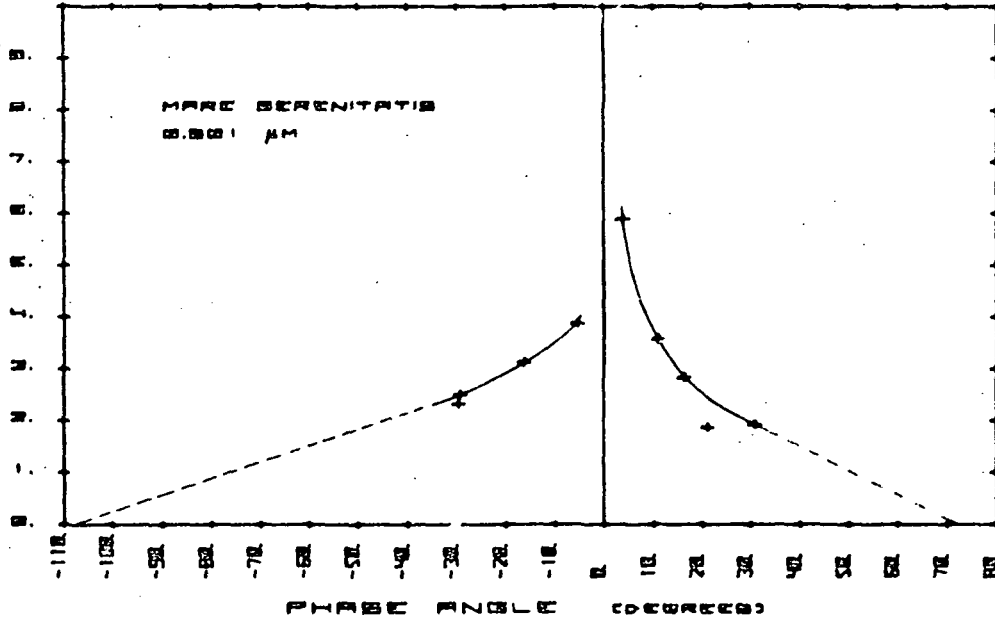


Figure B-1 (continued)

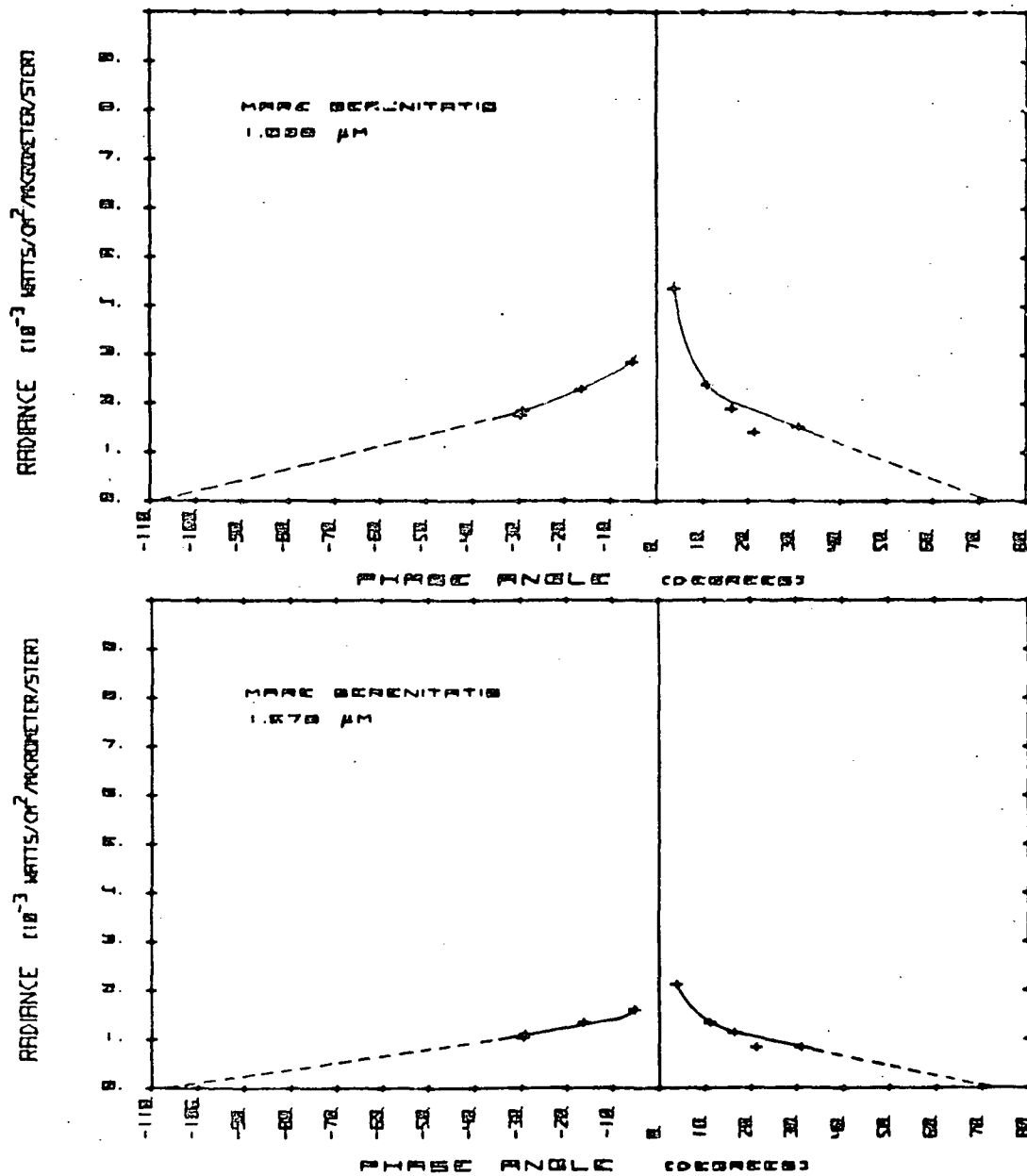


Figure B-1 (continued)

MSC-05546

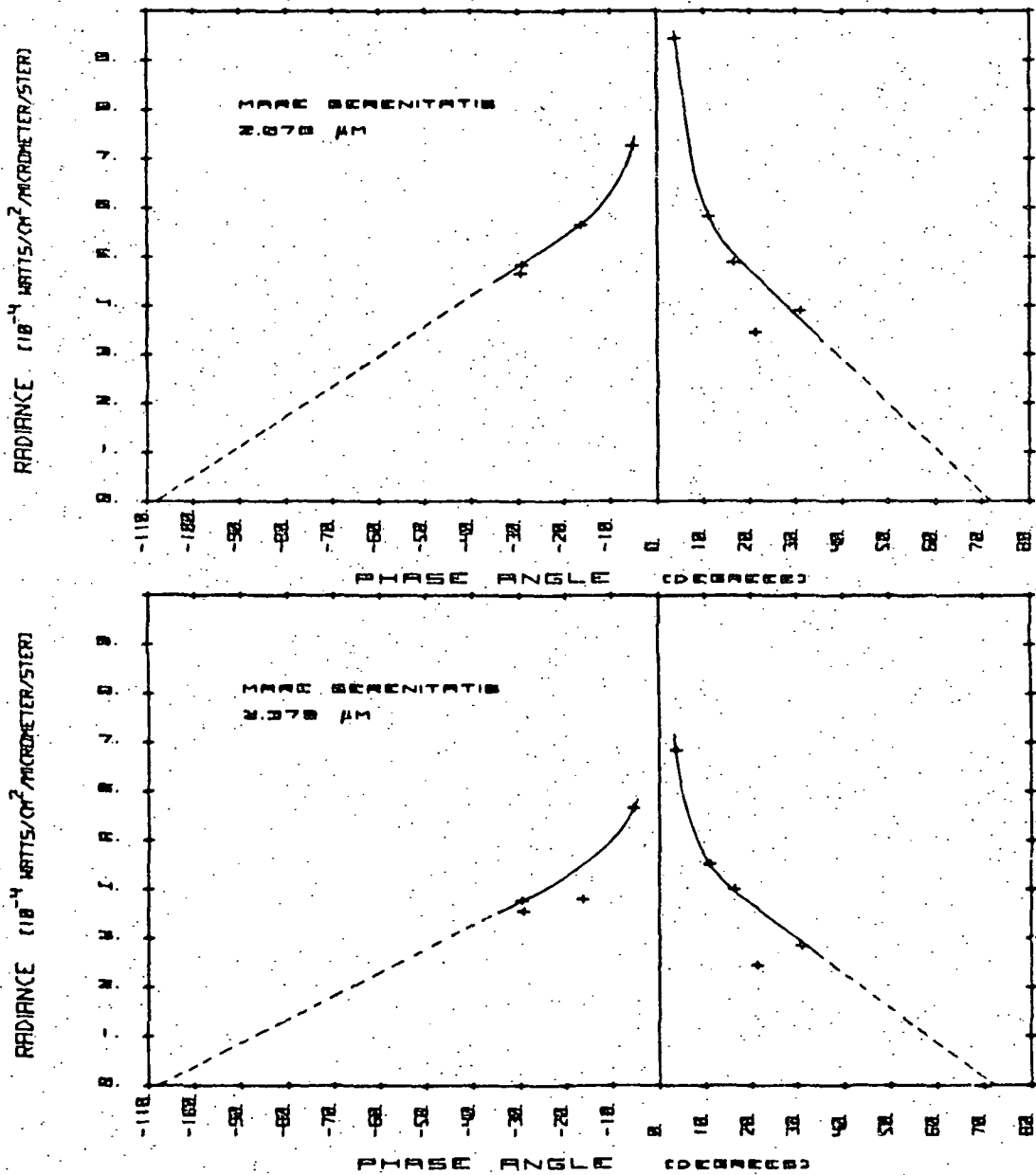


Figure B-1 (concluded)

MSC-05546

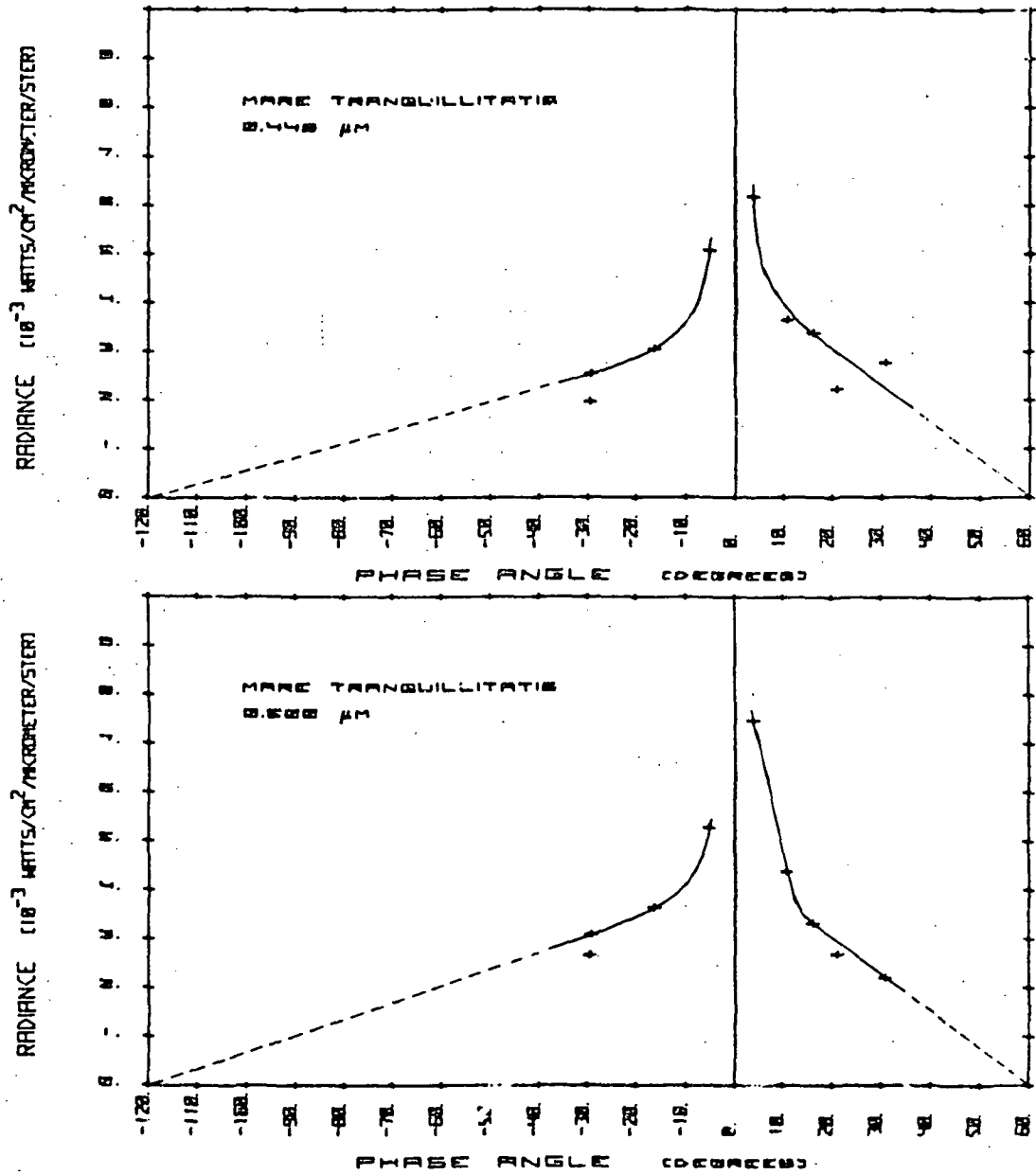
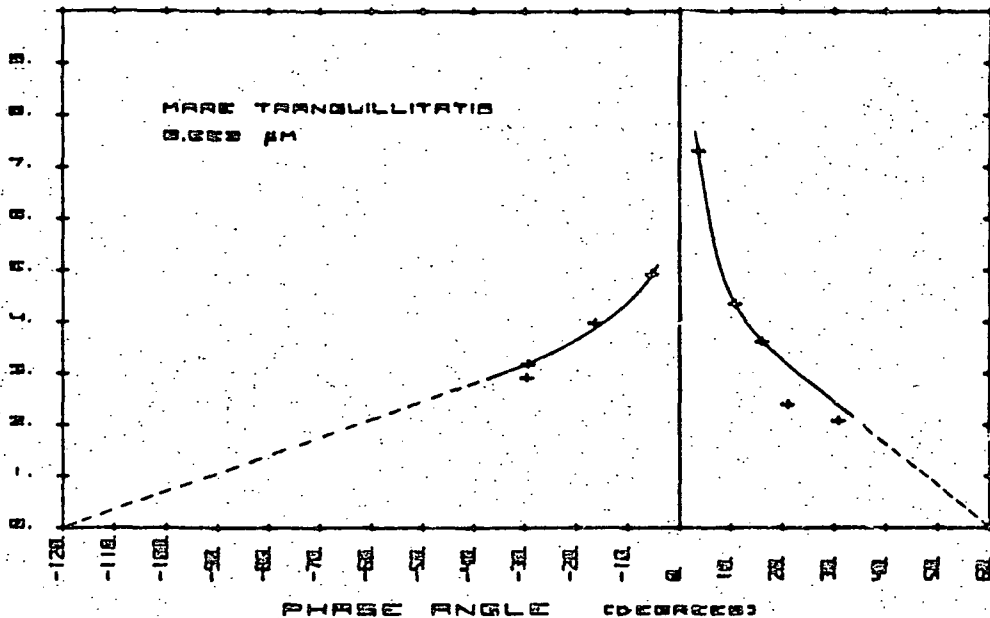


Figure B-2 Absolute Radiance of Mare Tranquillitatis

MSC-05546

RADIANCE (10⁻³ WATTS/CM²/METER/STER)



RADIANCE (10⁻³ WATTS/CM²/METER/STER)

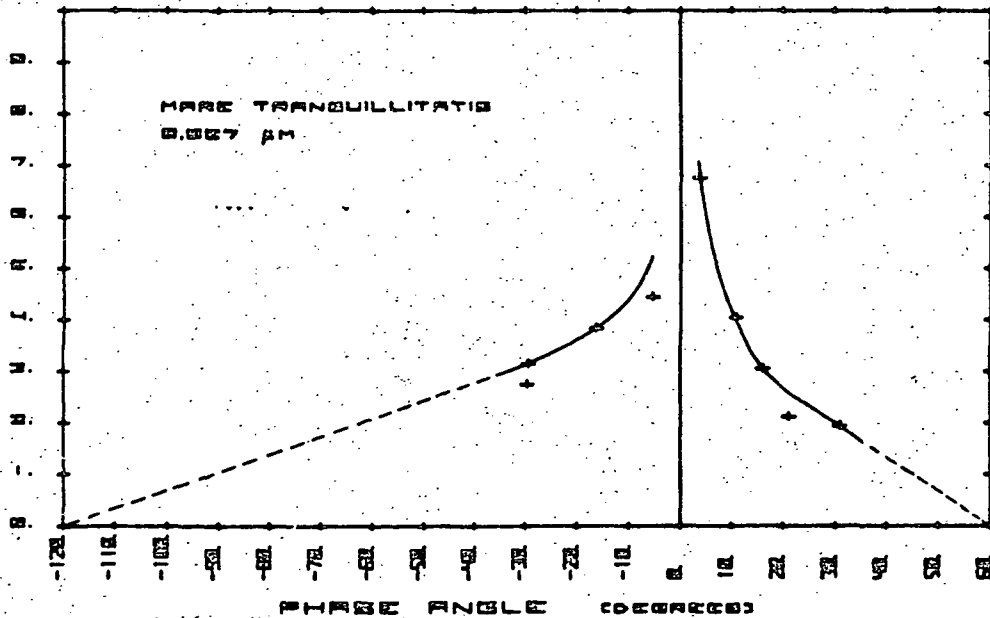
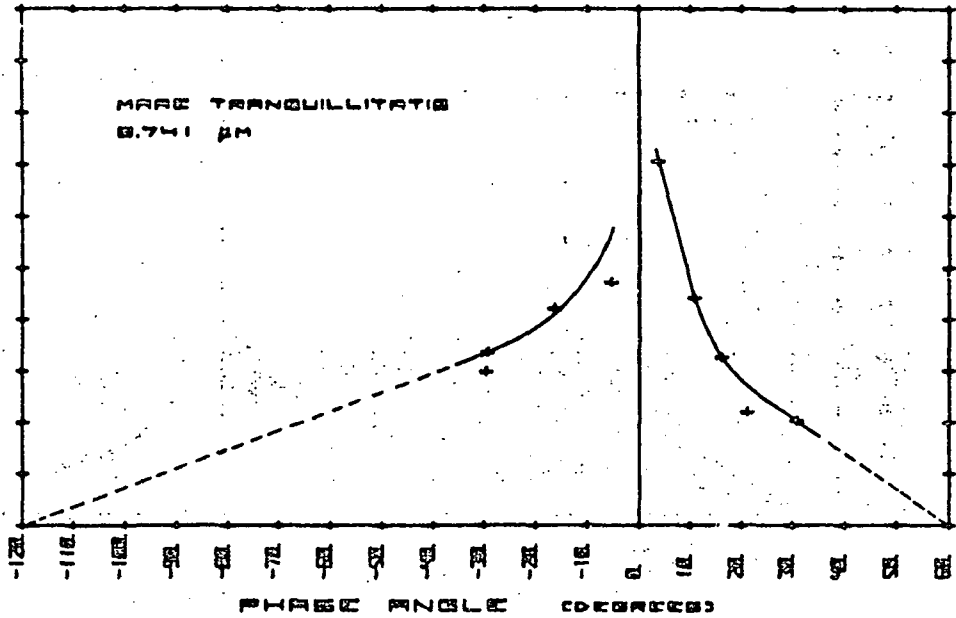


Figure B-2 (continued)

C-2

MSC-05546

REFERRANCE (10⁻³ WATTS/CM²/ACROMETER/STER)



REFERRANCE (10⁻³ WATTS/CM²/ACROMETER/STER)

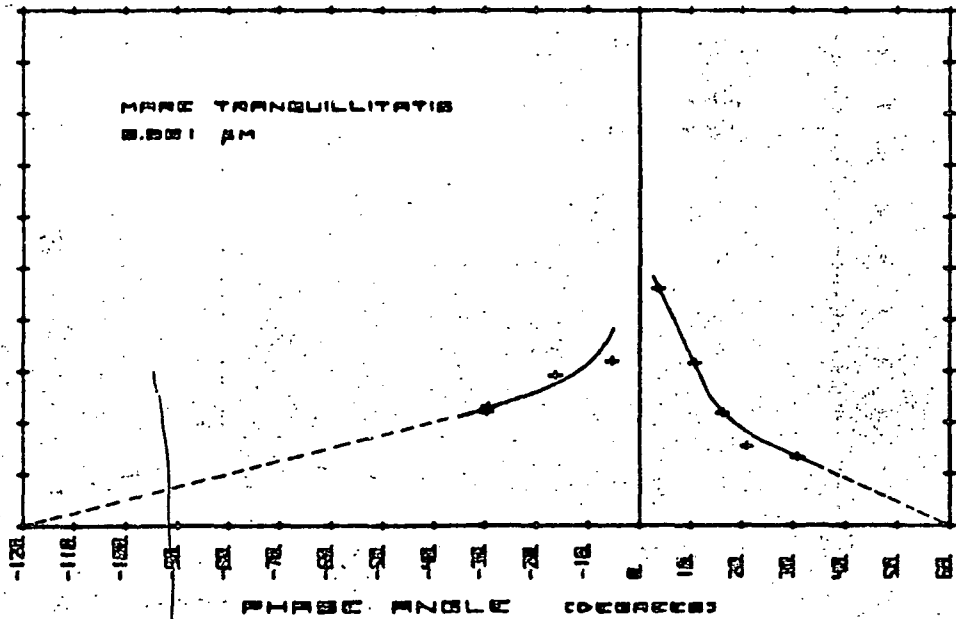
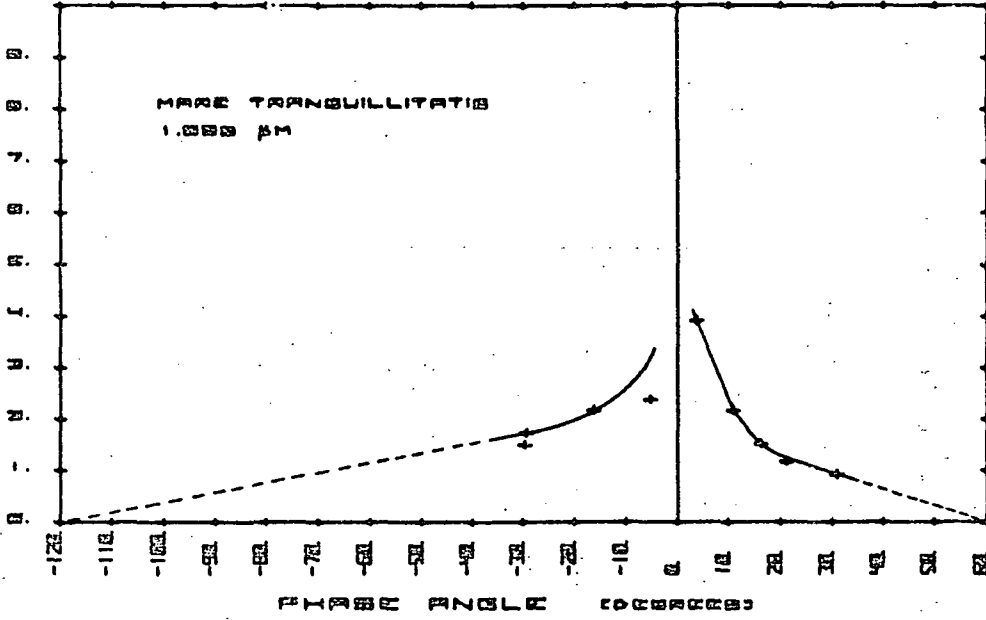


Figure B-2 (continued)

POSDRANCE (10⁻³ WATTS/CM²/MAGNETR/STDR)



POSDRANCE (10⁻³ WATTS/CM²/MAGNETR/STDR)

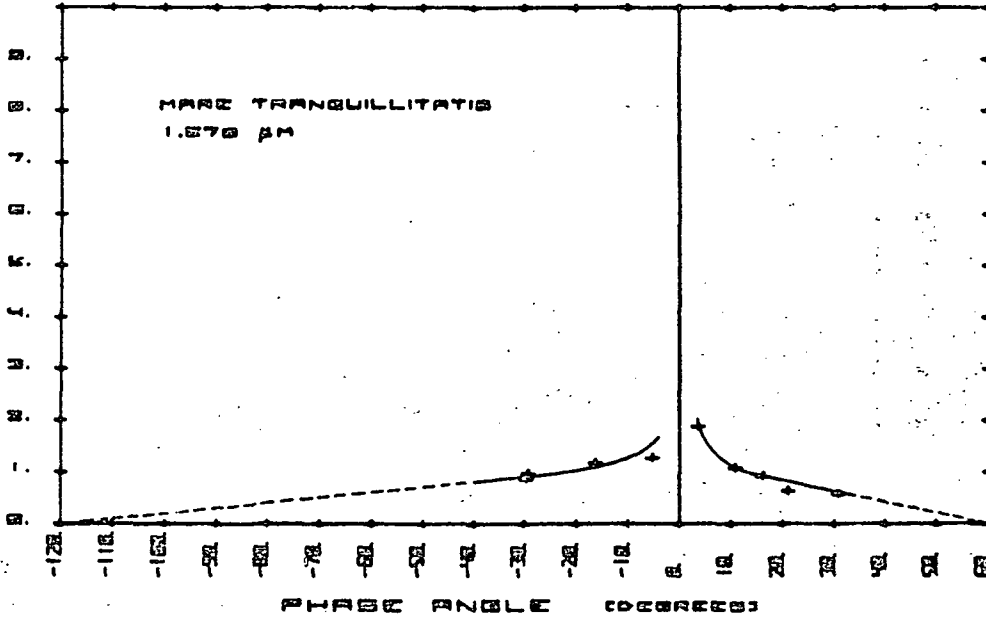
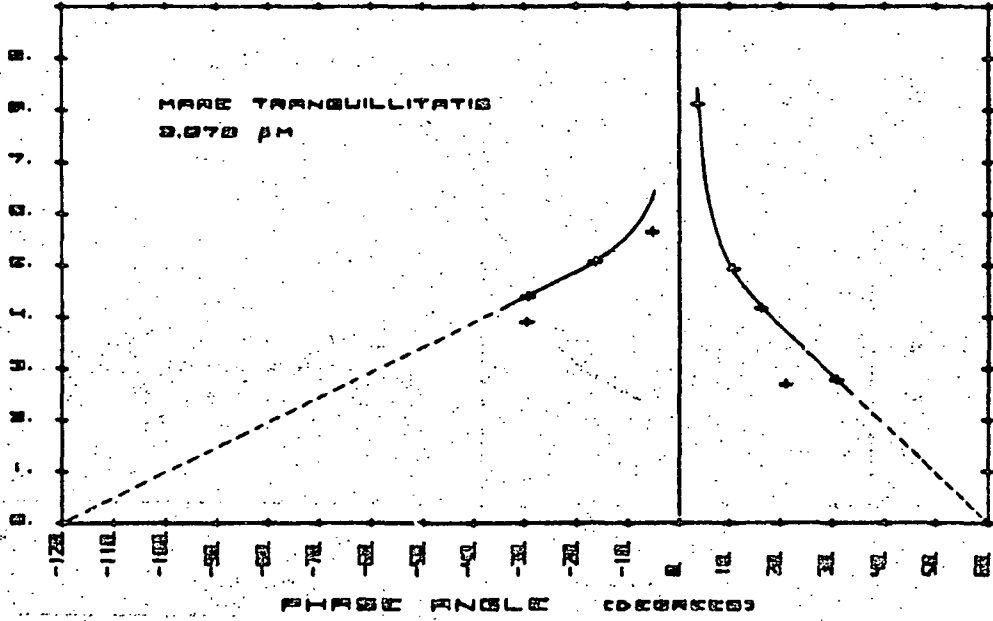


Figure B-2 (continued)

HSC-05546

IRRADIANCE (10⁻⁴) WATTS/CM²/MICROELECTRONS



IRRADIANCE (10⁻⁴) WATTS/CM²/MICROELECTRONS

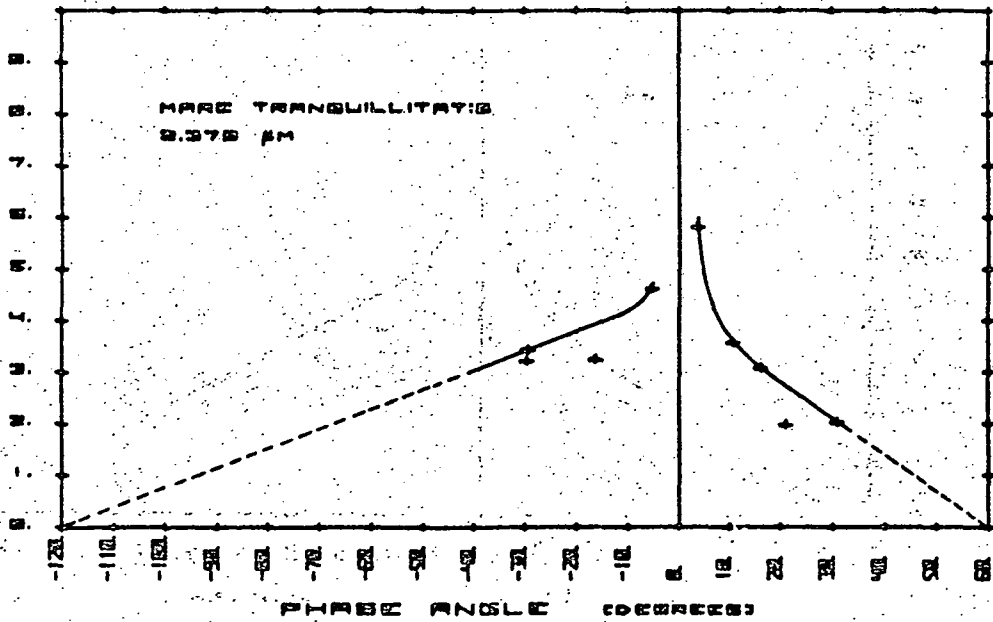


Figure B-2 (concluded)

MSC-05546

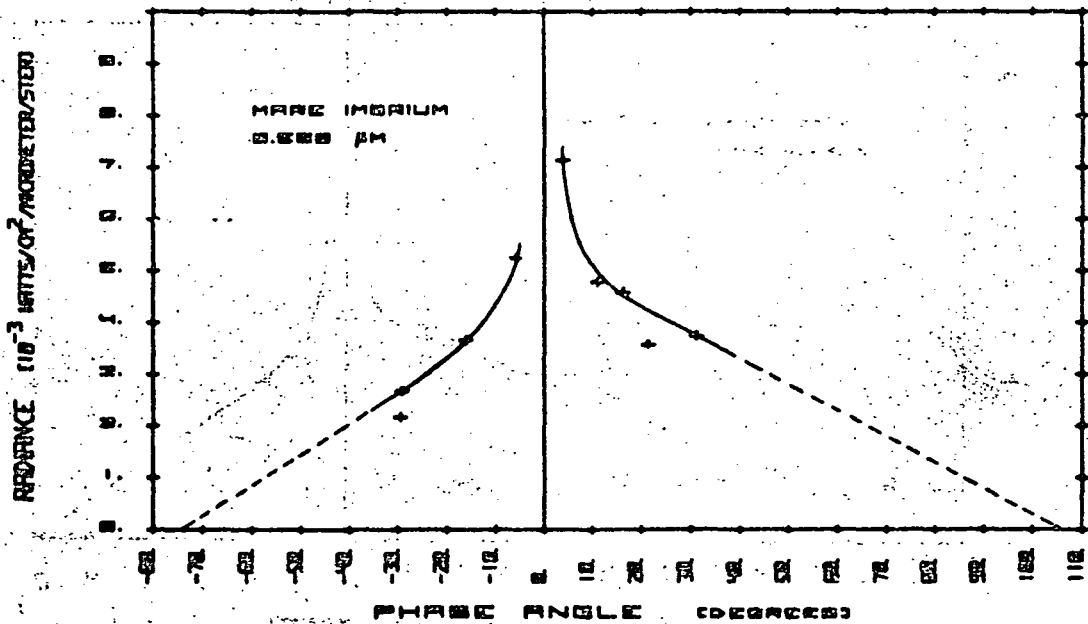
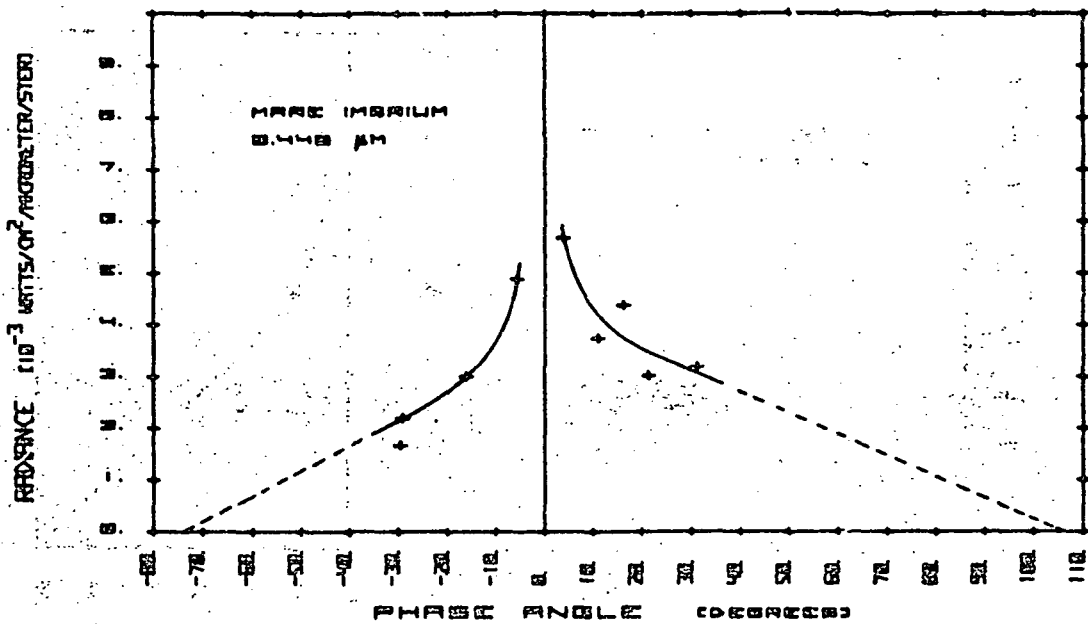
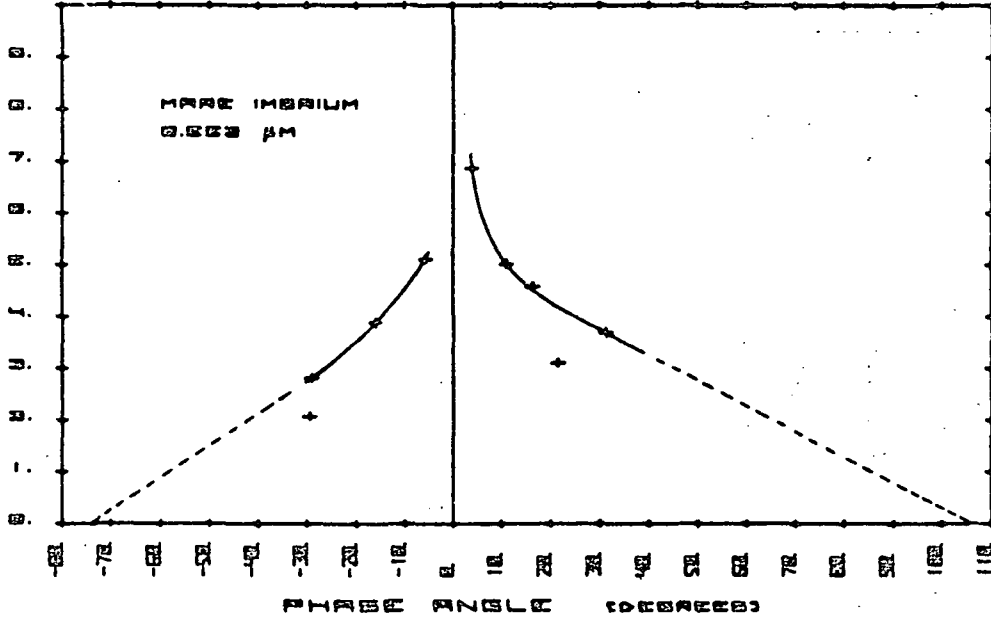


Figure B-3 Absolute Radiance of Mare Imbrium

MSC-05546

RADIANCE (10^{-3} WATTS/CM²/METER/STER)



RADIANCE (10^{-3} WATTS/CM²/METER/STER)

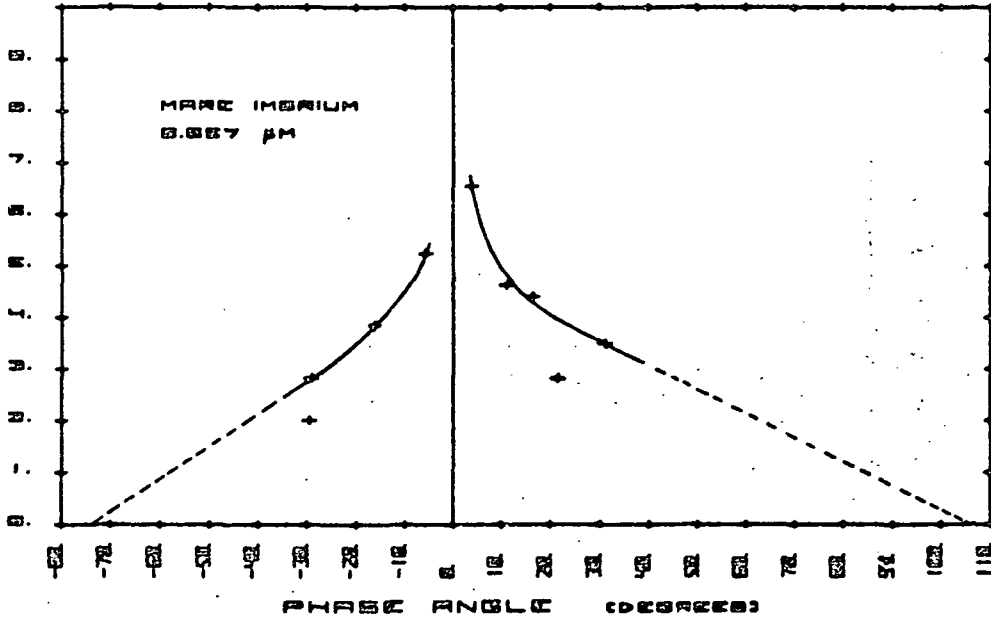
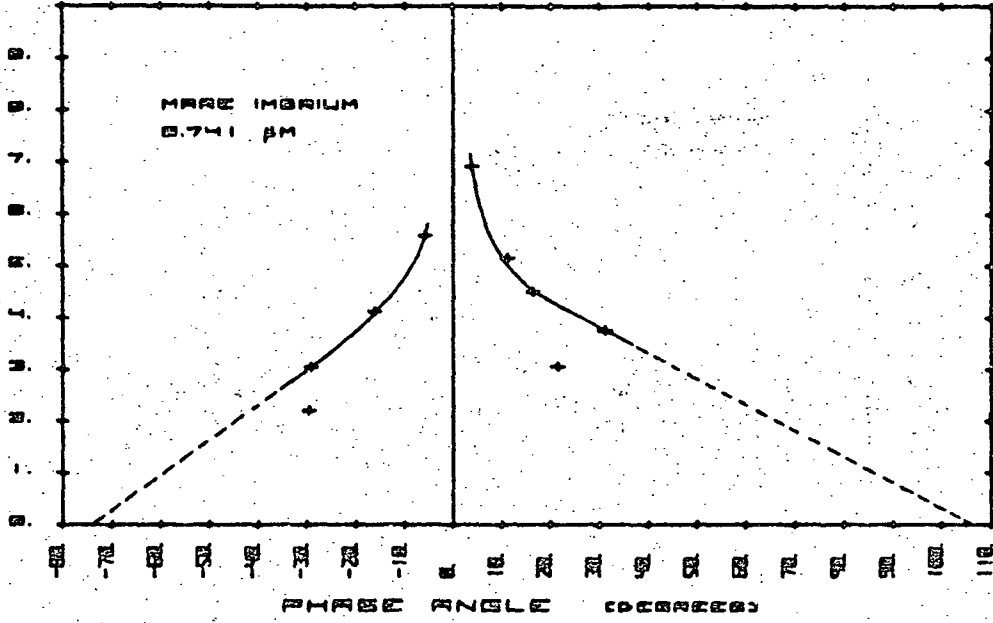


Figure B-3 (continued)

MSC-05546

REFERENCE (10⁻³ WATTS/CM²/METER/STERO)



REFERENCE (10⁻³ WATTS/CM²/METER/STERO)

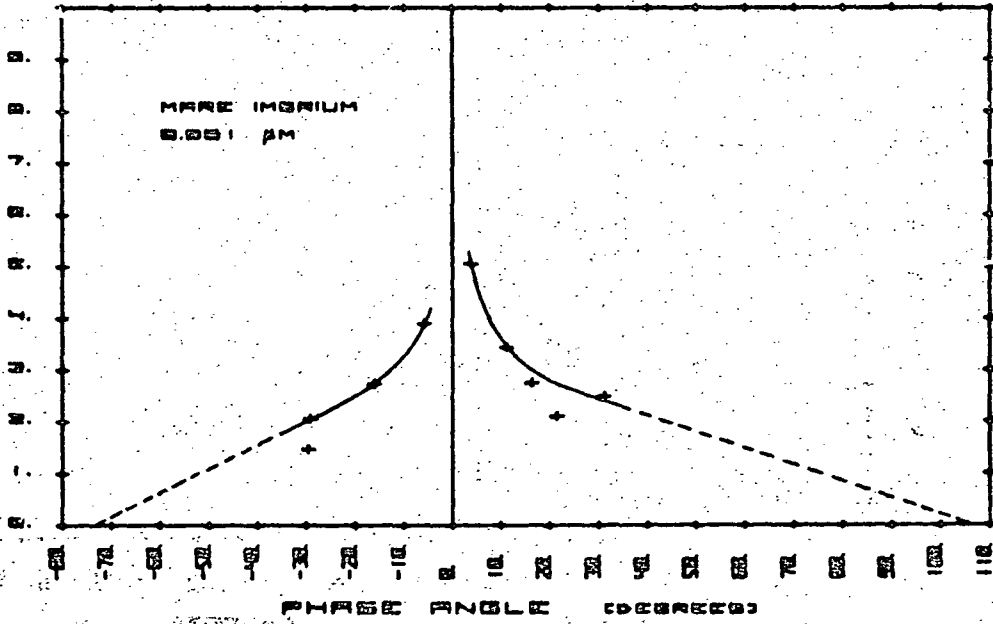
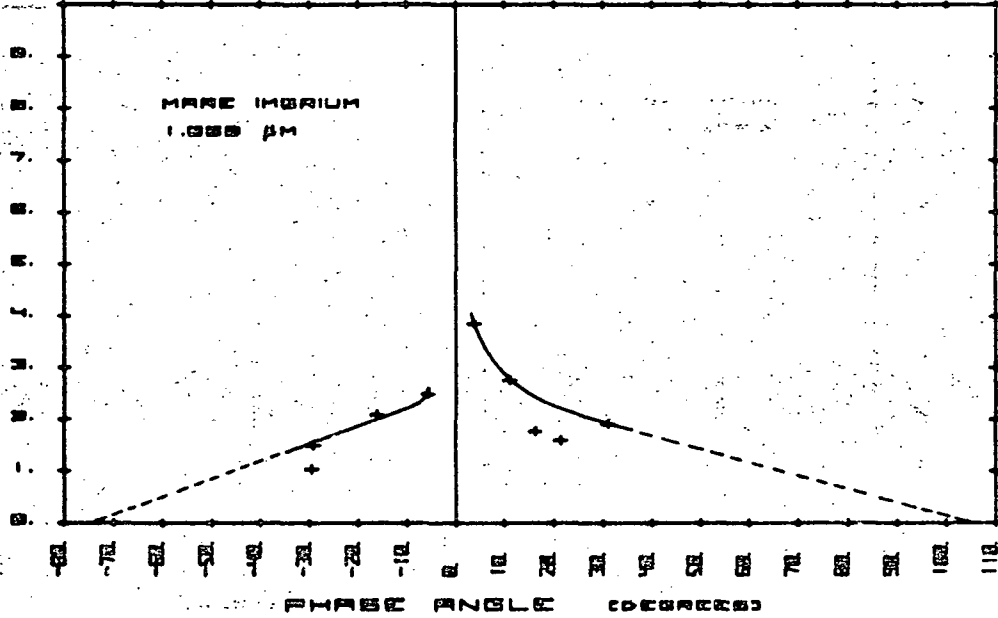


Figure B-3 (continued)

MSC-05546

REFLECTANCE $(10^{-3}$ WATTS/CM²/MICROMETER/STERE)



REFLECTANCE $(10^{-3}$ WATTS/CM²/MICROMETER/STERE)

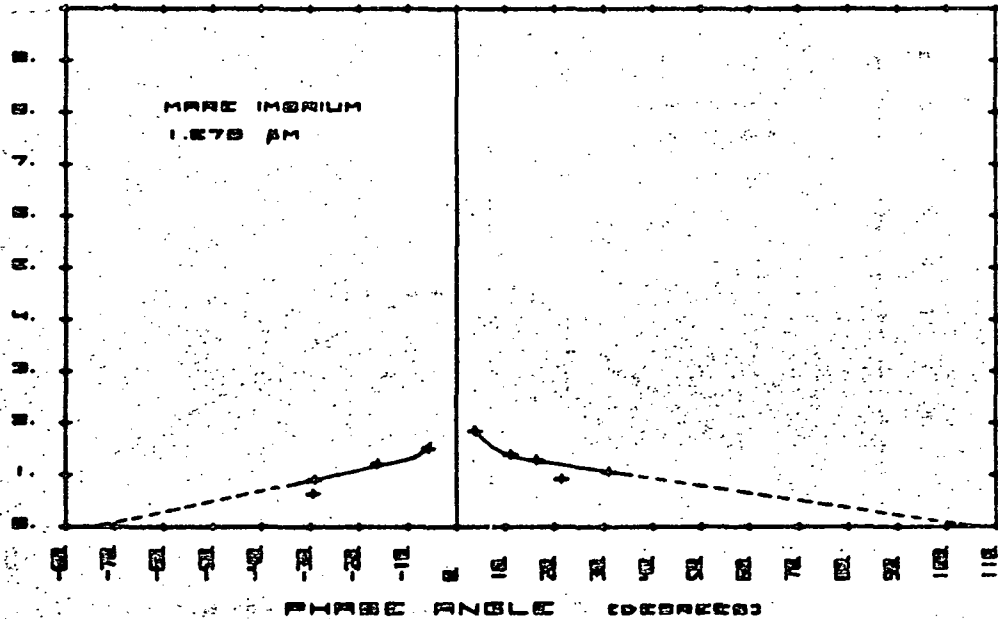


Figure B-3 (continued)

MSC-05546

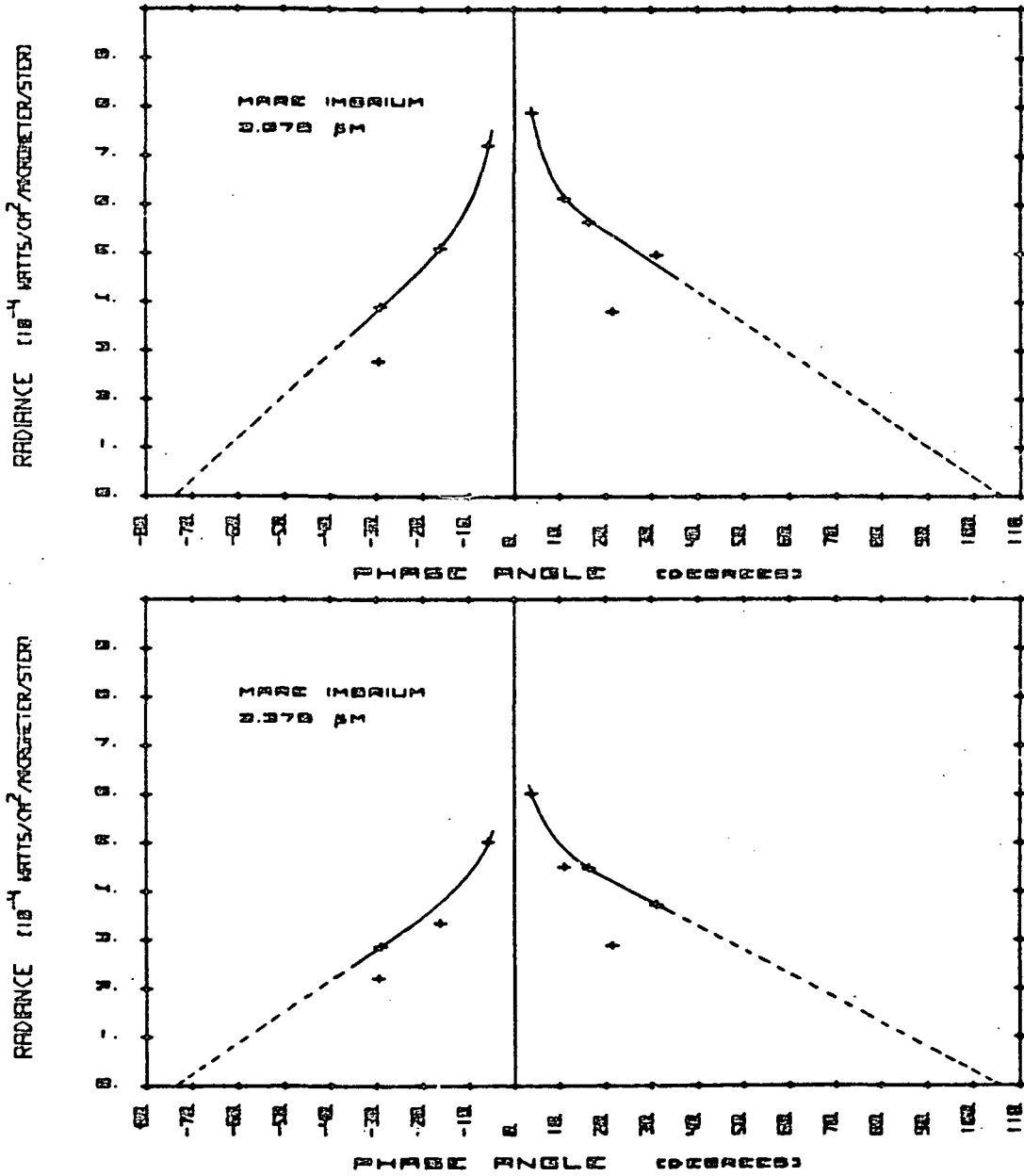


Figure B-3 (concluded)

U.S. GOVERNMENT PRINTING OFFICE: 1975-671-200/1972